UNIVERSITY OF SOUTHAMPTON

Faculty of Engineering, Science and Mathematics

Optoelectronics Research Centre

Simultaneous all-optical processing of wavelength division multiplexing channels

b y

Lionel André Provost

A thesis submitted for the degree of

Doctor of Philosophy

February 2012

UNIVERSITY OF SOUTHAMPTON

ABSTRACT

FACULTY OF ENGINEERING, SCIENCE AND MATHEMATICS

OPTOELECTRONICS RESEARCH CENTRE

Doctor of Philosophy

SIMULTANEOUS ALL-OPTICAL PROCESSING OF WAVELENGTH DIVISION MULTIPLEXING CHANNELS

by Lionel André Provost

In this thesis, the possibility of simultaneous all-optical regeneration of wavelength-division multiplexed (WDM) signals within the same optical device is investigated. The optical regeneration scheme discussed in this thesis relies on the exploitation of the SPM induced by the optical Kerr nonlinearity within an optical fibre. In the work presented in this thesis, I report the extension of a particular single-channel all-optical 2R regenerator suitable for on-off keying return-to-zero modulation format to WDM operation. The device is referred to as the Mamyshev regenerator, and provides both Re-amplification and Re-shaping capabilities for the incoming optical signal.

An in-depth analysis of the single-channel device reveals that remarkable and simple scaling rules can be established to relate the output properties of the optical regenerator to the characteristics of the incoming signal to be regenerated and key physical parameters defining the optical regenerator. The analysis allows general conclusions to be drawn on the mitigation strategies to be implemented to extend the scheme to the multi-channel case.

The extension to the multi-channel scenario is then examined. Minimization of the interaction time between adjacent channels is introduced by inducing a sufficient walk-off between co-propagating signals. The strength of the inter-channel nonlinearities can be sufficiently reduced to preserve the optical regeneration capabilities. Two techniques are therefore reported. One is based on the counter-propagation of two optical signals within the same piece of nonlinear fibre. The second relies on polarization multiplexing of two co-propagating signals. Theoretical aspects and experimental demonstrations at 10 Gb/s, 40 Gb/s, and 130 Gb/s are reported.

Contents

List of figures

List of tables

List of acronyms

ASE	Amplified spontaneous noise
BER	Bit-error rate (or ratio)
CWDM	Coarse wavelength division multiplexing
DCF	Dispersion compensation fibre
DGD	Differential group delay
DSF	Dispersion-shifted fibre
EDFA	Erbium doped fibre amplifier
FWHM	Full-width at half maximum
FWM	FWM
GVD	Group velocity dispersion
HNLF	Highly nonlinear fibre
NLSE	Generalized nonlinear Schrödinger equation
NOLM	Nonlinear optical loop mirror
OSNR	Optical signal-to-noise ratio
PC	Polarisation controller
PMD	Polarisation mode dispersion
PM-HNLF	Polarisation-maintaining highly nonlinear fibre
PRBS	Pseudo-random binary sequence
RZ	Return-to-zero

SBS	Stimulated Brillouin scattering
SMF	Single mode fibre
SPM	SPM
SRS	Stimulated Raman scattering
SSMF	Standard single-mode fibre
WDM	Wavelength-division multiplexing
XPM	XPM

Declaration of authorship

I, Lionel A. Provost, declare that the thesis entitled Simultaneous all-optical processing of wavelength division multiplexing channels and the work presented in the thesis are both my own, and have been generated by me as the result of my own original research. I confirm that:

- this work was done wholly while in candidature for a research degree at this University;
- where I have consulted the published work of others, this is always clearly attributed;
- where I have quoted from the works of others, the source is always given. With the exception of such quotations, this thesis is entirely my own work;
- I have acknowledged all sources of help;
- where this thesis is based on work done by myself jointly with others, I have made clear exactly what was done by others and what I have contributed myself;
- parts of this work have been published in the journal articles and conference proceedings reported in the List of Publications at the end of the thesis.

Lionel A. Provost

September 2010

Acknowledgments

I first thank Professor David Richardson and Doctor Periklis Petropoulos for welcoming me in the Optical Fibre Communications Group. I am extremely grateful for their supervision and valuable support throughout my PhD studies.

I want like to thank my colleagues I have the opportunity to meet during my stay at the Optoelectronics Research Centre, and more particularly people working in the group: Dr Francesca Parmigiani, Dr Trina Ng, Dr Symeon Asimakis, and Dr Michaël Roelens. I am extremely grateful to Dr Francesca Parmigiani for teaching me about the use of the numerous equipments in the laboratory. She was also involved in much of the experimental work reported in this thesis. I really appreciate her involvement and her motivation to get things done.

I would like to express both professional and friendly acknowledgement to Professor Christophe Finot. It was a real pleasure to have the opportunity to work (once again) with him and have discussions with him on numerous subjects whatever they were technical or not.

Working within the framework of the European Project TRIUMPH allowed me to meet and work with enthusiastic people, such as Christos Kouloumentas, and Philipp Vorreau.

Eventually, I would like to thank Kazunori Mukasa from The Furukawa Electric Company (Japan) for his generous and valuable support in providing me with some of the special optical fibre used within the experiments. Without these fibres nothing would have been possible.

Chapter I: Introduction

Over the two last decades, data communications traffic has demonstrated continuous growth and driven mostly by the development of Internet traffic and the development of new services such as High-Definition television, video on demand, Internet browsing, online gaming and remote computing to name but a few. All of these new multimedia services are ever more bandwidth-consuming as compared to traditional voice and sources data traffics (e.g. email), and drive an unprecedented demand for more complex communication networks of higher bandwidth and capacity. With the development of new broadband services (e.g. Fibre-to-the-Home), that allows the delivery of up to 100 Mb/s today and up to 10 Gb/s in the near future [1], the growth for more bandwidth is not expected to end anytime soon.

Addressing such a growth demand is not a straightforward challenge as numerous technical and economic factors must be taken into consideration [2]. Among these, one can identify infrastructure installation and maintenance costs, upgrade possibilities to address the unrelenting bandwidth growth and the introduction of service quality as critical issues.

Because of its huge bandwidth capacity as compared to copper or wireless transmission, optical fibre can transport a large amount of data within the same medium over several thousands of kilometres. The advent of optical amplifiers, wavelength-division multiplexing (WDM) [2] or

Optical Time Division Multiplexing (OTDM) [3] and advanced modulation formats [4] have allowed the demonstration of ever high capacity transmission experiments in the laboratory. A transmission capacity above 100 petabit per second.kilometer over 7,200 km has been reported in [5], equivalent to the simultaneous transmission of the content of 400 DVDs per second between London and Chicago.

In addition to this pure capacity increase, future optical networks will also need to provide advanced functionalities for traffic switching, allowing for example an optical signal to be routed from a source to a destination between interconnected optical networks. Such traffic routing is commonly achieved within an optical cross-connect switch, which can be considered as a multi-input/output fibre port device enabling an optical channel on any input fibre to be redirected to any output port in a static or reconfigurable way [6].

This switching equipment is considered the major bottleneck mostly because of their poor scaling properties with the number of channels and they are costly to replace whenever network upgrades are needed. Current fibre optical communications networks rely on optical/electronic/optical (OEO) conversion routing schemes, for which the optical signal is fundamentally processed in the electrical domain and which necessitate a prior stage of Optical-to-Electrical conversion before the signal is finally converted back into the optical domain thanks to an Electrical-to-Optical conversion stage.

The development and adoption of new technologies capable of allowing fully optical routing and switching capabilities at ultra-high-speeds are envisioned as the only sustainable solution [7]. One proposed approach is to develop all-optical switching and processing techniques to alleviate

the speed limitations of the OEO schemes as imposed by electronics. Among the functions that are likely to be implemented using an all-optical scheme, we find wavelength conversion [8], multiplexing/de-multiplexing of Optical Time-domain signals [9], format conversion [10], and all-optical regeneration [11, 12] to name but a few. Over the two past decades, numerous designs were proposed and their abilities to operate at high bit-rates well above 100 Gb/s demonstrated. They rely largely on two approaches either those based on active semiconductor devices such as semi-conductor optical amplifiers (SOAs), or those that exploit nonlinear optical effects in optical fibres.

One of the main drawbacks of all-optical processing technology arises from the lack of a disruptive advantage as compared to OEO schemes for the Wavelength Division Multiplexing environment, as each WDM channel usually has to be separately processed one would need as many optical devices be it OEO-based or optical-based as the number of channels. The techno-economical advantage of an all-optical approach is therefore not so significant and for that reason limits the attractiveness of the solution. It would be highly desirable if multiple WDM channels could be processed simultaneously within the same device, as this would substantially change the economics of the value proposition. Among the signal processing operations, all-optical signal regeneration would certainly benefit from the extension to support multi-channel operation within the same device since single-channel OEO regenerators could be saved - thereby offering major cost reduction.

1. Origin of signal distortion in optical networks

When an optical signal propagates within an optical network, several signal impairments can be observed arising from the optical fibre, and optical components the signal has gone through. The physical origin of this degradation arise from: i) degradation of the optical to noise ratio (OSNR) due to accumulation of noise coming from amplified spontaneous emission noise (ASE), ii) the fibre chromatic dispersion and nonlinearities and their interaction. As the signal bit-rate is increased, additional sources of degradation can arise from polarization-mode dispersion and the more significant interactions between the signal and noise. Network elements such as add-drop multiplexers, optical filters also distort the signal by introducing spectral distortions and phase ripple accumulation in the case that numerous elements are cascaded.

If the signal encoding method relies on On-Off Keying Return-to-Zero (RZ) intensity modulation, so that each bit is directly coded into the optical domain by one optical pulse (or mark) in the case of a '1' bit, or an empty slot (or space) corresponding to a '0' bit, the impairments that distort the signal are readily identified and arise from the presence of intra-channel nonlinear effects (Four-Wave Mixing (i-FWM), and Cross-Phase Modulation (i-XPM)) [13]. Signal impairments manifest themselves through the generation of new optical frequencies in initially empty bit-slots (ghost pulses), and amplitude fluctuations are experienced on mark pulses (amplitude jitter). A variable temporal delay can be furthermore impressed onto the pulses (timing-jitter) owing to i-XPM. In addition to these intra-channel nonlinearities, similar interacting mechanisms occur between adjacent channels in a WDM environment. Depending on the characteristics of the physical medium and the detailed engineering of the optical

transmission line, the relative impact of these effects can vary such that the limitations can arise from the presence of ghost pulses (inter or intra-channel FWM), and/or strong timing-jitter (i-XPM), and/or Optical Signal-to-Noise Ratio (OSNR) limitation for which ASE-accumulation predominates.

In order to preserve the signal integrity and ensure it can be transmitted over long distances and/or be routed across several optical nodes, signal restoration (or regeneration) can be used periodically along the transmission path. The operation consists of removing the accumulated noise and the elimination of any amplitude and spectral distortions. A review of the different solutions proposed to provide all-optical regeneration, capable of restoring the signal quality is proposed in Chapter II.

2. PhD research project

My PhD research project was thus to study the possibility to extend a particular single-channel optical all-regenerator approach (referred to as the Mamyshev optical regenerator) to the multi-channel environment [14]. Because of their large flexibility in term of optical properties, optical fibres were considered as a good candidate to implement such a mitigation scheme because both dispersion and nonlinearities can be easily tailored to suit the application.

This research work was carried out within the framework of the 3-year long European Specially Targeted Research Project TRIUMPH. The main objective of this project was to provide a Transparent Ring Interconnection Using a Multi-wavelength PHotonic switch, having transparent optical grooming/aggregation and multi-wavelength all-optical regeneration

capabilities [15]. The initial objectives were to propose and implement two all-optical 2R regenerator schemes and to demonstrate simultaneous processing of 3x40 Gb/s channels and 2x130 Gb/s optical channels as required within two final node demonstration trials.

The extension of the Mamyshev technique to multi-channel operation is limited by the presence of inter-channel nonlinearities resulting from XPM and FWM inter-channel interactions, which directly compete with the nonlinear effect used for the regeneration operation (Self-Phase Modulation (SPM)). Only a few research groups had investigated the possibility to extend all-optical regeneration schemes to multi-channel operation at the outset of the project. As discussed in more detail below, the difficulty of such an extension lies in the necessity to efficiently mitigate the inter-channel interaction within the optical regenerator. The design of a reliable mitigating scheme is therefore key to sustain simultaneous processing of WDM channels.

Prior to this project, only few demonstrations of simultaneous all-optical WDM regeneration had been reported. Basically, the implementation of such all-optical regenerators was based on three operating principles. The first and most obviously straightforward solution consists in linearly scaling the number of regenerators with the number of channel to be processed such as reported in [16]. Doing so, WDM channels are processed in parallel, and it is clear that no decisive advantage from a cost-effective viewpoint is brought as compared with OEO schemes. The second approach is more refined and consists in using a single regenerator to process WDM channels in a serial fashion within the regenerator [12]. The main drawback of this serialization approach is that channel synchronisation means must be implemented (e.g. multiplexing/demultiplexing operations and use of appropriate time-delay lines). Following this

approach, simultaneous all-optical Retiming operation was however demonstrated on 4x40 Gb/s WDM signals using a WDM cross-talk free regenerator formed by a single electro-optical InP Mach-Zehnder modulator [17]. Another serial processing strategy was proposed in [18, 19] by interleaving the WDM signals in the temporal domain before being processed, which imposes the use of RZ pulses with low-duty cycle to prevent any inter-channel cross-talk caused by pulse overlapping within the regenerator. In [19], all-optical Re-amplification and Reshaping regeneration of 6x10 Gb/s WDM signals using a fibre-based Sagnac interferometer was thus reported using ~7 ps pulse duration. Finally, the third solution consists of an all-optical regenerator with reduced prerequisites for channels synchronicity or signal preconditioning. Such a solution was proposed by Kuksenkov et al. [20, 21], and Vasilyev et al. [22] as an extension of the single-channel Mamyshev Re-amplification and Reshaping regenerator to a WDM environment for 10 and 40 Gb/s WDM channels. The principles of these two approaches and differences with my PhD work are thoroughly reviewed in the next Chapter.

3. Thesis outline

The general background for this work is discussed in Chapter II. First, I review the principle of all-optical regeneration in terms of operating principles and signal processing functionalities. Several implementation schemes proposed for all-optical regenerators are described with stronger emphasis on the fibre-based implementations that rely on SPM, (the class of device to which the Mamyshev regenerator belongs). This description is worthwhile to better appreciate the rationale of the solutions already proposed to address the extension to multi-channel optical regeneration. This chapter concludes with a review of such technical solutions.

Chapter III: deals with the analysis of the Mamyshev optical regenerator in a single-channel environment. Because the choice of the various parameters involved in such a regenerator is not straightforward, a new design approach is proposed and allows a drastic reduction in the design complexity. Selecting the operating parameters as a function of the key regenerator properties is made possible by the use of a normalized contour plot that relates the physical parameters of the regenerator to the optical regeneration performance. In this chapter, I detail the numerical modelling I have used to describe the pulse evolution within the regenerator, and detail how the normalized contour plot is constructed. Modelling and experimental validation of the design rules are presented and discussed. The chapter concludes with a summary of important conclusions drawn from the analysis.

In Chapter IV: two schemes are reported that I have studied to extend the single-channel optical regenerator to a multi-channel environment. The first part of the chapter details the applicability of the mitigation schemes in light of the conclusions of the design rules of the single-channel case, and considers how the inter-channel cross-talk manifests itself on the regeneration performance. Then, I will present the first multi-channel mitigation principle I studied and which is based on a counter-propagating architecture. Here the mitigation is obtained by the minimization of the walk-off time between two WDM channels when they propagate with the same fibre but in opposite directions. An original contribution of this work arises from the characterization of an additional source of cross-talk that arises due to the Rayleigh backscattering spectrum. The applicability of the scheme is experimentally reported at 10 Gb/s and 40 Gb/s. In the third part of this Chapter, I extend the processing capability to 4 channels within a Highly nonlinear polarization maintaining fibre by adding to the former counter-

propagating scheme, a second mitigation effect that exploits the large pulse walk-off which is induced by the differential group delay inside between the two polarization axes. Finally, I report the experimental results that addressed the implementation and the performance of the optical regenerator for the 2x130 Gb/s channels as proposed within the project.

Chapter V concludes this manuscript, in which the key results and further directions for this work are discussed.

Chapter II: General background

All-optical regeneration is a generic term, which in fact designates a collection of elementary signal processing functions that may be applied to an optical signal. These signal processing operations provide a means to remove different kinds of distortion that can affect an optical signal by manipulating the incoming signal directly in the optical domain. Depending on the nature of the signal degradation and its strength, different techniques have been implemented to suitably restore the signal integrity. Multiple processing operations can in many instances be achieved within the same optical device.

In the first part of this chapter, the different signal processing functionalities used for all-optical regeneration are introduced. The fundamental properties used to implement them are then described.

In the second part of this chapter, I examine the different all-optical regeneration devices operating in a single-channel environment. Because my work contribution involves highly nonlinear fibres, a particular emphasis is placed on optical fibre-based techniques. In particular,

the optical regenerator based on spectral broadening and offset filtering is considered in more detail given its relative simplicity.

Finally, I will outline the fibre-based technical solutions proposed so far in the literature to support multi-channel operation.

***

1. All-optical regeneration

1.1. General principles

In the context of optical transmission, signal distortions arise from the presence and the accumulation of amplified spontaneous noise, and the effects of the chromatic dispersion, and fibre nonlinearities. In Wavelength Division Multiplexing networks, additional sources of signal distortion are brought by the nonlinear cross-talk between co-propagating adjacent channels. Depending on the network architecture, other contributions can also be identified. Among those, we identify group delay ripples introduced by the optical components, or noise accumulation due to the limited extinction ratio of filtering elements as being particularly significant. Depending on the transmission distance and nature of the signal impairment the signal must be regenerated periodically so that noise and distortion are removed and the signal clean up allows satisfactory signal transmission detection from one end to another.

Figure II-1 schematically illustrates how these distortions translate onto an On-Off Keying RZoptical signal. Here we have considered an 80 km-long transmission span made of standard single mode fibres (SSMF). Dispersion compensation of the accumulated chromatic dispersion is achieved by using dispersion compensating fibre (DCF) at the end of the span. The input power has been intentionally set high to introduce a large amount of nonlinear signal distortion within the DCF fibre. No dispersion pre-compensation was used on the input signal. Several distortions are identifiable from the optical eye diagram .The first signal degradation obviously arises from the attenuation experienced along the propagating path due to the fibre attenuation, and which simply decreases the amplitude of the pulse. The second type of distortion manifests itself as strong amplitude fluctuations on the optical pulse, either in terms of noise on the mark pulses and the presence of excess energy in the space (also called ghost pulses), as well as modification of the pulse shape (temporal broadening, introduction of a profile asymmetry, etc.). Finally, the last source of signal distortion stems from the variation of the pulse position within its temporal slot and which is referred as to timing-jitter.

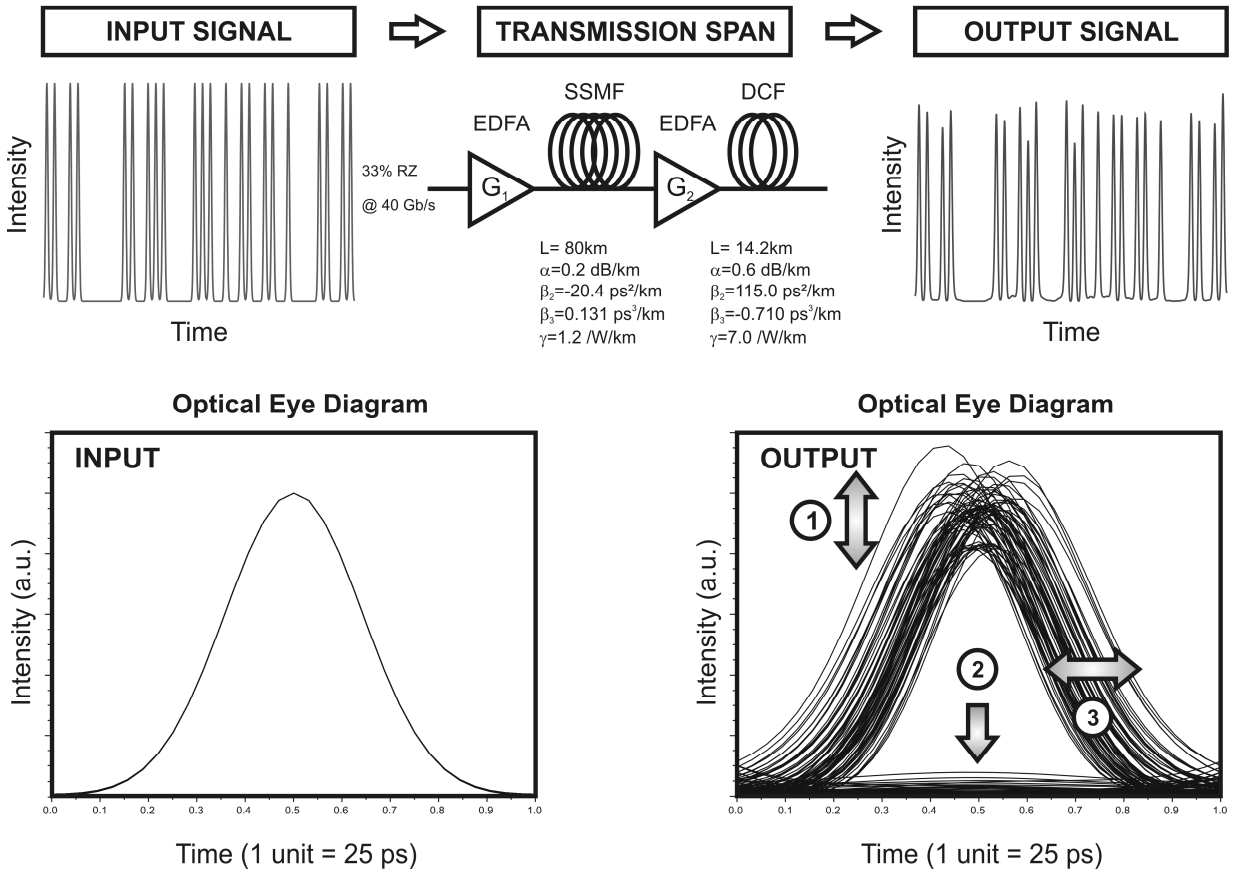

Figure II-1: Example of On-Off Keying RZ signal distortions. Top: Set-up used for the modelling and fibre parameters. The input signal was propagated within a link made of a Standard Single-Mode Fibre (SSMF) and a Dispersion Compensating Fibre (DCF). The gains of the two optical amplifiers were set so that the average powers at the SMF and DCF input are both -16 dBm. Bottom: Optical Eye diagram of the input signal and the output Signal. Signal distortions corresponding to amplitude fluctuations①, generation of ghost pulses②, and timing-jitter ③ are depicted. For the purpose of these calculations the Optical amplifiers are assumed to be both ideal and noiseless.

The purpose of the signal regeneration is therefore to remove these distortions and to restore the characteristics of the optical signal to a suitable level so that a high overall transmission quality is maintained.

In light of the different types of signal distortion, three elementary signal processing operations are defined:

- ***RE-AMPLIFICATION*:** this operation compensates for the power loss experienced by the optical signal along the transmission path.

- ***RESHAPING*:** this operation consists of restoring the intensity profile (pulse shape) and average power level of the incoming signal. This requires the function of equalizing amplitude fluctuations on the mark pulses, removing ghost pulses in spaces, restoring the nominal duration of the pulse, and finally removing accumulated noise within the signal bandwidth.

- ***RETIMING*:** This operation aims at reducing the timing-jitter by re-synchronising the pulse position within its temporal bit-slot.

Depending on the network-case scenario, it is not always beneficial to systematically provide these three operations at each optical repeater and network nodes. This is motivated by the fact that the strengths of the system impairment caused by fibre loss, the amplitude fluctuation and the timing delay are different. Nevertheless, loss and amplitude fluctuation are usually considered to be the two major sources of signal impairment in most systems as compared to timing-jitter,

which is more critical in long-haul transmission systems. The Retiming operation is therefore required less frequently.

Signal regeneration therefore designates any combination of the three aforementioned operations. The distinction between those combinations is required and conveniently achieved using a number prefix such as 1R, 2R, and 3R. As illustrated in Figure II-2, the simplest regeneration scheme consists of a Re-amplification scheme (1R), and is simply implemented using optical amplifiers based on rare-earth doped optical amplifiers or Raman amplifiers. 2R-regeneration combines both optical Re-amplification and Reshaping functionalities. By adding a retiming operation to a 2R-regenerator device one obtains a 3R-regenerator.

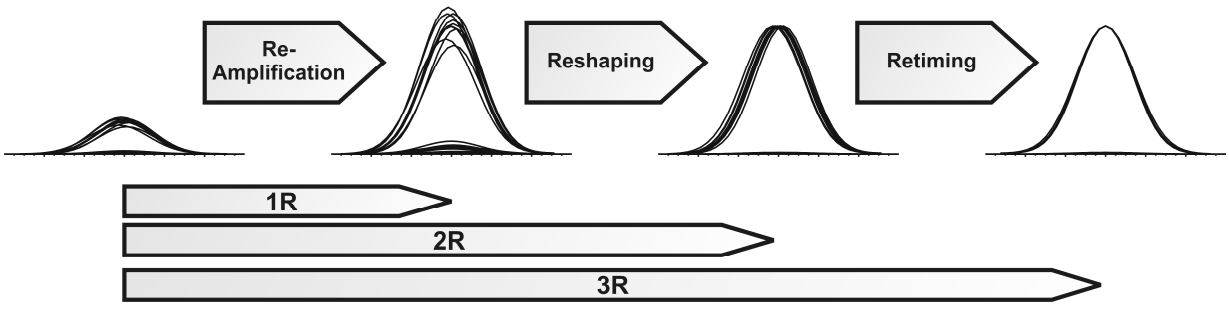

Figure II-2: Signal regenerator scheme illustrating the re-amplification, reshaping and retiming operations on an input signal. Note that the order of Reshaping and Retiming can be independently exchanged for 3R regeneration schemes.

The practical implementation of any 2R or 3R optical is advantageously appreciated by the description of four building blocks as illustrated in Figure II-3 (after [12]). It consists of:

- **Input and output adaptation interfaces:** (namely signal pre-conditioning and signal post conditioning). These two blocks are devoted to the (respectively post-) conditioning of the input and output signals in order to comply with the operating needs of the subsequent blocks. Conditioning operations can therefore be of different complexity, and address issues such as input/output power adjustment, pulse shaping, out-of-band noise filtering, format conversion, control of the signal polarisation states, signal de-multiplexing/multiplexing (be it in the time and/or frequency domain).

- **A nonlinear gate:** this is undeniably the central element of the regenerator. This block relies on the exploitation of a nonlinear transmission characteristic between the input and the output power of the regenerator (see the next section).

- **A Switching decision unit:** This element is used to control the state of the gate (open/closed) and is only relevant for retiming operations. The block requires an additional clock signal that is used to switch the nonlinear gate. This signal can either be retrieved from the signal or locally generated. In the case of 2R-regenerators the control of the gate is generally provided by the incoming signal alone or one of its replicas. On the other hand, 3R optical generation relies on configurations in which clock pulses are generated either using a local pulsed light source running at a clock rate retrieved from the incoming signal clock. The retiming operation is then achieved by switching the clock pulses by the incoming data signal using a nonlinear gate. Because the clock signal operates at a different wavelength, wavelength conversion usually occurs. This wavelength conversion can be advantageously exploited in optical switched networks to

better accommodate optical paths, and avoid wavelength blocking [8], or can be removed in a further wavelength conversion process.

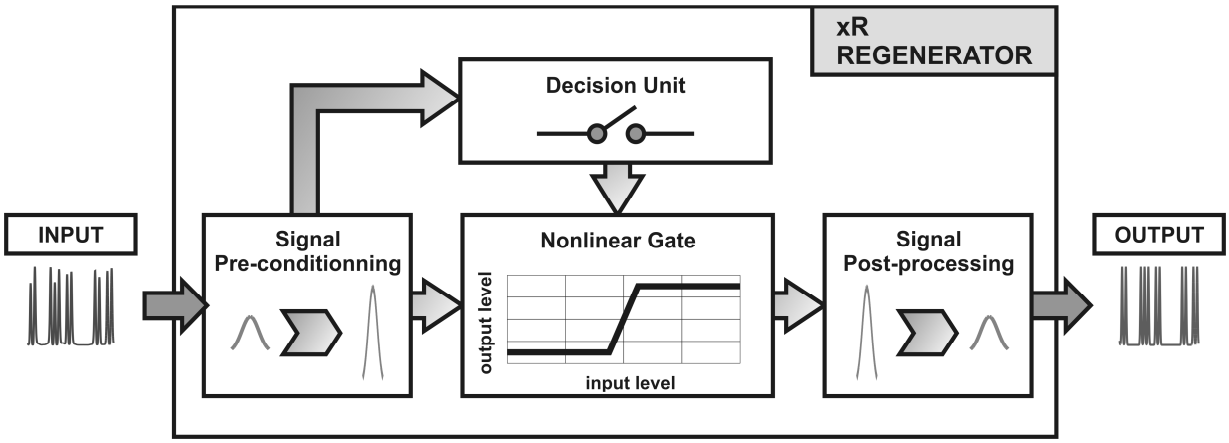

Figure II-3: Block diagram of an optical 3R regenerator showing the different building blocks (after [12]).

The nonlinear gate allows discrimination of low and high input levels owing to a power-dependent transfer function, which relates the output signal power to the input signal power. As illustrated in Figure II-4(a), the shape of the power transfer function (TF) is ideally a step-like curve exhibiting two output states to allow both amplitude equalisation on marks and complete rejection of the noise in space slots. Obtaining a steep transition is challenging from a physical point of view within a single non-linear gate. Power transfer functions with smoother profiles are usually obtained experimentally, resulting in an "S"-like shape as illustrated in Figure II-4(b). Sharper transitions are however obtained when cascading several regenerators so that a step-like function is obtained as illustrated in Figure II-4(b). Cascading optical regeneration stages can also

be employed to preserve wavelength transparency for optical regeneration schemes that change the carrier frequency of the output signal in each stage of regeneration.

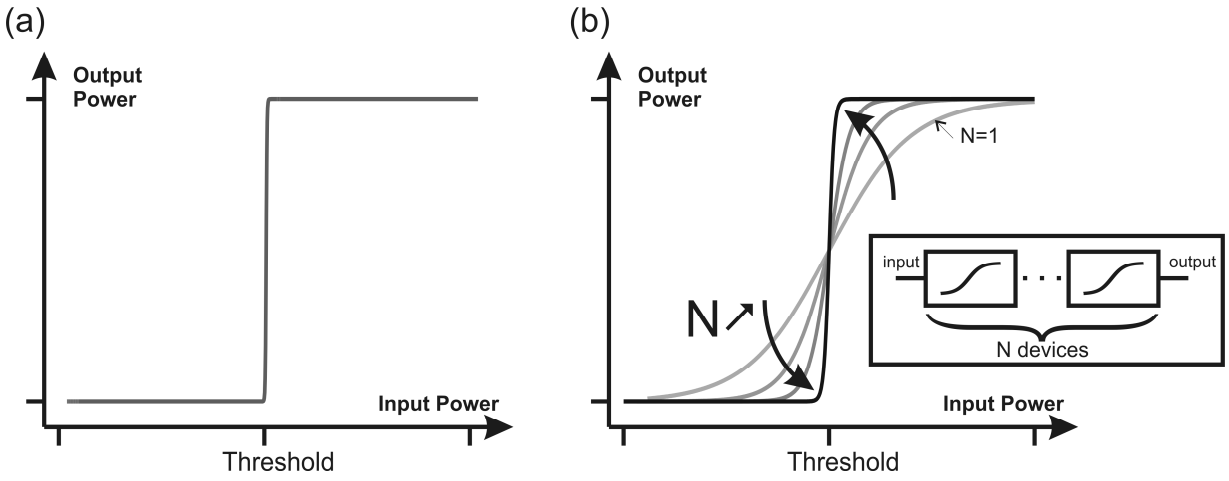

Figure II-4: (a) Ideal power transfer function of the nonlinear gate used for reshaping operation. (b) Power transfer function derived from multiple cascading of an elementary power transfer function.

1.2. Optical nonlinear gates

In the context of all-optical regeneration, the nonlinear gate is the most distinctive and critical element of the optical regenerator. To date, a variety of schemes have been proposed to provide step-like power transfer functions and each exploits an intensity-dependent nonlinear process in an optical material. Three types of nonlinear optical device are commonly based on optical semiconductors, Periodically Poled Lithium Niobate (PPLN) waveguides that exploit cascaded $\chi^{(2)}$ frequency mixing, and glass material exhibiting optical Kerr nonlinearities such as optical fibres. Corresponding nonlinear gates and implementations are reviewed below.

1.2.1. Optical Semiconductors-based nonlinear gates

Semiconductor Optical Amplifiers (SOA) have been the topic of intense interest over the past decades, mostly because they represent a cheap device with a small footprint suitable for large-scale integration. Three nonlinear effects can be exploited for semiconductors based nonlinear gates.

Amplitude fluctuation on the mark pulses can be removed by using the nonlinear saturation of the SOA gain characteristic. Although, this is a simple method, limitations arise from the impossibility to reject noise in space slots and dictates that the scheme be used in combination with a second stage that allows noise removal such as the use of a saturable absorbers [23].

Cross-gain modulation (XGM) and subsequent XPM within an SOA have also been reported. The operating principles stem from phase modification of the optical pulse that arises from the local change of the refractive index as the carrier density within the SOA is modified due to the excitation by the signal intensity. This effect makes use of the change of the SOA gain induced by the intensity pattern of an incoming pump signal (the incoming signal to be regenerated) so that the gain variations, and thus the intensity pattern, is directly transferred onto a probe signal. Because the output signal is inverted as compared to the input signal, an additional operation is required to restore the polarity. This can be achieved through several arrangement based either on advanced spectral filtering or interferometric techniques [24-27].

The limitations of the regeneration based on XGM in semi-conductor optical amplifiers arise from the consequence of the slow relaxation time given the limited recovery time of the carriers (from 50 ps up to the ns regime). This intrinsically limits their use at high bit-rates due to

pattering effects and restricts them to single-channel operation only. This is not the case with XPM based schemes [28]. Configurations have been proposed to overcome this issue either based on multiple SOA architectures or more recently quantum-dot-based SOAs (QD-SOA) which have a very short relaxation time (from 500 fs down to 100 fs) [29, 30], as such are suitable for high-bitrate applications.

Finally, exploitation of FWM in nonlinear SOAs was proposed [31]. The principle is based on the generation of new higher-order frequency components due to the interaction of two optical signals. Although the scheme is fully able to address high bit-rate signal processing, there are some practical limits due to the low efficiency of the scheme and its polarisation dependency. Finally there are constraints due to the spectral allocation of the pump and probe signals.

Using cross-absorption modulation in an electro-absorption modulator has been proposed for 3R optical regeneration [26, 27, 32, 33]. The principle relies on the intensity dependent absorption of a probe signal (consisting of the clock signal) induced by a pump signal (data to regenerate). Practical applicability of the scheme is however relatively limited since the absorption is both polarization and wavelength-dependent and requires relatively high input powers. Moreover, it cannot address high bit-rate signal due to the limited carrier recovery time.

Other nonlinear gates have been also proposed but interest in them is limited because of their restricted bandwidth and relative resemblance to optoelectronic emitter/receiver devices. Among these, we find electro absorption modulators [32-34], and self-pulsating gain-switched distributed feedback lasers diodes [35, 36]. Recently, the applicability of micro-ring resonators was reported from a numerical point of view in [37]. Finally, a new class of nonlinear optical waveguides

referred to as photonic nanowires have been recently proposed as promising nonlinear gates [38]. Because of their sub-µm transverse dimensions, such index-guiding waveguides provide a maximal confinement of light so that large optical nonlinearity can be obtained. Such devices are thus well suited for many applications among which nonlinear processing of optical signals (e.g. all-optical regeneration [39], wavelength multi-casting [40]). Such waveguides can be fabricated from glasses or semiconductors (e.g. silicon waveguide).

1.2.2. Periodically poled Lithium Niobate waveguides

These devices exploit the second-order nonlinear interactions in Quasi-Phase Matched (QPM) periodically poled Lithium Niobate. The principle of the quasi-phase matching is to modify the nonlinearity of the medium along the device by adding a periodic phase shift correction along the medium to ensure a continual build-up of the harmonic signal [41]. Such devices are manufactured using a multi-step lithographic and electric field poling process to induce a permanent change in the nonlinear properties.

Signal switching is achieved by a cascaded frequency generation scheme which exploits the QPM effect: specifically difference and sum frequency generation [42]. In the context of optical signal processing, Periodically poled Lithium Niobate waveguides are generally used for wavelength conversion as part of an 3R optical regenerator, [7], but could also be used as a small foot-print device for optical OTDM/WDM multiplexing and de-multiplexing operations [43].

1.2.3. Optical Kerr effect-based nonlinear gates

The second nonlinear gate category exploits the optical Kerr effect within optical fibres or optical planar waveguides [44]. The Kerr effect arises from the nonlinear response of the glass medium to a strong optical field of intensity $|E|^2$ that locally changes the refractive index of the medium $n(\omega)$, where ω stands for the frequency. In Equation *(II-1)*, n_0 stands for the linear refractive index; and n_2 is the nonlinear refractive index which is related to the third-order susceptibility $\chi^{(3)}$ [45], which is dependent on the physical properties of the optical glass:

$$n(\omega) = n_0(\omega) + n_2 |E|^2 \qquad \textit{(II-1)}$$

For the optical regeneration of On-Off keying RZ pulses, the direct consequence of the Optical Kerr effect is the introduction of an intensity-dependent phase modulation on the optical signal either induced by the signal itself (Self-Phase Modulation (SPM)) [46], or a second optical signal (Cross-Phase Modulation (XPM)).

SPM refers to the self-induced phase shift ϕ_{NL}^{SPM} imprinted on an optical field E_1 at frequency ω_1 during its propagation in an optical fibre. This quantity depends on the fibre length L and optical intensity $|E_1|^2$ and is obtained by:

$$\phi_{NL}^{SPM} = \frac{2\pi\omega_1}{c} L n_2 |E_1|^2 \qquad \textit{(II-2)}$$

Similarly, the XPM refers to the nonlinear phase shift induced on optical field E_1 at frequency ω_1 induced by another field E_2 propagating at a different frequency ω_2. Due to the tensorial nature of the third-order susceptibility $\chi^{(3)}$, the nonlinear phase shift experienced for the field at ω_1 is dependent on the states of polarization of the two co-propagating fields. When the two optical fields are linearly co-polarized, the resulting nonlinear phase shift ϕ_{NL} experienced at ω_1 is maximized and expressed by:

$$\phi_{NL} = \frac{2\pi}{\lambda} L n_2 \left(|E_1|^2 + 2|E_2|^2 \right) \qquad (II\text{-}3)$$

The first term in Equation *(II-3)* is due to SPM (see Equation *(II-2)*), whereas the second is attributed to XPM. For optical fields of equal amplitude ($|E_1|=|E_2|$), the contribution of the XPM is therefore twice that of SPM for linearly polarized optical fields.

As the optical Kerr effect benefits from a quasi-instantaneous response time – which is considered to be in the femtosecond domain (i.e. few fs), optical processing of high bit-rate signal (>100 Gb/s) can be more easily addressed. Single channel optical regenerators using optical fibre can be designed to exploit nonlinear effects offered by SPM, (XPM), and FWM (FWM) [45].

Three major schemes for fibre-based optical regenerator are distinguished. We describe them hereafter and highlight their pros and cons.

1.2.3.1. Sagnac-interferometer-based optical regenerator

The first scheme is based on a Sagnac interferometer of which the fibrerized version is called the nonlinear-optical loop mirror (NOLM) [47]. As depicted in Figure II-5(a), the principle relies on splitting the signal to be regenerated into each arm of the interferometer incorporating a highly nonlinear fibre (HNLF). The two arms of the interferometer are formed by the counter-propagation of two replicas of the input signal within the same optical fibre. Switching is possible thanks to a power splitter of unequal power coupling ratio α. The input peak power of the '1' pulses propagating in one path of the interferometer (e.g. path A) is set so that the pulse propagation corresponds to the nonlinear regime, whereas propagation regime for path B essentially remains linear. The asymmetric nature induced by the different power coupling ratio between the two paths A and B determines the amount of nonlinear phase difference generated by SPM between paths A and B.

Depending on the amount of phase shift added, the counter-propagating signal in the two arms interfere either destructively or constructively so that resulting signal is either reflected back to the input port or switched to the output port. Figure II-5(b) depicts the ideal power transfer function (i.e. sinusoidal shape) corresponding to the case where only the presence of SPM is considered [47].

As the scheme relies on an interferometric effect, the technique is known to be relatively sensitive to environmental perturbations and is polarization dependent, so that polarisation control inevitably needs to be considered. Addressing high bit-rates is as straightforward, although it is necessary to consider the effect of the XPM-induced nonlinear phase shift

contribution added by the counter-propagating signal on the power transfer function [48]. An experimental demonstration of such a 2R regenerator is reported in [49] and enabled a Forward Error Correction (FEC) compatible transmission over 10,000 km of a 42.66Gb/s Dispersion-Managed RZ WDM signal.

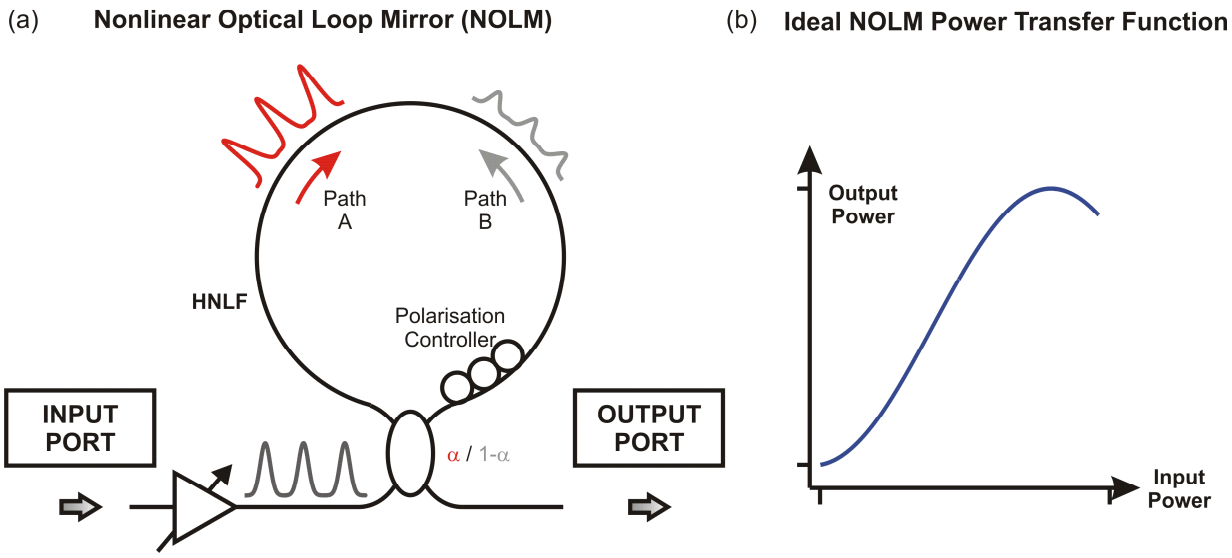

Figure II-5: (a) Nonlinear optical loop mirror scheme in a 2R optical regeneration. (b) Corresponding ideal power transfer function.

1.2.3.2. FWM-based optical regenerator

The second scheme relies on the generation of frequency components due to FWM between an incoming signal and a pump signal [50]. Most common implementations exploit the degenerate FWM effect and for which the pump signal is placed at one of the zero dispersion wavelengths of a dispersion-shifted highly nonlinear fibre.

A FWM-based 2R optical regenerator is depicted in Figure II-6(a). The signal to be regenerated is fed into a Dispersion-shifted HNLF together with an intense continuous-wave (CW) pump. Through multiple FWM processes new frequency sidebands are generated - equally spaced by the initial frequency detuning ΔF between the input and pump beams – (see on the output spectrum in Figure II-6(b)). A narrow-band output filter is used to select the corresponding signal sidebands as the output signal. The choice of the sideband to be filtered is essential in order to provide suitable optical regeneration (i.e. a power transfer function having a step-like transition). As explained in references [51-53], the idler wave cannot be employed to simultaneously provide both noise rejection on the marks and power equalization on the spaces under the depleted pump regime. On the contrary, the first cascaded sideband reported in Figure II-6(b) is more suitable since i) at low input signal power the output power scales quadratically with the signal input power, ii) at high input signal powers and under the depleted pump regime, a plateau can be reached, resulting in a step-like nonlinear power transfer function.

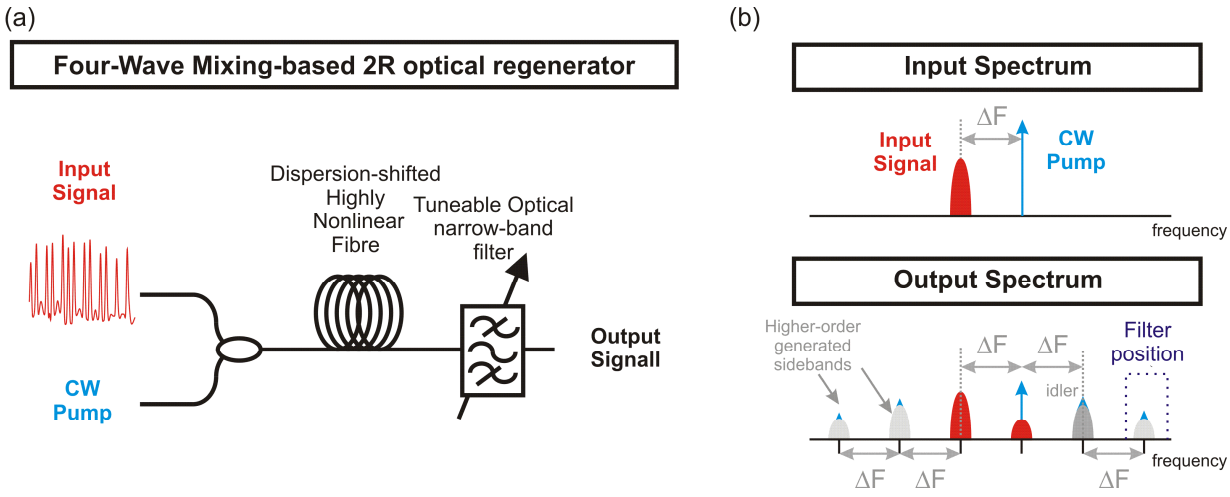

Figure II-6: (a) FWM-based optical regenerator. (b) Spectral content at the input and output of the dispersion-shifted HNLF, and position of the output filter. ΔF is the frequency detuning between the signal and the pump frequencies.

In practice the generation of higher-order frequency products requires high input power so that spectral broadening of the pump is mandatory to suppress stimulated Brillouin scattering (SBS) [45, 54, 55]. As spectral broadening is also imprinted on the regenerated signal, additional distortion and signal-to-noise degradation are generally observed. Using a non-degenerate dual-pump configuration allows minimization of the signal broadening while suppressing the SBS effect [56].

Because FWM is a parametric process, phase-matching conditions need to be preserved to guarantee high power conversion efficiency. The process is therefore more dependent on the polarization state of the incoming signals along the fibre, and requires with fibres with excellent longitudinally uniformities in order to preserve the position of the zero-dispersion wavelength [57, 58]. Numerous experiments are reported [51-53, 55, 56, 59-66]. Although experimental works were only reported at 10 Gb/s both for Non-Return-to-Zero and RZ signal, the applicability to higher bit-rates is not limited by the response time. However a strong alteration of the pulse shape due to the chromatic dispersion in association with nonlinear effects can take place as presented in [67].

1.2.3.3. XPM-based optical regenerators

The third category encompasses the combination of SPM (for 2R regeneration) or XPM (for 3R regeneration) and a non-interferometric switching method. The regenerator architecture was first

proposed by Suzuki *et al.* in [68]. As depicted in Figure II-7(a), the device consists of an optical clock signal centred at a frequency F_{clock}, a dispersion-shifted highly nonlinear fibre and a narrow-band filter centred at F_{clock}. The clock pulse signal is generated from a clock-recovery circuit that provide pulses of shorter duration than the pulse to regenerate at a same repetition rate. The signal to regenerate and the clock pulse are fed into the HNLF. An optical delay line is used to adjust the timing of the clock pulse so that it is located on the leading edge (or trailing edge) of the signal pulse as shown in Figure II-7(b). In the presence of an incoming 'one' pulse, the centre frequency of the clock pulse spectrum is shifted due to XPM within the HNLF. In the figure, the centre frequency is shifted towards shorter frequencies at the fibre output. As the amount of the wavelength shift is directly proportional to the gradient of the signal pulse intensity profile, the spectral shift is dependent on the input peak power of the incoming pulse. Using a narrow band optical filter centred at F_{clock} allows conversion of this spectral shift into power fluctuation by discriminating spaces and marks pulses. In this configuration, it is clear that the output signal is inverted as compared to the input signal.

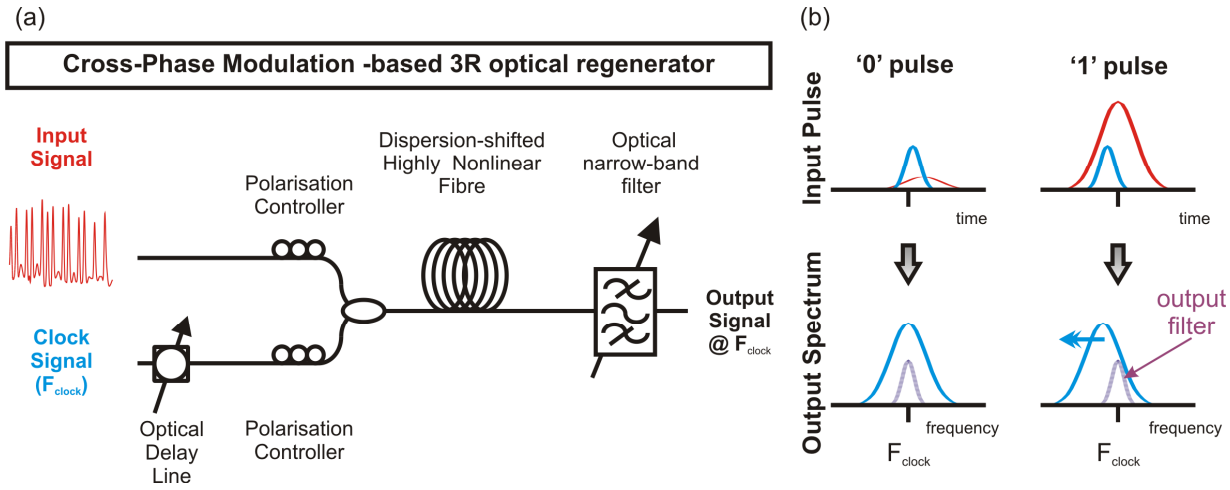

Figure II-7: (a) XPM-based optical regenerator. (b) Principle of operation in case of '0' and '1' pulses.

In practice, XPM-based schemes require to control of the state of polarization of the pump and probe signals to maximize the XPM effect and spectral shift, even if polarization independent XPM schemes have recently been demonstrated [69]. Because of their reduced environmental instabilities, these types of optical regenerators are among the most studied (see next section). Finally, other methods have also been proposed but which have more stringent requirements for their set-up and fibre characteristics. This includes: exploitation of the nonlinear polarization rotation effects used in a Kerr shutter configuration. [70, 71], or parametric amplifiers [72].

Finally, regenerators based on Stimulated Raman Scattering were also demonstrated and reported in [73].

2. Single-channel SPM-based regenerator

Optical regenerators that exploit SPM are addressed in this section. SPM is the simplest nonlinear effect to stimulate and utilize because the effect is self-induced, and the added nonlinear phase shift is proportional to instantaneous the pulse intensity profile [45, 46].

As the phase profile is differently affected by the chromatic dispersion whether it is normal or anomalous, we distinguish between two types of regenerator: the first one is only applicable in the anomalous dispersion regime taking advantage from the soliton effect, and the second

solution preferably operates in the normal dispersion regime and is based on spectral broadening of the pulse.

2.1. Soliton-based regenerator

Here, the principle relies on the exploitation of the fundamental soliton effect. The fundamental soliton pulse refers to a particular pulse intensity profile - which corresponds to a $sech^2$ for which the nonlinear phase induced by the SPM and the phase change induced by group-velocity dispersion cancel each other. The direct consequence is that both the intensity profile and the spectrum of the pulse remain unchanged whilst the pulse is propagating within a loss-less fibre. The condition is obtained for a particular combination of the temporal width, and the pulse energy for given fibre properties. One condition is therefore to operate in the anomalous dispersion regime.

The soliton effect refers to the mechanism that forces any pulse to evolve to a fundamental soliton – potentially with some shedding of dispersive radiation in the process due to high order dispersion [74]. The convergence consists of a progressive self-reshaping of the pulse thanks to a redistribution of the frequency content, while excess frequency content, that does not belong to the soliton pulse, is radiated away. The conditions for soliton convergence are provided by selecting the input power conditions and adjusting the fibre length with respect to the optical fibre properties.

By implementing a soliton conversion stage and applying a narrow-band optical filter centred at the optical carrier frequency at the end of the stage, it was proposed to filter excess noise to the mark pulses. This method is referred to the spectrally filtered soliton method and was reported at 20 Gb/s [75], and 160 Gb/s [76]. Although this method exhibits a reshaping capability and a power equalization of the marks, the presence of in-band noise remains, so that an additional stage must be provided to remove this noise - such as the use of saturable absorbers (SA) [12, 17].

Retiming operation was also demonstrated by applying a Phase and/or intensity modulation to the signal. As described in [17], jitter reduction arises as a consequence of the soliton effect (for intensity modulation), whereas phase-modulation imposes a time-position-dependent frequency shift that may be compensated for by the group-velocity-dispersion of the fibre. The scheme is referred to as synchronous modulation and an optical 3R-regenerator was demonstrated in [17] over 10,000 km for a 4x40 Gb/s system.

2.2. SPM-based and offset filtering

In this part, we describe the operating principle of the 2R optical generator based on SPM-induced spectral broadening and subsequent offset filtering and which formed the focus of my PhD project.

The regenerator was introduced in 1998 by P. Mamyshev [14], and is also referred as to the Mamyshev optical regenerator, as a large amount of attention has been paid to it. As illustrated in Figure II-8, the regeneration principle is straightforward and relies on spectral broadening on the incoming pulse due to SPM. A simplified Mamyshev optical regenerator is reported in Figure II-8, consisting of a Highly-nonlinear fibre, which is used to imprint the SPM to the incoming pulses, followed by a tuneable optical narrow-band optical filter. The operating principle is also schematically described in Figure II-8, by considering the spectral evolutions of a high-peak power and a low-peak power input pulses at different locations along the regenerator.

As low-peak-power pulses (nominal ‘zeros’) experience less spectral broadening than high-peak-power pulses (nominal ‘one’), discrimination between marks and spaces is achieved by placing an output narrow-band optical filter spectrally offset from the input signal carrier. The detuned optical filter collects only a small fraction of the energy of low-peak-power pulses, and a larger energy fraction of the high-peak-power pulses. Moreover, as high-peak-power pulses experience more spectral broadening, the amount of power that is passed within the filter bandwidth saturates at high peak powers. As the spectral evolution of the pulse along the fibre length leads to the presence of input peak power-dependent spectral ripples in the filter bandwidth (as illustrated in Figure II-8), a variety of shapes can be achieved (as seen in the text chapter). A

direct consequence is that the shape of the power transfer function is dependent on numerous parameters (i.e. details of the input pulses and fibre characteristics, frequency detuning of the filter, etc). The shape of the offset filter acts as a pulse-reshaping element by slicing into the broadened spectrum pulse and the filter bandwidth sets the output temporal width. Nonlinear propagation within the normal dispersion regime is preferable in that it does not allow the development of modulation instability due to nonlinear interaction between the signal and ASE [17]. Furthermore, the SPM spectra generated under conditions of normal dispersion are generally flatter, thus leading to smoother pulse shapes at the output of the regenerator [14].

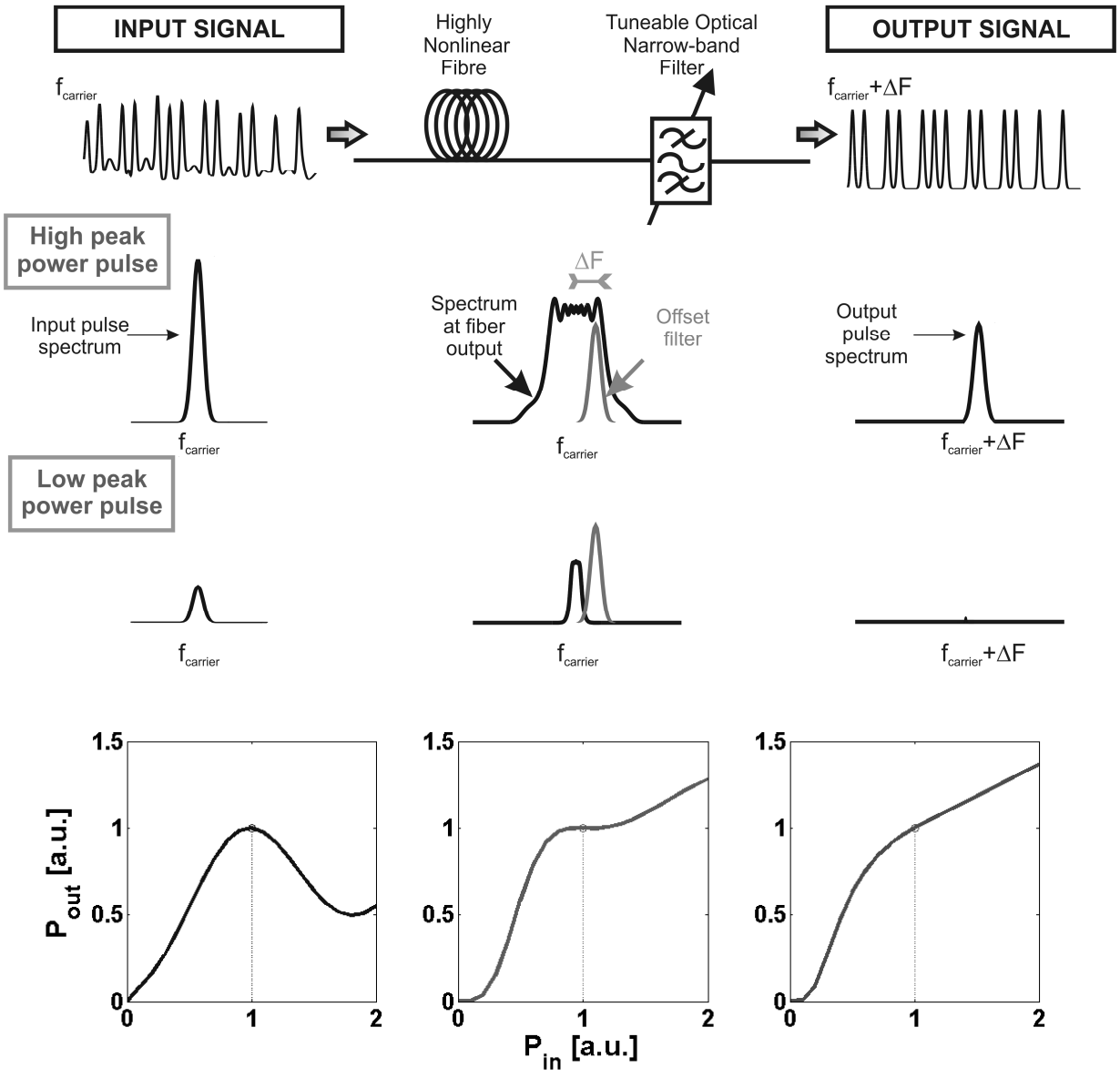

Figure II-8: Top: operating principle of the SPM-based spectral broadening and subsequent offset filtering optical 2R regenerator. Bottom: Examples of power transfer functions obtained for different output filter detuning and input powers.

The corresponding set-up is shown in Figure II-9. The degraded optical pulse streams are first fed into an optical amplifier, which is used to boost the power to a suitable level at the input of the highly nonlinear fibre (HNLF). An ASE noise rejection filter can be employed to remove out-of-band excess noise. The amplified pulses are then propagated in the HNLF. A narrow-band filter is used to carve into the broadened spectrum at the output of the HNLF providing pulse reshaping.

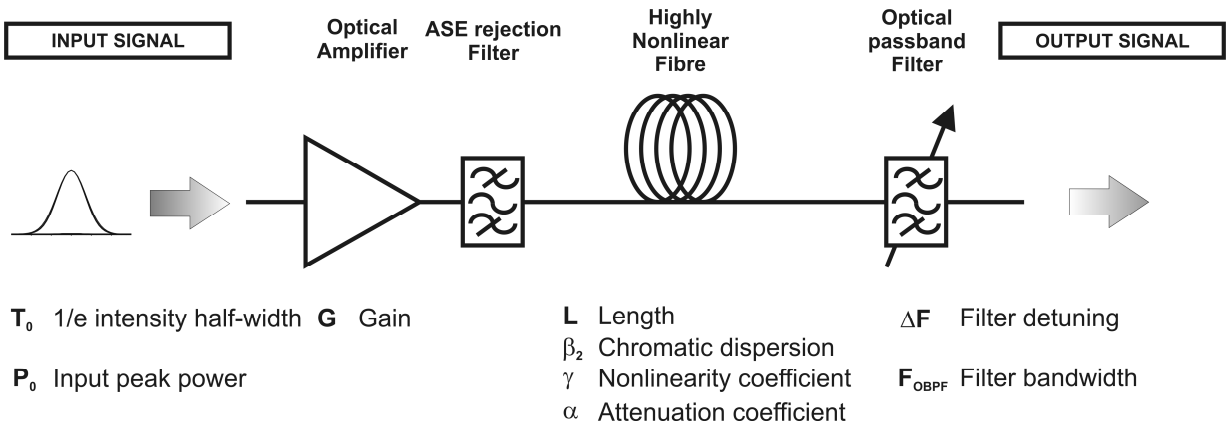

Figure II-9: Typical implementation of a 2R optical regenerator based on SPM-based spectral broadening and subsequent offset filtering, with corresponding parameters.

The applicability of the scheme to operate at 10 Gb/s [14], 40 Gb/s [77, 78], and 160 Gb/s [70] enabling for the last experiment error-free transmission up to 1 million kilometres (in association with a retiming unit has been demonstrated). Numerous experimental studies have been carried

out regarding pulse width restoration [79], polarisation-mode dispersion mitigation [80], tolerance to residual dispersion [81], BER improvement [82-84], etc.

In addition to the simple set-up, the scheme is appealing since the requirement of the fibre characteristics are extremely reduced as compared to other fibre-based optical regenerators, and the scheme offers simultaneous noise rejection and amplitude power equalization.

One of the most important drawbacks of the technique arises from an additional timing-delay that is imprinted onto the pulses of the output signal [14, 67, 85, 86]. This variable amount of time delay can be caused by any deformations in the intensity and phase profiles present on the incoming pulse (e.g. peak-intensity and/or pulse-width fluctuations). The origin of this timing-jitter arises from the different amount of pulse frequency chirp induced by nonlinear propagation along the HNLF for input pulses of differing power, and more specifically from the amplitude-phase conversion caused by the interaction of the SPM effect and group velocity dispersion. As illustrated in Figure II-10, the different arrival time is the result of the power-dependent chirp rate (i.e. chirp slope) value. Furthermore, depending on the relative position of the offset filter, this power-dependent delay is mapped in an asymmetrical fashion onto the output pulses. Figure II-10 shows that if the filter is offset by ΔF ($-\Delta F$) from the carrier frequency of the input signal then pulses with higher (lower) peak power would arrive at the end of the regenerator faster (slower) than a pulse with the mean peak power.

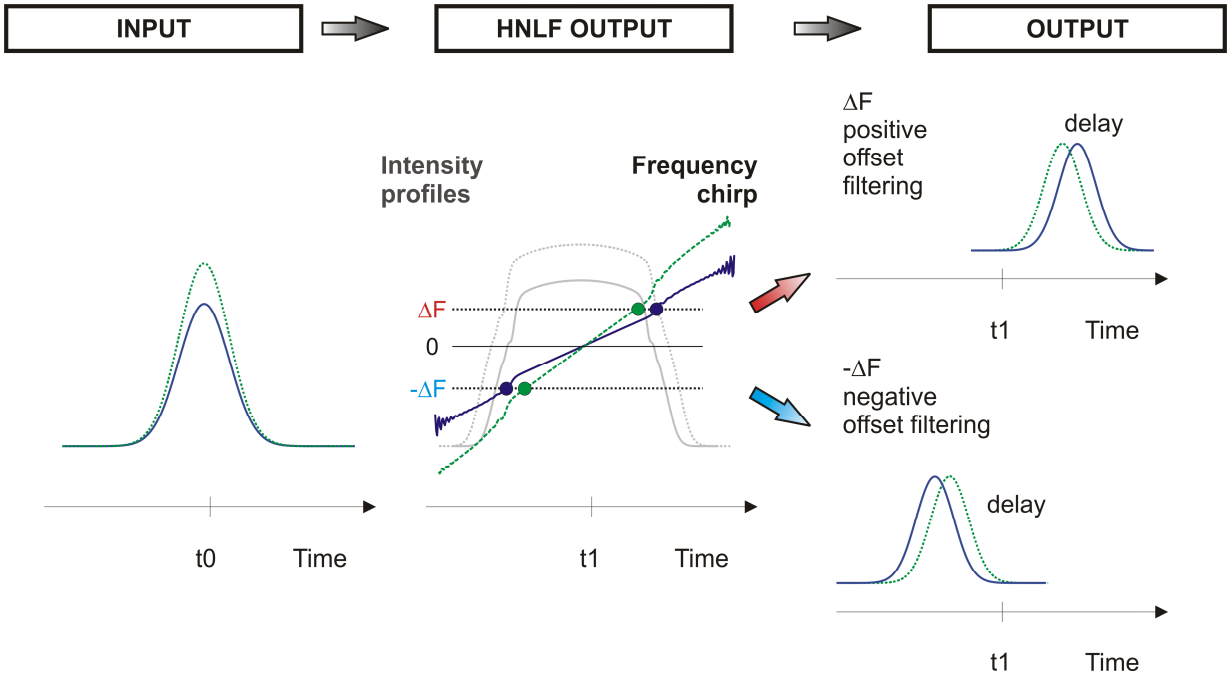

Figure II-10: Temporal delay mapping as a function of the input power and the position of the offset filter of the Mamyshev 2R optical regenerator. Temporal pulse intensity and frequency chirp profiles corresponding to two incoming pulses of same temporal duration but different input peak powers are represented at different locations along the optical regenerator.

Different chirp fluctuations across the temporal profile of the output pulse can therefore be obtained. As the detuned filter selects only the frequency content of the pulse around a specific instantaneous frequency, corresponding spectral content may be extracted at instant that may vary from pulse to pulse due to chirp fluctuation, thus resulting in timing-jitter. This power-dependent delay is mapped in an asymmetrical fashion onto the output pulses and basically depends on the

relative position of the offset filter - e.g. if the filter is offset by ΔF (-ΔF) from the original central frequency then pulses with higher (lower) peak power will arrive at the end of the regenerator faster (slower) than a pulse with the mean peak power. Unless a retiming stage is employed to compensate for this timing-jitter such as in Ref. [87], the maximum achievable error-free transmission would be reduced because of the accumulation of timing-jitter along the transmission path. As the Mamyshev regenerator is considered alone, it seems possible however to reduce the amount of the timing-jitter by either changing the operating parameters of the regenerator [88] or by cascading a second Mamyshev regenerator stage [89].

3. Extension to multi-channel processing

Simultaneous optical processing of multiple optical WDM channels within the same optical element is undoubtedly a desirable functionality for all-optical telecommunications networks, potentially offering major technical and economical benefits as compared to any single channel-based approach. Since optical networks are expected to become more transparent moving forward a strong interest in multi-channel optical regeneration has developed during recent years.

The extension to multi-channel operation is however limited by the presence of inter-channel nonlinearities, as they directly compete with the nonlinear effect used within the nonlinear gate. In light of the description of the various regeneration principles used for the single-channel case, suitable multi-channel mitigation is not straightforward to address. For instance, single channel optical regenerators using optical fibre can be designed to exploit SPM (SPM), XPM (XPM), FWM (FWM), and Stimulated Raman Scattering but the extension to multi-channel operation is limited by the presence of inter-channel nonlinearities resulting from XPM and FWM inter-

channel interactions, which directly compete with the nonlinear effect used for regeneration. From this, one expects an additional source of noise and power fluctuations which degrade the reshaping performance for individual channels as discussed in the next section and Chapter IV in more detail.

In a multi-channel regenerator, a robust mitigation must be provided to limit the cross-talk levels arising from the inter-channel interactions while preserving the regeneration performances for each of the WDM channels as achieved for the single-channel case. Besides the pure reshaping performance, the robustness of the regenerator to the properties of the incoming WDM signals is also a key issue worth investigating. Two additional conditions can be identified. The regenerator might be able to ultimately cope with: i) no assumption on the temporal synchronism across the WDM channels, so that no precise timing between incoming signals can be *a priori* set, ii) a lack of knowledge of the polarization states of the incoming signals.

Only a few demonstrations of multi-channel 2R all-optical regeneration had been reported. This section summarises the existing solutions and reported performances.

3.1. Semiconductor-based schemes

For semi-conductor-based nonlinear gates, only Quantum Dot SOAs are reported to be of potential relevance for multi-channel processing though this is only supported by numerical predictions [90]. The reduction of the cross-talk between optical channels arises from the spatial isolation of dots, which prevents transfer of carriers amongst different spectral regions, provided these are outside of the inhomogeneous broadening region.

3.2. Fibre-based schemes

Fibre-based regenerators are obviously more attractive given the great design provide flexibility for tailoring the dispersive and the nonlinear properties of the fibre. Modification of the single-channel regenerator set-up is facilitated enabling more efficient mitigation of the inter-channel nonlinearities due to FWM and XPM. SPM-based regenerators are the most suitable solution to support multi-channel operation based either on soliton effect or spectral broadening followed by optical filtering. An interferometric scheme was also proposed using a dispersion-unbalanced NOLM Sagnac interferometer but which required precise timing between the incoming signals to be established [3] at its input.

3.2.1. Fibre-based 2R-regenerator using soliton effect

A direct extension of the spectrally filtered optical soliton method has been proposed in [91] for a WDM configuration. An experimental demonstration of 4x40 Gb/s-channel regeneration was reported using a chromatic dispersion managed scheme with polarization multiplexing to reduce XPM [91]. The dispersion management was realised by a collection of fibre assemblies comprising fibres of opposite signs of chromatic dispersion [92, 93]. Although power equalization can be achieved, the scheme still suffers from an inability to remove in-band noise. One possibility for alleviating this problem using a distributed offset filtering approach has been proposed [94]; though the practical viability of this has still to be demonstrated experimentally because of the extremely small values of offset detuning required.

3.2.2. Fibre-based 2R-regenerator using spectral broadening and offset filtering

In [21], the use of a specially tailored dispersion decreasing fibre to process 4x40 Gb/s Carrier Suppressed RZ channels was reported. Due to the high power efficiency of the soliton pulse compression effect, strong spectral broadening without significant inter-channel nonlinear effects was possible at low input powers (45mW/channel), whereas no deleterious effects due to pulse interaction was reported. Nevertheless, only modest improvements in the Q^2 factor (0.7 dB) were reported due to an excessive amplified spontaneous emission noise contribution.

A less demanding solution in terms of fibre requirements was theoretically proposed by Vasilyev *et al.* [22] based on a direct adaptation of the set-up proposed by P. Mamyshev. The operating principle relies upon introducing a rapid walk-off between adjacent channels through dispersion chromatic management along the device. Significant SPM-induced spectral-broadening can still be preserved when maintaining a low path average chromatic dispersion over the complete regenerator length. Doing so, the pulse temporally broadens and shrinks at periodic stages along the regenerator.

The corresponding set-up is reported in Figure II-11(a). The original design comprised a series of individuals “cells” made of one highly dispersive nonlinear fibre (e.g. dispersion compensating fibre (DCF)) followed by a chromatic dispersion compensator (Figure II-11(b)). Vasilyev *et al.* suggested to use a Periodic Dispersion Group-Delay Device (PGDD) acting as a lumped and channelized dispersion compensator [95] (Figure II-11(c)). This configuration allows the channels to continuously walk-through each other so that the group delay difference between adjacent channels monotonously increases with regenerator length ((Figure II-11(e)).

Nevertheless the consideration of both the phase and amplitude response of the PDGG noticeably complicates the design of the regenerators and the optimisation of the fibre parameters [96] and in the end would complicate any experimental implementation.

To overcome this issue, it was proposed to replace these PGDDs by standard single mode fibre (SSMF) so that the device can be fully-fibrerized [22, 97]. The latter solution differs fundamentally from the former since the group delay variation between two adjacent signals periodically returns to zero (Figure II-11(e)). Because of the monotonous variation of the group delay within the SSMF (Figure II-11(d)), each pulse interacts with the same set of neighbouring pulses, whereas for the PGDD approach, each pulse briefly interacts with a large number of adjacent pulses. The mitigation performance is slightly degraded as a slight dependence on the relative time delay between incoming channels is reported [98].

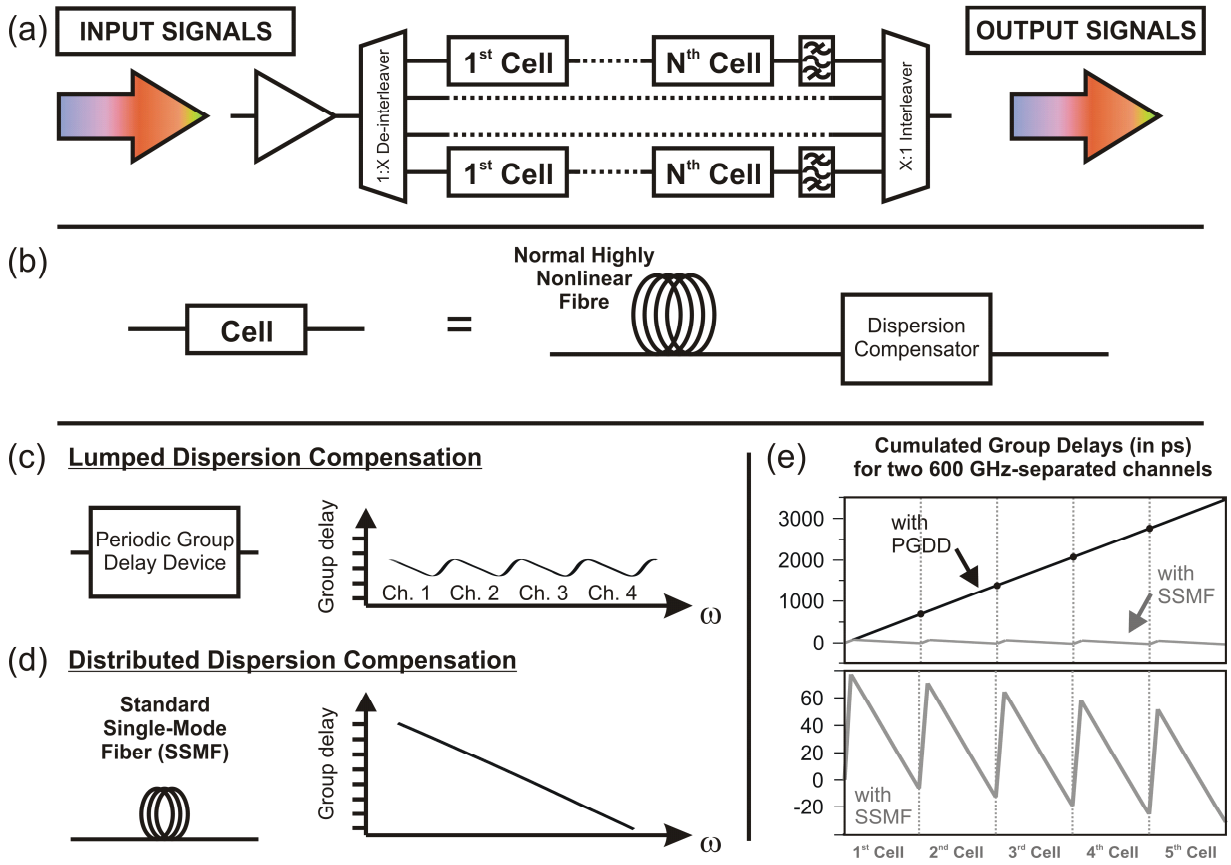

Figure II-11: Schematic of a typical optical regenerator based on SPM. (a) Schematic of the proposed dispersion-managed multi-channel optical 2R regenerator after [22]. (b) Detailed description of the optical cell used in the multi-channel optical regenerator consisting of a piece of normally dispersive highly nonlinear fibre and a dispersion compensator unit. (c). Dispersion compensator implementation using periodic group delay devices as proposed in [22], and corresponding group delay variations. (d) Dispersion compensator implementation using Standard Single-Mode fibre as proposed in [97], and corresponding group delay variations. (e) Comparison of the group delay evolution as a function of the position within five cells when the dispersion compensator unit made of a periodic group delay device (top graph) or standard single mode fibre (both top and bottom graphs) based on data from [98].

In the framework of the European project TRIUMPH, I had the opportunity to participate in the realisation of an all-fibrerized regenerator designed for 33%-RZ 40 Gb/s channels, and to perform its early characterization [98] at 4x10 Gb/s. The characterization showed that the effects of inter-channel nonlinearities could be suppressed with a residual power penalty of 0.5 dB between multiple- and single-channel operations (in the absence of any signal degradation). A maximum 1.5 dB power penalty improvement was achieved for an artificially degraded input signal but with significant variation between channels. Based on the same approach further experiments were conducted for two 33% RZ 43 Gb/s data stream (1,200 GHz spectral separation) and a power penalty improvement of 2.5 dB was achieved for both channels for an artificially degraded input signal [16]. Three-channel operation (600 GHz channel spacing) was still feasible albeit at the expense of slightly degraded performance due to an increased XPM-induced timing-jitter contribution that highlights the presence of a remaining contribution caused by inter-channel interactions within the optical fibre assemblies. Corresponding results are reported in references [98, 99].

Based on this review, one can wonder whether simpler architecture can be thought about given that multi-channel optical processing has only been reported for a limited number of channels (up to 4). The purpose of this thesis is thus to investigate alternative schemes to mitigate the inter-channel cross-talk within the optical nonlinear gate. The motivation to do so is to examine whether simpler architectures over a fibre dispersion-managed solution can be considered, and to evaluate their performances and possible limitations with respect to single-channel operation. Among the different approaches, the fibre-based 2R-regenerator using spectral broadening and offset filtering was considered over the other techniques because of its easier implementation.

Due to the lack of detailed analysis in the literature, I first study the single-channel Mamyshev regenerator in Chapter III, in order to examine the regenerator performance with respect to the operating conditions and nonlinear fibre properties. In Chapter IV, I examine the various solutions that could be considered to extend the scheme to a multi-channel when using a single piece of fibre.

Chapter III: Single-channel 2R-optical regenerator design

This chapter reports the new contributions during my PhD work on the design of the single channel optical 2R optical regenerator based on spectral broadening and subsequent offset filtering. Taking benefit of fundamental scaling properties, I identified general rules, which drastically reduce the design complexity of the optical regenerator, be it in the absence or presence of fibre attenuation. This approach facilitated the drawing of fundamental conclusions that are bit-rate independent.

The presentation of these results and conclusions are given in Publications A and B. Publication A reports the presentation of the model used and the theoretical scaling rules proposed for the regenerator in the absence of any fibre attenuation. The second Publication presents the experimental validation of the design rules, and for which the impact of the fibre attenuation loss has been included.

The complete reference of Publication A (see page 109) is:

> L.Provost, C.Finot, P.Petropoulos, K.Mukasa, D.J.Richardson, "**Design scaling rules for 2R-optical SPM-based regenerators**", Optics Express 2007 Vol.15 pp.5100–5113.

The complete reference of Publication B (see page 125) is:

> L.Provost, C.Finot, K.Mukasa, P.Petropoulos, D.J.Richardson, "**Generalisation and experimental validation of design rules for SPM-based 2R-regenerators**", Optical Fiber Communication conference (OFC 2007), 25-29 Mar 2007, OThB6.

The chapter is divided into three sections. First, we will present the model and the theoretical argument used to derive the design rules. In the second section, we will present the experimental validation showing the applicability of the proposed rules, and finally we will highlight important aspects on the applicability of these design rules.

***

1. Introduction

Though the regeneration scheme based on spectral broadening and offset filtering was introduced by P. Mamyshev in 1998 [14], its design has only been addressed in a few works [14, 67, 100].

Although the reported conclusions of those works are undeniably helpful, no exhaustive guidance was provided to build up such regenerators from scratch and to size it accordingly with the desired reshaping performance.

The reason for such a difficulty fundamentally lies in the large number of parameters one has to consider and the difficulty to relate parameters with the reshaping properties. As highlighted in the previous chapter, the design complexity of the Mamyshev regenerator scales up rapidly when considering the numerous parameters involved (as seen in Figure II-9): fibre parameters (fibre length, fibre attenuation, chromatic dispersion, chromatic dispersion slope, and nonlinear coefficient), offset position of the output filter, input power budget, input pulse duration, etc. In addition, because the requirements imposed on the characteristics of the Highly Nonlinear Fibre (HNLF) are more relaxed than for other regeneration schemes, fibre parameters can extend over large ranges. The last argument is even truer when considering the variety of glass materials that could be employed within the nonlinear medium. The progress made on the manufacturing process allows non-silica fibre-based devices to be considered as serious contenders.

As far as fibres with normal dispersion are concerned, two types can be distinguished and have been proposed as viable candidate for nonlinear signal processing:

1. Silica-based fibre types. This is the most usual and traditional category. It includes full-solid silica HNLF, chromatic dispersion compensating fibres (DCF) [101], and silica-based microstructured optical fibres.

2. Compound-glasses fibre types. This type corresponds to fibre formed of non-silica glass (chalcogenides, tellurite, Bismuth glasses). Those glasses were proposed as alternatives to silica-based fibres because of their higher nonlinear coefficient – about 1000 times that of fused silica [102-104]. They have been therefore considered to be of a potential interest to exploit Kerr nonlinearities using a reduced power budget.

Figure III-1 shows the nonlinear coefficient and group velocity dispersion ranges associated with the aforementioned fibre types. Individual fibre data coming from either the literature (see Ref [105-116] for corresponding figures) or from in-house fibres are reported. It is noticeable that the two fibres types essentially differ in their nonlinearity levels, and to a lesser degree in terms of chromatic dispersion. However, the two types significantly differ in their intrinsic attenuation as compound glasses exhibit attenuation levels of a few dB per meter while silica-bases fibre exhibits attenuation of a few tenths of dB per kilometre.

Although several proof-of-principle experiments on the Mamyshev regenerator have been demonstrated in silica-based holey fibres [115, 116], compound glasses such as chalcogenide glasses [117-119], or bismuth-oxide [110, 120, 121], a direct cross-comparison of the pros and cons of each glass type is not simple because of the different operating conditions and implementation set-ups (different lengths, different bit-rates) existing among the reported works.

The existence of such a large range of nonlinear properties combined with the lack of sufficient feedback on the influence of each parameter involved in the reshaping operation are the two major issues that are considered in my analysis for the single-channel case and represent my major contribution to the field.

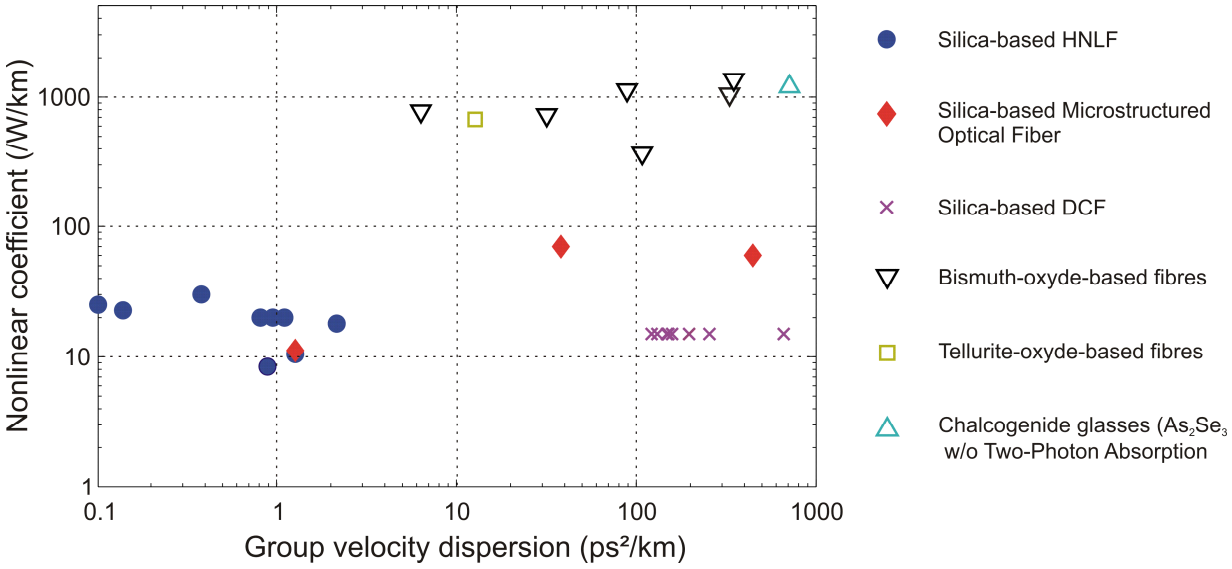

Figure III-1: Overview of the group-velocity dispersion and nonlinear coefficient for different fibre structures and glass material. Data are reported at 1550 nm. Full-symbols: silica-based optical fibres; Open symbols: non-silica compound glass optical (Refs. [117-119]) fibres and bismuth oxide-based (Refs. [110, 120, 121]) fibres.

2. *Description of the numerical model*

2.1. Nonlinear propagation of an optical pulse within a nonlinear Kerr medium

The evolution of an optical pulse within a nonlinear fibre is governed by the well-known Nonlinear Schrödinger Equation (NLSE) [45].

Let us consider an optical fibre having an attenuation coefficient $\alpha(\omega,z)$, a nonlinear coefficient $\gamma(\omega,z)$. Let $\beta_0(\omega,z)$ be the mode propagation constant , where ω stands for the frequency, and z

the longitudinal position along the fibre. For sake of clarity all frequency dependence will be dropped throughout the rest of this thesis, and the longitudinal homogeneity of the fibre will be considered to be uniform so that the longitudinal dependence in z is also dropped. Let A(t,z) be the slowly varying pulse envelope of the electrical field of the optical pulse of which the carrier frequency is ω_0 and initial temporal width is T_0.

$$A(t,z) = \sqrt{P_p}U(t,z) \qquad \textit{(III-1)}$$

Where: U(t,z) being the normalized amplitude, and Pp the peak power of the pulse. For instance, for input Gaussian pulse, $U(t,0)= \exp[-{}^{1}/_{2}(t/T_0)^2]$, where the T_0 is the $1/e^2$ half-width. For a Gaussian pulse, the full-width at half maximum T_{FWHM} of the pulse intensity relates to T_0 with: $T_{FWHM} = 2\sqrt{\ln(2)}T_0$.

The NLSE Equation considered is reported in Equation (III-2). Consideration of the nonlinear contribution has been limited to the SPM term (RHS term) so that both the Raman Scattering contribution and self-steepening term are neglected. Such a simplification is justified by the fact that both contributions are only expected to become significant for optical pulse durations of less than 1 ps, which is significantly smaller that the optical pulse-widths under consideration here. The Stimulated Brillouin Scattering contribution has also not been considered too, since the line-width of the pulses we will consider are much larger than the Brillouin line-width.

(III-2)

$$\frac{\partial A}{\partial z}+\frac{\alpha}{2}A+\beta_1\frac{\partial A}{\partial t}+\frac{i\beta_2}{2}\frac{\partial^2 A}{\partial t^2}-\frac{\beta_3}{6}\frac{\partial^3 A}{\partial t^3}=i\gamma|A|^2A$$

Where: β_1, β_2, and β_3 being respectively the group velocity, group velocity dispersion and third-order group velocity and defined as the first, second, and third coefficients of the Taylor expansion of β_0 around ω_0 respectively [45].

The definition of the following normalized quantities allows the NLSE to be recast into the standard form provided by Equation ***(III-3)***. These quantities are standard normalisations introduced in the soliton theory as presented in [45]. Note that we implicitly set the third order dispersion term β_3 to 0.

$$u(z,t)=\sqrt{N^2}U(z,t)$$

$$N^2=\frac{L_D}{L_{NL}}$$

$$\xi=\frac{z}{L_D}$$

$$\tau=\frac{T}{T_0}=\frac{t-\beta_1 z}{T_0}$$ Scaled time variable expressed in the reference frame moving with the pulse at the group velocity vg (retarded frame)

$$L_D=\frac{T_0^{\,2}}{|\beta_2|}$$ Dispersion length

$$L_{NL}=\frac{1}{\gamma P_p}$$ Nonlinear length

$$i\frac{\partial u(\xi,\tau)}{\partial \xi} - \frac{\mathrm{sgn}(\beta_2)}{2}\frac{\partial^2 u(\xi,\tau)}{\partial \tau^2} + |u(\xi,\tau)|^2 u(\xi,\tau) = -\frac{i}{2}\alpha\, L_D\, u(\xi,\tau) \qquad \textit{(III-3)}$$

Where: sgn(x) being the *sign* function (if x>0 sgn(x)= +1, else -1)

An analytical solution of the differential equation ***(III-3)*** only exists in particular cases so that the integration of the equation for the general case can only be achieved numerically. The numerical solution of the equation can be achieved using the widely known Split-Step Fourier method of which a complete description and implementation is reported in [45].

2.2. Scaling factor properties on the NLSE Equation

The form of the standard NLSE Equation ***(III-3)*** is valuable as it is possible to generate an infinity of solutions once a particular normalised solution is known. If we assume a loss-less medium by setting α=0, so that the RHS of Equation ***(III-3)*** is cancelled and $u(z/L_D,T/T_0)$ is found to be a solution of the NLSE Equation ***(III-3)***, then it can be shown $\delta.u(\delta^2.z/L_D,\delta.T/T_0)$ also represents a solution for any real number δ [45].

This scaling property can be further interpreted into a more useful assertion. By considering two optical pulses of amplitude $A_1(t,z)$, and $A_2(t,z)$ propagating in a Fibre 1 (with length L_1, nonlinear coefficient γ_1, and group velocity dispersion β_{2_1}), and fibre 2 (with length L_2, nonlinear coefficient γ_2, group velocity dispersion β_{2_2}) respectively, it can be demonstrated that the two pulses will evolve to the same scaled profiles in both the time and frequency domains if the two following conditions are fulfilled.

1- The initial ratio (i.e. at z=0) between the fibre and the dispersion lengths are equal so that:

$$\frac{L_1}{L_{D1}} = \frac{L_2}{L_{D2}} \qquad \textit{(III-4)}$$

2- Their respective initial N^2 ratio (i.e. at z=0) are equal so that

$$\frac{L_{NL1}}{L_{D1}} = \frac{L_{NL2}}{L_{D2}} \qquad \textit{(III-5)}$$

In other words, the study of a single optical pulse of a prescribed initial envelope is sufficient to predict the evolution of any replica having different temporal and/or amplitude scaling in an optical fibre having a different fibre length and/or different group velocity dispersion or/and nonlinear coefficient. Using the two previous conditions one can compute corresponding fibre parameters as well as amplitude and temporal scaling parameters.

A similar conclusion can be drawn when the fibre attenuation is also considered. Noticing that the loss contribution to the NLSE equation is only achieved thanks to the αL_D term of the RHS of Equation ***(III-3)***, the previous two pulses will evolve to the same scaled profiles in both time and frequency domains when a third condition is fulfilled:

3- Their initial αL_D products are equal

$$\alpha_1 L_{D1} = \alpha_2 L_{D2} \qquad \textit{(III-6)}$$

Where: α_1 and α_2 are the attenuation losses of fibre 1 and fibre 2 respectively.

Despite the apparent simplicity of these three conditions (which are easily derived from the NLSE analysis), a drastic and significant reduction of the modelling requirement is enabled for the Mamyshev regenerator. Global bit-rate independent conclusions can be derived on the propagation of a single optical pulse in a given optical fibre for which the four parameters T_0, P_p, β_2, γ, are arbitrarily fixed. The extent of such a conclusion is however reduced for a lossy media, as the scaling properties are only valid when the αL_D value remains constant, and this therefore needs to be addressed for many cases of αL_D values.

2.3. Parameterisation of the power Transfer Function

In this part, attention is paid to the analysis and parameterisation of the different operating regimes that are offered by the Mamyshev regenerator. Depending on the regenerator parameters settings, three operating regimes can be identified and characterized by the shape and the power dependence monotony of the power transfer function. As depicted in Figure III-2(a), in which an ideal Mamyshev regenerator set-up is considered (see regenerator parameters in the figure), we compute the propagation of an input un-chirped optical Gaussian pulse-width of T_0=5 ps duration (corresponding to 33%RZ 40 Gb/s optical signal) and a peak power P_{p1}. The output (Gaussian) filter bandwidth is set to match the initial spectral bandwidth and spectral shape of the incoming pulse.

An idealized optical amplifier (i.e. no noise is added in the amplification process) is used to describe the corresponding power transfer function by increasing or decreasing the input peak power of the optical pulse at the fibre input port. By varying the fibre length by -25% and 25% around the initial length L_0, three operating regimes are observed as depicted in Figure III-2(b), and which differ from one another by the variation of the power transfer function which can be either be; non-monotonous (regime 'A') producing some oscillatory structure at high input power levels, exhibiting a locally flat region (plateau) on the one-level (regime 'B'), or a purely monotonic response (regime 'C').

The differences in behaviour result from the ripple due to SPM within the pulse spectrum and the position of the output filter relative to these ripples as depicted in Figure III-2(c). The pulse spectrum becomes flat-top for longer propagating distances and the Transfer Function hence becomes hence monotonic. It is also clear that the noise rejection in empty slots is different for the three operating regimes as seen by the shape of the transfer function at low input power (low G_1 value).

Based on the transfer function evolution, we define a nominal input power for the incoming pulse mark levels, which locally shows a maximum output power compression (mathematically determined by the position at which the first derivative of the Transfer Function is either zero (for regimes A or B) or minimum (for regime C)). Those points are reported as G_A, G_B, and G_C in Figure III-2(b). Intensity and frequency chirp profiles of the output pulses corresponding to these three operating settings are reported in Figure III-2(d).

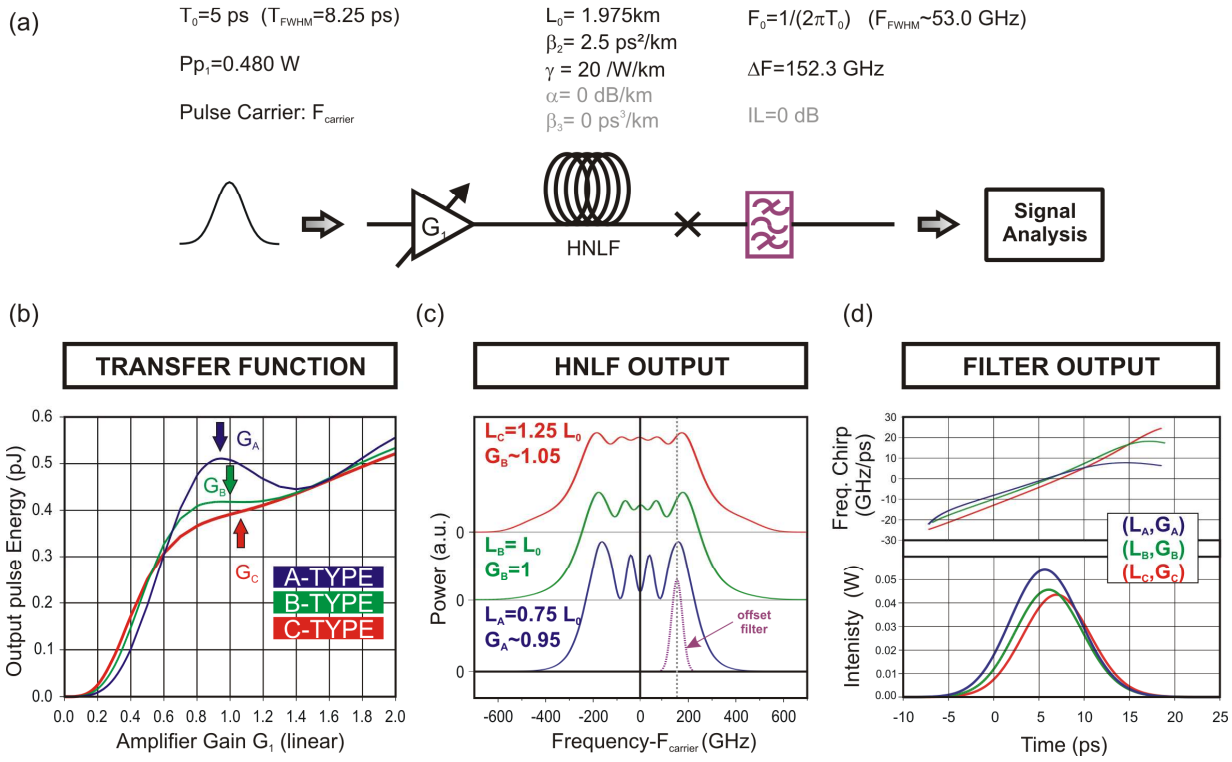

Figure III-2: Illustration of the three possible operation regimes for the Mamyshev regenerator. (a): parameters of the regenerator set-up considered for the numerical modelling. (b): Power transfer functions and corresponding type (A, B, and C) when the fibre length is changed by -25%, 0%, and +25 % respectively as compared to the initial length L_0. Vertical arrows depict the position on the transfer function where the output power compression is locally maximum. (c): Corresponding spectrally broadened spectra at the fibre output for the three operating regimes. The spectra were intentionally offset along the vertical axis for better readability. The central position and amplitude of the offset filter is also reported. (d): Pulse intensity profile (bottom) and frequency chirp (top) at the output of the offset filter. The pulses are plotted in a moving reference frame attached to the input pulse.

In order to encompass these different regimes and associated operating input parameters (nominal input mark power and output extinction ratio), three parameters are defined: 1) the input peak power for the mark pulses P_1^{in} that provide a locally maximum output power compression, 2) the output power compression ρ ratio of the marks obtained when considering a uniform amplitude fluctuation window of ± 7.5 % centred around P_1^{in}, and 3) the output extinction ratio ER^{out} considering an input extinction ratio ER^{in} of -10 dB, ER^{in} being defined as the ratio between the input peak powers of 'zero' and a 'one' pulse having a peak power of P_1^{in}. Corresponding definition of the three former quantities can visually derived from the power transfer functions and eye diagram in the figure below:

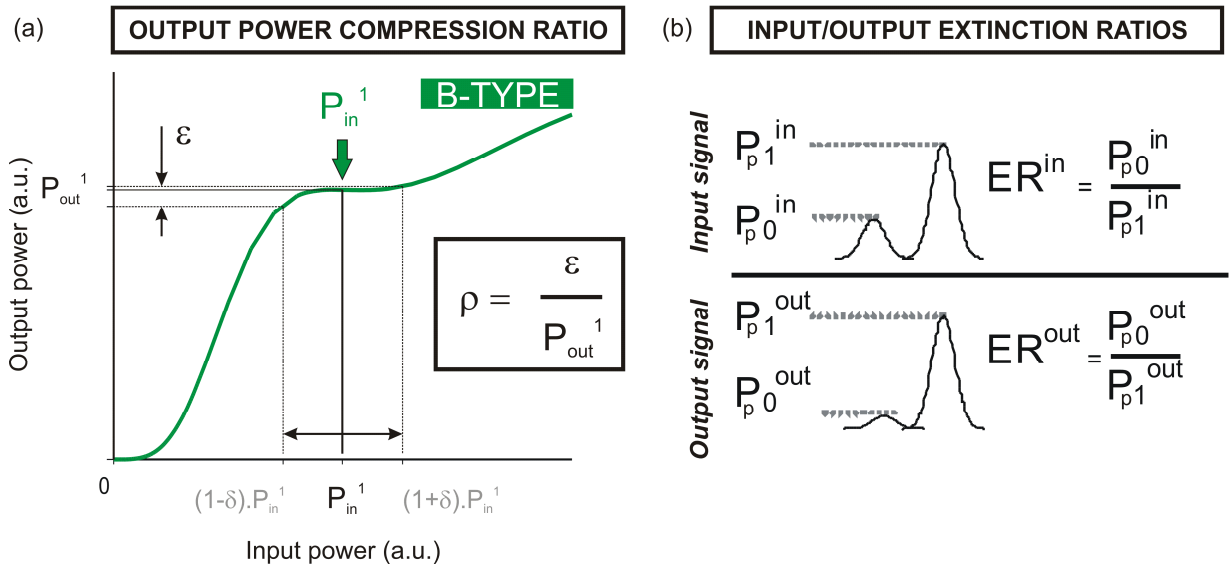

Figure III-3: (a): Definition of the output power compression ratio ρ for an operating regime corresponding to the Type B with δ=7.5%. (b): Definitions of the input and output extinction ratios.

Additional parameters quantifying the performance of the regenerator can also be defined such as the energy yield, time-bandwidth product and timing delay - as reported in Publication A.

3. Design rules and parameter scaling

We now present in this section design rules for Mamyshev regenerators obtained by combining the previous observations and scaling properties of the NLSE Equation. First, we report numerical modelling results considering a loss-less case situation (a good approximation for silica fibres) (Publication A). Then we report experimental results for which the applicability of the design rules is experimentally validated (Publication B).

3.1. Loss-less case

This section presents one of the most important contributing results of this chapter which consists of a contour map plot. Thanks to a careful selection of the representation space, a synthetic relationship between the physical parameters associated with the regenerator and the reshaping capacity of the regenerator is established using the parameters defined earlier in this chapter.

Considering the propagation of a single and un-chirped Gaussian pulse fed into the input of the regenerator and the use of normalized parameters, it is possible to produce a general contour map as shown in Figure III-4 considering a loss-less fibre (α=0).

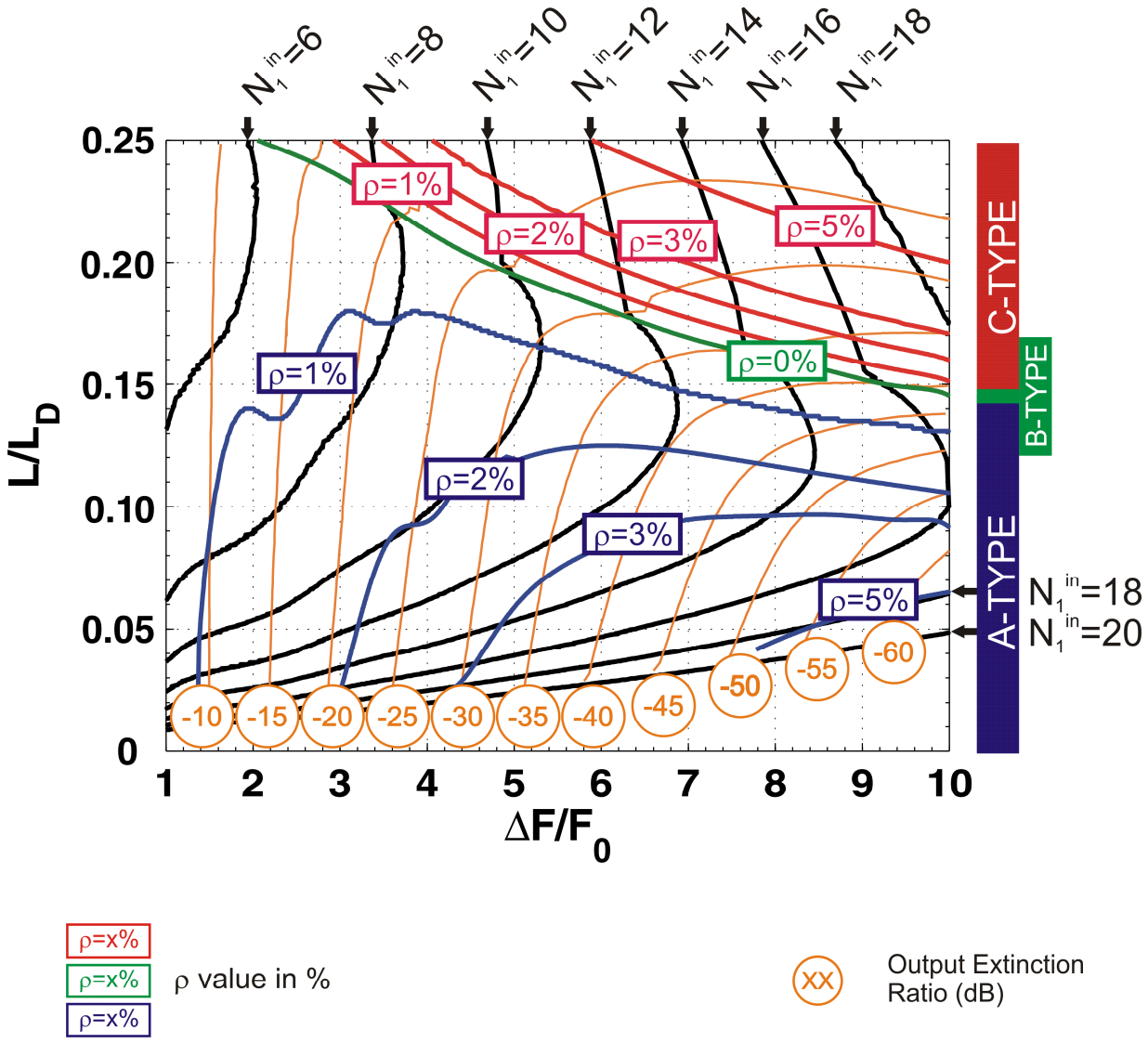

Figure III-4: Normalized map for input un-chirped Gaussian pulses linking the regenerator parameters to the regeneration performance: Bold plain lines correspond to ρ contours. Orange plain lines correspond to ER^{out} contours (in dB), and black lines correspond to N_1^{in} contours.

As the reported information on the map is dense, it is necessary to provide some guidance on how the map was constructed and should be read.

First, the horizontal axis is the ratio between the offset detuning of the output filter ΔF and the filter bandwidth F_0. F_0 is set to match the initial input pulse bandwidth (i.e. $F_0 = 1/(2\pi T_0)$). ΔF is computed with respect to the incoming carrier of the input signal. The vertical axis is the ratio between the fibre length L and the dispersion length L_D.

Choosing a combination within this space constrains each parameter of the regenerator to be set except two, namely the input peak power and fibre nonlinear coefficient. By setting the nonlinear coefficient to a prescribed value, the input peak power remains as the only free parameter, so that the power transfer function regime is completely defined. Following the definition of the parameters used to characterize the power transfer function, the operating conditions associated to the selected (L/L_D; $\Delta F/F_0$) are completely set. It is therefore possible to compute the input peak power parameter $P^1_{in.}$

The rest of the information is thus reported using iso-lines curves representing output power compression ratio ρ and corresponding operating regime (A, B, or C), operating input peak power Pp_1^{in} (or equivalently by the N_1^{in} quantity: $N_1^{in}=L_D/L_{NL}=L_D.\gamma.P_{p1}^{in}$), and output extinction ratio ER^{out} (considering an input extinction ratio of ER^{in}=-10dB).

The particular results depicted in the presented map of Figure III-4 are however only applicable to un-chirped Gaussian-shaped pulses. Considering different input pulse shapes or chirp profiles

such as those reported in [70, 122, 123] would however not restrict the applicability of the proposed method, but would merely result in different contour plots.

Finally the state of polarisation of the incoming signal is an input parameter one needs to consider when applying the previous design rules. Since the nonlinear refractive index n_2 depends on the polarization state of the fields - owing to the tensorial nature of the optical Kerr effect [45, 46], the value of the nonlinear coefficient (γ value) is modified accordingly. However, for most commonly used HNLFs (i.e. relatively long and non-polarization maintaining fibres), this dependence is greatly reduced as the state of polarization is assumed to evolve randomly along the fibre. This is attributed to the presence of small physical disturbances along the fibre giving rise to birefringence. Under these assumption, it results that an average value for the nonlinear coefficient γ can be employed whatever the incoming polarization states of the incoming signal [124].

3.2. Lossy case

As the design rules were derived for a loss-less fibre case, their practical applicability for realistic highly nonlinear fibres might be restricted, as the fibre attenuation must be taken into consideration in many cases of practical interest. Since fibre loss manifests itself as a reduction of the spectral broadening, proposing a more general analysis that includes the effect of fibre attenuation is thus relevant. This next part discusses the inclusion of such a loss by extending the scaling rules found in the loss-less case.

3.2.1. Extension of the design rules to a lossy environment

We report that the extension to a lossy environment of the contour map plot presented in the previous paragraph was possible if the normalized L/L_D quantity of the vertical axis of the map (Figure III-4) is replaced by the quantity $(L_{eff}L)^{1/2}/L_D$, where L_{eff} stands for the effective length of the fibre. From a physical point of view, the effective length can be understood as the actual length over which nonlinearities would have been experienced in the absence of any fibre loss. L_{eff} is defined as:

$$L_{eff} = \frac{1-\exp(-\alpha L)}{\alpha} \qquad \textit{(III-7)}$$

The introduction of the normalised quantity $(L_{eff}.L)^{1/2}/L$ cannot be straightforwardly appreciated. In fact, it is motivated by some previous published works addressing the description of the optical wave-breaking phenomenon in fibre [125, 126]. In those works, the description of the phase evolution of the pulse along the fibre is proposed by assuming that the two chirp contributions induced by SPM and group velocity dispersion are independently imprinted onto the pulse. As we report in [127], the effective length L_{eff} quantity is introduced to take into account the effect of the fibre loss on the nonlinear phase shift generated by SPM [45].

It is mandatory to recall once again that the applicability of the scaling rules on a contour plot map in a lossy environment is only valid if the αL_D quantity remains constant as previously discussed.

3.2.2. Experimental validation

The validity of the scaling rules was experimentally assessed. Using the parameter of the highly nonlinear fibre reported in Table III-1, a two dimension contour plot was computed and is reported in Figure III-5 at 1545 nm. The map was computed by considering an input Gaussian pulse width of with T_{FWHM}=6.15 ps corresponding to the nominal pulse-width experimentally obtained. The corresponding experimental set-up is reported in Figure 1(a) of Publication B.

Fibre Type	β_2	β_3	γ	α	**L**	**Leff**	L_D	αL_D	$L.L_{eff}/L_D^2$	$(L.Leff)^{1/2}/L_D$
	ps^2/km	ps^3/km	/W/km	dB/km	m	m	m	dB	-	-
HNLF	2.3	0.034	18	-2.13	1,000	790	59311	12.6	0.022	0.014

Table III-1: Parameters of the highly nonlinear fibre used for the experimental validation of the design rules of the single channel optical regenerator.

The contour plot Figure III-5 was computed considering an ideal output filter (with no phase response) whose bandwidth matches the initial and ideal pulse width. The third order group velocity term was not considered here. The operating regime B was achievable for a nominal input peak power of 3.1 W, corresponding to an offset filter position of ~-3.0 nm.

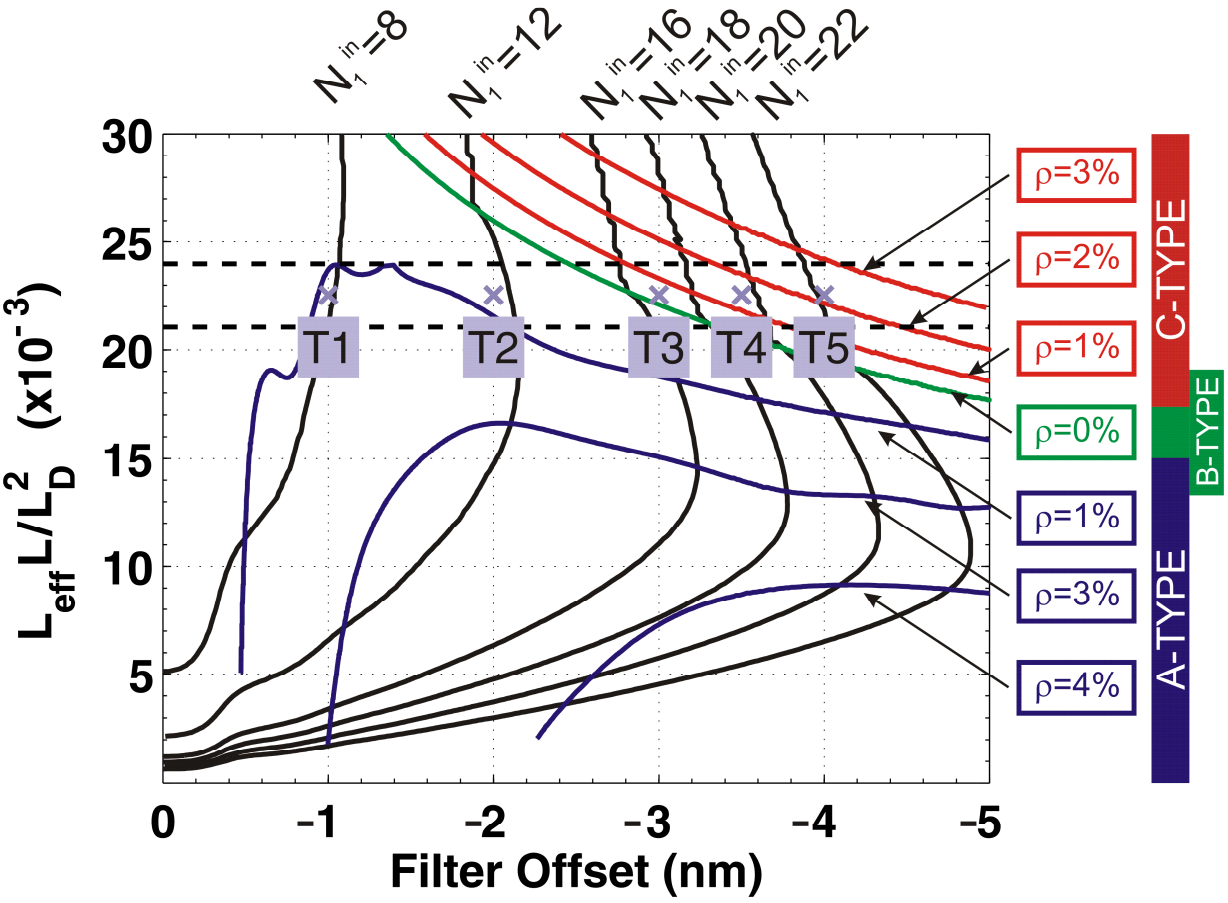

Figure III-5: Contour map corresponding to the experimental fibre used with iso-lines plots for several N_1^{in} and ρ values. The positions of the experimental points (crosses) are shown with corresponding upper and lower bound due to the uncertainty in the pulse width estimation (dashed lines). The carrier wavelength is 1545 nm.

From an experimental point of view, we were able to experimentally operate within the area of the map delimited by the two dashed line in Figure III-5, due the uncertainty on the experimental pulse width (+/-0.1 ps). This area was indeed the most interesting as these power transfer function regimes could be scanned simply by changing the filter position. Five positions ranging from T1 to T5 were selected, corresponding to offset detunings of -1.0, -2.0, -3.0, -3.5, and -4.0 nm respectively (see Figure III-6).

We depict in Figure III-6 the five experimental TF functions, with corresponding ρ values. The progressive change in the TF as the filter position is set further from the carrier wavelength is confirmed. We also report the modelling results based on the experimental data considering the contribution of the chromatic dispersion slope and the various insertion losses within the system. A relatively good agreement is found over the five filter positions. As discussed in Publication B, the discrepancies at higher input peak power levels were attributed to the differences in the detailed evolution of SPM generated spectral side lobes associated with residual chirp on the initial pulses (as seen in the retrieved intensity profile and frequency chirp reported in Figure 3(a) of Publication B).

.

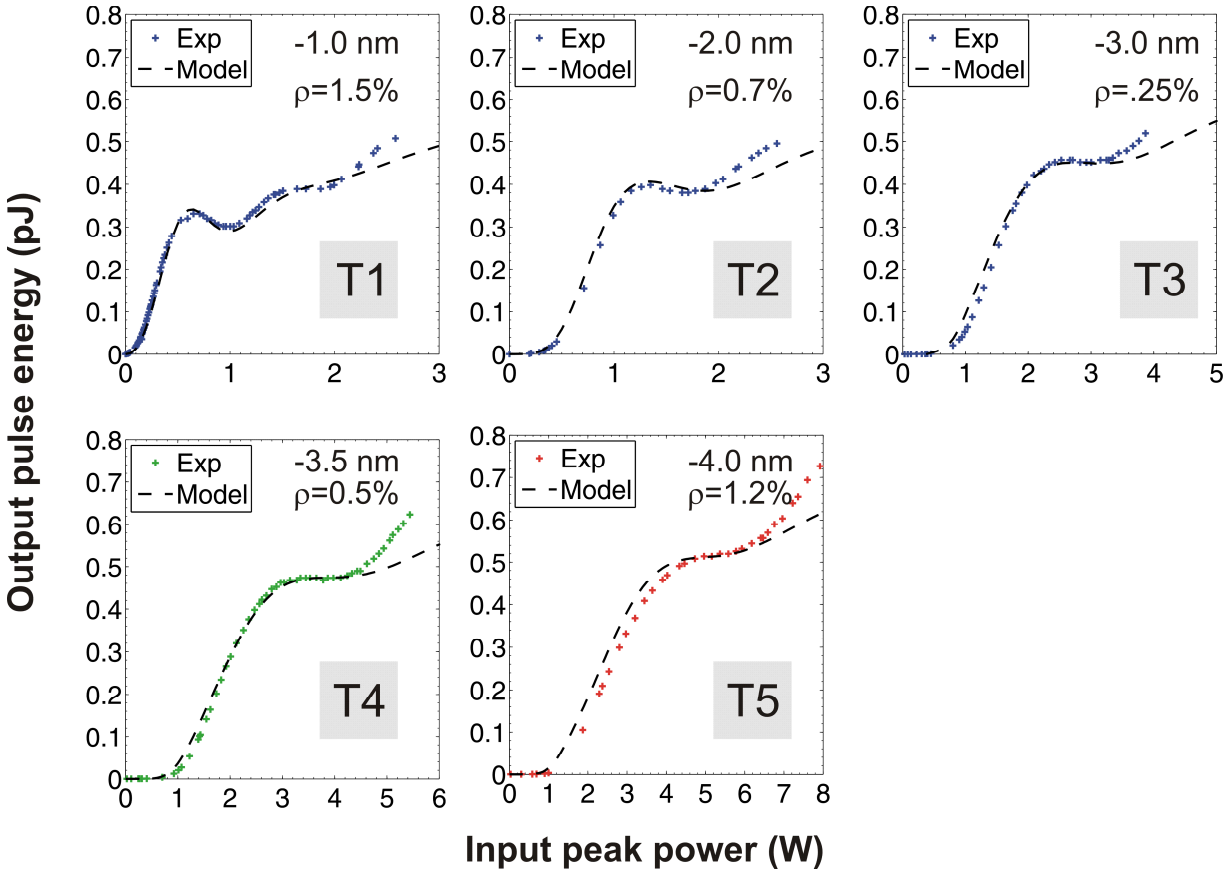

Figure III-6: Experimental and modelled transfer functions for the five filter positions (-1nm, -2 nm, -3nm, -3.5 nm, and -4 nm). Estimated output power compression ratio ρ derived from experimental data is also reported for each filter position.

4. Additional design consideration

In this part, we highlight some of the main observations and conclusions drawn from the analysis of the presented scaling properties. Publications A and B further detail those aspects as well as other design consideration such as energetic yield, sensitivity to the third order chromatic dispersion, and impact of the timing-jitter.

4.1. Limitations induced by intra-channel effects

The design rules are derived based on a single pulse approach. As already highlighted in [77], an additional restriction must be considered when considering a train of optical pulses. Such a limitation arises from the temporal broadening of the optical pulses during their propagation in the highly nonlinear fibre, which means that optical pulses can extend well outside of their initial temporal bit-slot. In such a case, nonlinear interactions take place through intra-channel FWM, resulting in the presence of pattern-dependent fluctuation in the transfer function. The deleterious intra-channel effects are more prone to occur for large duty-cycle input signals (i.e. large temporal pulse widths). In Publication A, this issue is illustrated in Figure 9(a), where we have reported the variation of the temporal profiles of the oncoming pulse when the regenerator operates at different N^1_{in} values and the pulse extends within adjacent bit slots as a function of the pulse duty cycle.

As shown in Figure 9(b) of Publication A, it is possible to estimate an upper limit on the N^2 value to avoid intra-channel interactions caused by excessive broadening of the pulse in neighbouring slots [128, 129]. This upper value is derived by computing the distortions in the output power for 'one' bits in the presence of neighbouring 'one' pulses with the single-pulse case, so that conclusions drawn for the single-pulse case are preserved for a train of optical pulses. When fibre attenuation is included, the restrictions on the parameter N^2 are actually more stringent and the corresponding upper limit depends on the αL_D quantity, since that the temporal broadening is always larger as compared to the loss-less case when operating at the same input power level.

4.2. Influence of the nature of the signal distortions and the assessment of regeneration performance

One of the main aspects of these modelling findings to be taken into consideration is that the transfer assessment was chosen using incoming pulse signals of identical shape and temporal duration but of variable input peak powers. However because the pulse intensity profile directly affects the SPM process, the regenerator is expected to exhibit different power transfer function for different input pulse shapes for the same operating settings [82].

In order to assess the consequence of such variations, two possible contributions were considered for the loss-less case: i) a variation of the input pulse width, and ii) the presence of linear chirp on the incoming pulse (i.e. due to residual dispersion). Such contributions actually induce a different evolution in the spectral broadening of the pulse and which can result in power fluctuation on the output mark levels of the regenerator when one nominally operates in the B-regime. As seen in the results reported in the Figure 7 of Publication A, the shape of the power TF can be substantially modified both by altering the monotony of the TF and changing the output power of the ‘one’ pulses.

Addressing this intrinsic sensitivity is not straightforward when considering realistically distorted optical signals propagating within an optical network. Since the degree of distortion of the optical signal would be highly dependent on the transmission system and network characteristics considered, such an analysis is obviously well beyond the scope of the present work. It was also the reason why the impact of the presence of the amplified spontaneous emission noise was also not considered within this analysis. A few works are worth mentioning regarding the impact of

the ASE noise or nonlinear intra-channel effects on the regeneration capability [77, 82, 84, 89, 130]. The conclusions highlight the fact that operating in the B regime and matching the input power to the plateau range may lead to too much sensitivity to individual input pulse variations so that the degree of amplitude jitter reduction would be intrinsically limited. However, fortunately by increasing the operating power improvements in the amplitude jitter reduction can be obtained, as the regenerator exhibits less sensitivity with respect to pulse shape variations as observed in Figure 7(a) of Publication A. This was further confirmed with additional modelling computations as reported in [89] when considering realistically distorted input optical pulses. Finally, in Ref. [131] the authors report a general approach to directly relate the Q-factor improvement with the characteristics of the HNLF used in the Mamyshev regenerator in the presence of noise and fibre loss.

4.3. Impact of fibre attenuation loss of on the regenerator performance

The exploitation of the proposed scaling representations is helpful to assess the existing trade-offs between different nonlinear fibre parameters of different glass material.

In Table III-2, the physical properties of five types of highly nonlinear fibre with typical parameters are reported, namely a Dispersion Shifted Fibre (DSF), two silica-based highly nonlinear fibres with different attenuation loss, a DCF and a highly nonlinear bismuth oxide fibre. The required fibre length L, average input power, energetic yield, output extinction ratio ER^{out} - considering an input signal extinction ratio of -10 dB, are reported for the case of a B-type operating regime (except for Bismuth-oxide fibre, for which such a regime could not be achieved

as it was well beyond the upper limit to avoid adjacent pulse interaction). The corresponding regime for this case is thus type A, with a ρ figure of 0.005%. The contribution of the third order group velocity term was ignored in order to simplify the comparison. The incoming signal considered is a Pseudo-Random Bit Sequence (PRBS) RZ pulse train with a data rate R=40 Gb/s and 25 % duty cycle, the frequency detuning was (arbitrarily) set to 2.5 x R (i.e. 100 GHz).

Fibre Type	**Chromatic Dispersion**	**γ**	**α**	**L**	**Input Average Power**	**ER^{out}**	**Energetic Yield**	**N**	**αL_D**
	ps/nm/km	/W/km	dB/km	m	dBm	dB	-		dB
DSF	-7	1.8	0.2	402	32.9	-13.5	15.5%	6.45	0.32
HNLF 1	-0.87	20	1	3,602	14.8	-13.2	6.7%	7.57	12.7
HNLF 2	-0.64	20	0.5	4,712	13.0	-13.3	9.0%	7.21	8.66
DCF	-120	5	0.6	23	40.8	-13.6	15.8%	6.44	0.055
Bismuth Oxide fibre	-260	1100	900	15	24.0	-13.5	0.76%	9.46	38.7

Table III-2: Fibre properties, lengths and power requirement to provide the transfer function in the regime B except for Bismuth oxide fibre of which parameters corresponds to type A with ρ=0.005%.

A clear trade-off between fibre length/dispersion and the required input power budget is observed. Achieving compact devices therefore dictates the use of fibre with high dispersion values, such as DSF or DCF. On the contrary achieving good performance at practical power levels requires highly nonlinear fibres. However, as those fibres are usually designed to have low-

dispersion values, several kilometres of highly nonlinear fibre are required and the corresponding optical regenerators would be more prone to be limited by Stimulated Brillouin Scattering [100] and likely more demanding in term of fibre homogeneity required. More interestingly the output extinction ratio is also slightly different and is dependent on the actual αL_D considered: the higher the αL_D, the smaller the extinction ratio improvement[1].

In [132], we propose to use a multi-segment fibre arrangement to overcome such observed limitations when using a continuous single fibre. This allows better management of the chromatic/nonlinear interaction along the regenerator length. We demonstrate that the proposed scheme allows a reduction in the length requirements and an increasing output extinction ratio for the same filter position.

5. Conclusion

In this chapter, I have reported my major contributions regarding the design of the Mamyshev optical regenerator in a single-channel configuration. Based on numerical modelling and consideration of the properties of the equations governing the propagation of optical pulses within nonlinear fibre, the complexity of the design is significantly reduced thanks to the definition of some normalized parameters. Such quantities allow one to relate the general physical fibre parameters with parameters derived from the power transfer function of the regenerator and the

[1] This conclusion is however not applicable to Bismuth-Oxyde fibre as the operating regime corresponds to the A-type, so that the output extinction ratio is expected to be better than for regime B.

incoming signal characteristics. Such relationships can be efficiently arranged in a concise two-dimensional representation using contour plots.

We also demonstrated that it was possible to extend those scaling rules to the case in which the fibre attenuation needs to be taken into account. The experimental validation demonstrates a satisfactory agreement with the model. This validation emphasizes some of the important tradeoffs existing among the different types of highly nonlinear fibres, and how the chromatic dispersion and fibre losses impact on the scaling properties of the optical regenerator.

Chapter IV: Multi-channel 2R-optical regenerator

In this chapter, I review the solutions I have proposed to extend the optical regeneration scheme proposed by P. Mamyshev to the multi-channel environment. Taking benefit of the design rules I established for the single-channel case, two novel schemes are presented. A suitable mitigation of the inter-channel cross-talk generated within the nonlinear optical gate of the optical regenerator is achieved thanks to the introduction of a large walk-off between the optical channels under process. Using direction- and polarization- multiplexing, I show that up to 4 channels can be simultaneously regenerated within the same piece of highly nonlinear fibre.

The chapter is divided into three sections. First, I examine the key aspects to be considered to extend the single-channel regenerator to a multi-channel case (not only from a cross-talk mitigation aspect but also in light of the conclusions found for the single channel design). From this analysis, several strategies to extend the single-channel scheme are then discussed. Following this review, I describe the two technical solutions I have implemented and analyse their principle

of operation and performance both from a theoretical and experimental point of view. In the last section, the experimental demonstration of simultaneous processing of 2x130 Gb/s channels within the same fibre is presented before concluding this chapter.

The corresponding experimental results are reported in the following 4 papers C, D, E, and F.

The complete reference of Publication C (see page 127), is:

L.Provost, F.Parmigiani, C.Finot, K.Mukasa, P.Petropoulos, D.J.Richardson, **"Analysis of a two-channel 2R all-optical regenerator based on a counter-propagating configuration",** Optics Express 2008 Vol.16(3) pp.2264-2275.

The complete reference of Publication D (see page 141), is:

L.Provost, F.Parmigiani, P.Petropoulos, D.J.Richardson, **"Investigation of simultaneous 2R regeneration of two 40 Gb/s channels in a single optical fibre"**, Photonics Technology Letters 2008 Vol.20(4) pp.270-272.

The complete reference of Publication E (see page 143), is:

L.Provost, F.Parmigiani, P.Petropoulos, D.J.Richardson, K.Mukasa, J.Takahashi, J.Hiroishi, M.Tadakuma, **"Investigation of four-wavelength regenerator using polarization-and-Direction-Multiplexing"**, Photonics Technology Letters 2008 Vol.20(20) pp.1676-1678.

The complete reference of Publication F (see page 145), is:

F.Parmigiani, P.Vorreau, L.Provost, K.Mukasa, M.Takahashi, M.Tadakuma, P.Petropoulos, D.J.Richardson, W.Freude, J.Leuthold, **"2R regeneration of two 130 Gb/s channels within a single fibre"**, OFC 2009 San Diego 22-26 Mar 2009 JThA56.

***

1. Introduction

1.1. Cross-talk mitigation strategies

As previously described in the preceding chapter, the Mamyshev optical regenerator relies on the exploitation of the SPM generated due to the optical Kerr effect. The extension of this scheme to a multi-channel case consists in establishing a sustainable scheme for simultaneous processing of several optical channels within the same nonlinear gate. The design of the multi-channel regenerator must therefore provide a suitable mitigating scheme to limit the deleterious impact of inter-channel nonlinearities (XPM and FWM) as soon as a several optical channels are co-propagating.

The strength of the non-linear interaction between adjacent channels is usually mitigated by engineering the chromatic dispersion map along the propagation path to ensure strong FWM

mismatch conditions and a fast walk-off between pulses to diminish the contribution of the XPM and aimed at ensuring that the pulses undergo a complete walk-though.

The FWM interaction is efficiently decreased by cancelling the phase matching conditions between co-propagating signals, and is achieved by ensuring that propagating optical channels propagate at a different group velocity along the fibre and/or in different polarization states.

Mitigation of the XPM is however more demanding. Similar to SPM, XPM results in an intensity-dependent nonlinear phase modulation on one optical pulse induced by a second co-propagating optical pulse. The total amount of nonlinear phase shift added by the second pulse is thus dependent on the interaction time during which the two pulses are spatially overlapped, the intensity profile of the interacting pulses, as well as the polarization states of the two interacting channels. The nonlinear phase shift induced by the second pulse is at a maximum for linearly co-polarized polarization states, and minimum when linearly cross-polarized [45]. For the co-polarized case, the nonlinear phase shift induced by XPM is twice the SPM nonlinear phase shift for the same pulse intensity. For the Cross-polarised case, XPM still predominates over SPM but the ratio between XPM and SPM nonlinear phase shifts reduced to 2/3 (for the same pulse intensity).

All of these aforementioned cross-talk effects directly impact the regenerator ability to exhibit a nonlinear power transfer function, because of the presence of large spectral distortions arising from large energy transfers and the generation of new frequencies. Consequently, large output power fluctuations are introduced onto the power TF associated with each channel as illustrated

in Figure IV-1. In addition, these fluctuations are highly dependent on the temporal synchronisation of the adjacent channel.

Figure IV-1 depicts the variation of the power transfer functions of one optical channel when an additional second channel is fed into the regenerator. The parameters of the optical regenerator were set using the design rules proposed for the single-channel case, so that an optimal transfer function for the first channel is exhibited. The pulse width was Gaussian 8.25 ps for the two channels (Bit-slot duration Tb=25 ps). The interfering optical signal is arbitrarily formed of alternating mark/space pulses and the channel separation is 600 GHz. The polarization states of the two signals are collinear, and this corresponds to the worst-case scenario.

Several power TF are been reported for Channel 1, considering several values of initial delay between the two optical channels, as well as the position of the offset filter (either positively or negatively offset with respected to the incoming frequency carrier $f_{carrier1}$. The shapes of the computed Transfer Functions clearly demonstrate that the key regeneration requirements are completely lost for most of the cases (either power equalization on the marks pulse, and/or ghost pulse rejection).

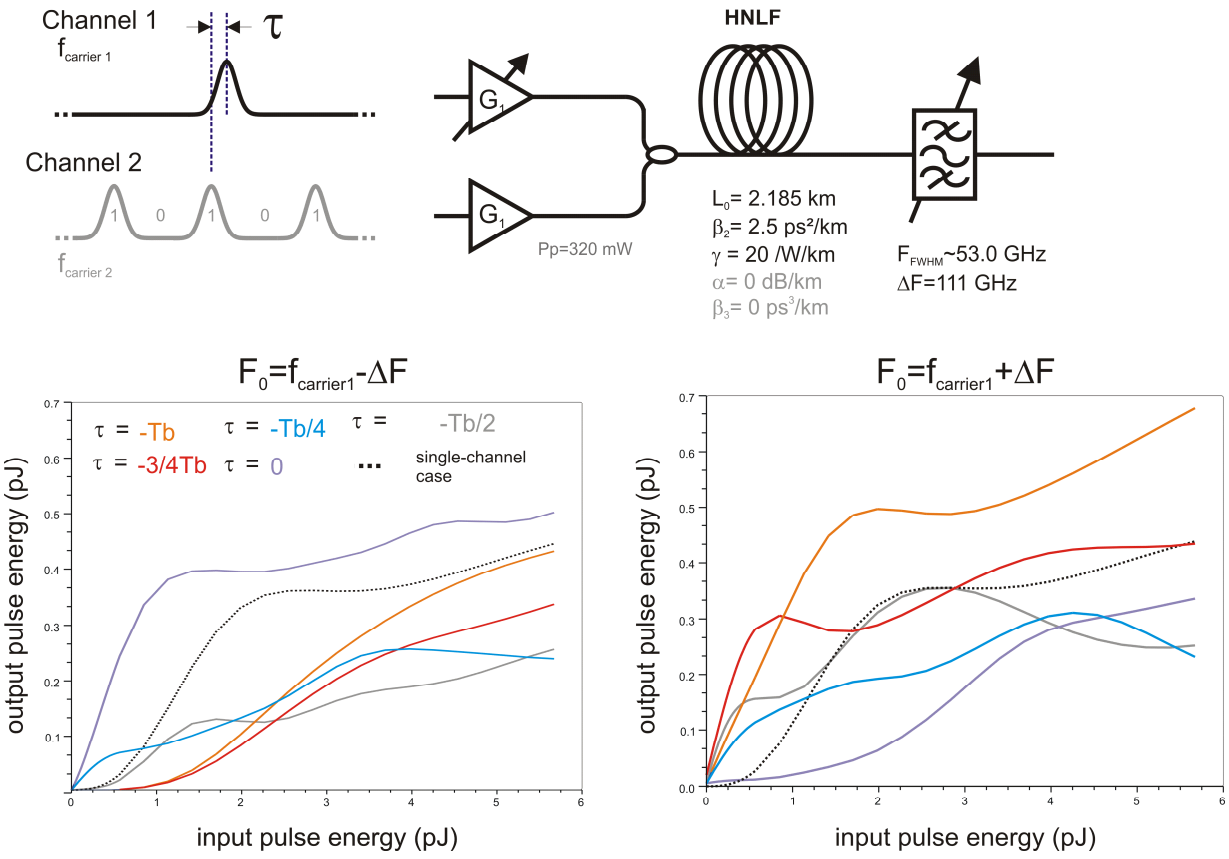

Figure IV-1: Impact of the inter-channel nonlinearities on the regeneration performance. Top: regenerator set-up considered for the modelling. Bottom: Comparison of the computed power TF for channel 1 as function of the output filter position F_0, and the initial relative delay between Channel 1 and 2. Incoming power of Channel 2 remains unchanged and is set so that the marks input peak power corresponds to P_{pin}^1. The channel separation is set so that $f_{carrier2}=f_{carrier1}+600$ GHz.

As reported in Chapter II, several solutions based on dispersion managed solutions have therefore been proposed to mitigate the large inter-channel nonlinearities by providing a relatively complex set-up using either a multi-fibre assembly [96] or dispersion decreasing fibre [21]. One of the motivations of this work reported in this manuscript was to investigate whether it was possible to propose a scheme based on a single and continuous piece of fibre, since it was definitely of an easier implementation and operation.

1.2. Pulse walk-off rate vs. single channel optical regenerator design

In light of the previous paragraph, two solutions can be proposed to extend the single channel optical regenerator to a multi-channel scheme either by decreasing the interaction time among pulses of adjacent channels and/or control of the polarization states of the individual channels. This approach implicitly assumes that a large statistical averaging effect shall take place so that interaction time between adjacent pulses is sufficiently reduced to minimize any pattern-dependence on the spectral broadening and will consequently force a given pulse to interact with *a large number* of co-propagating pulses.

The number of interacting pulses can be estimated by the walk-off rate W which represents the spatial separation rate at which two optical carriers moves away from each other while propagating within the optical fibre. Denoting the two optical carrier frequencies with ω_1 and ω_2, W is defined as the inverse of the group velocity difference $\left|\beta_1(\omega_1)-\beta_1(\omega_2)\right|$ and is expressed in km/ps. For convenience, a walk-off length L_W can be defined as the spatial separation over a prescribed duration (for instance the pulse duration T_0). L_W is thus defined as:

$$L_w = \frac{T_0}{W} = \frac{T_0}{|\beta_1(\omega_1) - \beta_1(\omega_2)|} \approx \frac{T_0}{|\beta_2.(\omega_1 - \omega_2)|} = \frac{T_0}{|\beta_2.\Delta\omega_{1-2}|} \qquad \textit{(IV-1)}$$

Where $\Delta\omega_{1\text{-}2}$ is the spectral separation between the two optical frequencies ω_1 and ω_2

The smaller the L_W, the faster the pulses are moving away from one another. From additional manipulation of Equation *(IV-1)*, one can deduce Equation *(IV-2)*, where the normalised length ratio L/L_D has been introduced.

$$\frac{L}{L_W} \approx T_0 |\Delta\omega_{1-2}| \frac{L}{L_D} \qquad \textit{(IV-2)}$$

The number of interacting pulses can be easily assessed using Equation *(IV-2)*. Considering two 33% duty-cycle RZ optical signals running at 40 Gb/s (T_0=5ps) with optical carriers spectrally separated by 600 GHz, we obtained an L/L_W ratio of $1.2*\pi$ when operating with a realistic L/L_D figure of 0.2. This ratio corresponds to a walk-off rate W~19 ps/km. Such a value is undeniably small as compared to the corresponding bit-slot period (T_b=25 ps), and typical fibre lengths would lead to the same pattern-dependence on the power transfer function as highlighted in the previous part: one pulse would only interact with at most two pulses of the adjacent channels if the fibre is one kilometre long.

The same conclusion holds if the spectral separation is increased as illustrated in Table IV-1, in which we have reported the walk-off W expressed as a fraction of the bit-slot duration per km of fibre considering different carrier separations and bit-rates.

From Table IV-1, the extension of the single-fibre arrangement of the Mamyshev regenerator within a single piece of fibre is therefore extremely limited due to the extremely low walk-off rate induced by the chromatic dispersion and the spectral separation of the channel. Owing to the scaling rules applicable to the single channel design rules, this conclusion holds whatever the dispersion value of the optical fibres used.

Signal Bit-Rate	**Bitslot duration**	**T_0**	**Walk-off rate for ΔF=600GHz**	**Walk-off rate for ΔF=900GHz**	**Walk-off rate for ΔF=1200GHz**	**Walk-off rate for ΔF=1800GHz**	**Walk-off rate for ΔF=2400GHz**
Gb/s	ps	ps	W/T_b (/km)	W/T_b (/km)	W/T_b (/km)	W/T_b (/km)	W/T_b (/km)
40	25.0	5.0	0.75	1.13	1.51	2.26	3.0
80	12.5	2.5	0.38	0.57	0.75	1.13	1.5
100	10.0	2.0	0.30	0.45	0.60	0.91	1.2
130	7.7	1.5	0.23	0.35	0.46	0.70	0.9

Table IV-1: Walk-off rate as a function of the channel separation and bit-rates. Rate is expressed as the fraction of bit-slot duration Tb per kilometre of HNLF fibre. Results are reported for a 33% duty cycle RZ signal.

In conclusion, no sufficient averaging effect can be obtained to mitigate XPM-induced cross-talk simply by increasing the chromatic dispersion value of the fibre. The chromatic dispersion and walk-off rate must therefore be de-coupled to guarantee an efficient mitigation of the inter-channel nonlinearities (arising from the walk-off rate) without compromising the role of the chromatic dispersion in the spectral broadening and subsequent power transfer function characteristics.

2. Counter-propagating scheme

In this part, I report the first mitigation scheme to enable processing of two optical signals within the same optical fibre. This scheme is referred to as the counter-propagating scheme and consists in propagating the two optical signals in opposite directions within the same optical fibre. In doing so, the walk-off rate is maximised - resulting in a very strong mitigating effect.

I highlight however the presence of a new cross-talk source arising from the Rayleigh backscattering due to the counter-propagating signal. I numerically and experimentally assess the level of this new source of cross-talk and demonstrate that is sufficiently low so that no detrimental effect should be anticipated.

The applicability of the scheme is experimentally demonstrated at various repetition rates ranging from 10 Gb/s through 40 Gb/s, and finally 130 Gb/s, taking benefit of the single-channel design rules.

2.1. Principle of operation

Figure IV-2 depicts the regenerator set-up based on a counter-propagating architecture. The scheme has the same design complexity as the single-channel regenerator, and can be envisioned as the superposition of two single-channel optical regenerators with common input/output ports. Two optical circulators on each end of the HNLF are used to feed and extract the input and output signals.

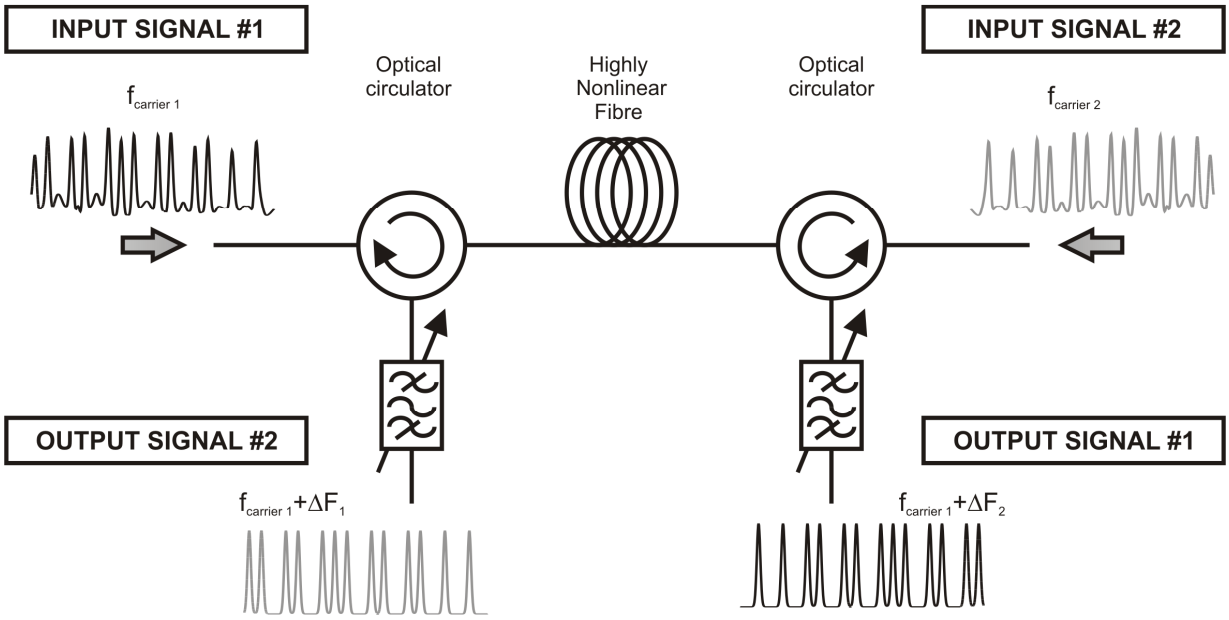

Figure IV-2: Schematic of the counter-propagating optical regenerator based on SPM spectral broadening and offset filtering.

One major advantage of the approach relies in the high similarity that can be anticipated for the design, operating conditions and more generally performance as compared to the single-channel case.

An interesting feature here lies in the extremely high relative pulse walk-off as compared to the co-propagating case. Whereas the walk-off time between two optical frequencies arises from the difference between group velocities in the co-propagating case, the counter-propagating scheme permits one to benefit from the summation of the group velocities. Given the small contribution of the chromatic dispersion to the group velocity, a complete de-correlation between the walk-off time and the chromatic dispersion is achieved, and W reduces to:

$$W = \frac{1}{\beta_0(\omega_1) + \beta_0(\omega_2)} \approx 2\frac{n_{eff}(\omega_1)}{c} \qquad \text{(IV-3)}$$

Where n_{eff} is the effective index of the fundamental mode at frequency ω_1.

For silica-based fibres (n_{eff}~1.45 at 1550 nm), the expected walk-off rate W is effectively 10 ns/m, whatever the channel separation. As compared to the co-propagating case (typical value of ~20 ps/km for a 33% RZ signal operating at 40 Gb/s), the walk-off rate is therefore increased by a factor of 5.10^5!

Such an arrangement is straightforward to propose. Even though a maximum number of just two optical channels can be processed, the scheme has some benefit - mostly arising from the possibility to independently operate the two optical channels taking into account the spectral properties of the HNLF and the single-channel design.

This solution is highly similar to the dual-stage single channel Mamyshev optical regenerator incorporating a bi-directional scheme as reported in [133]. The second regenerator was indeed implemented by counter-propagating the output signal of the first regenerator stage within the same fibre, to provide wavelength-conversion free operation.

2.2. Experimental demonstration for 2x10 Gb/s 2x40 Gb/s optical channels

Two experimental set-ups were investigated resulting in two sets of results achieved at 10 Gb/s and at 40 Gb/s. The first set-up was used to experimentally assess the cross-talk level arising from the Rayleigh backscattering (as shown in Figure 5 of Publication C) and the second to demonstrate the feasibility of the scheme in a case employing a realistic 25% duty cycle optical pulse train running at 40 Gb/s and to confirm the absence of any deleterious inter-channel cross-talks (see Figure 1 of Publication D).

The two experiments used the same operating conditions for the channel allocation and offset filter positions: the two channels were separated 5 nm apart, and the positions of the offset filters were set so that the initial carrier wavelength separation was preserved as reported in Figure 1 of Publication D.

The experimental assessment of the regenerating characteristics was conducted by measuring the static power TF function of the two channels in the absence and the presence of the interfering channel. The average input power of the interfering channel was set in order to operate on an appropriate portion of the corresponding TF for the mark pulse level. Results are reported in Figure IV-3 with corresponding nominal input power for the mark pulse levels of P1 and P2.

Some differences in the TF shapes of the two channels are observed, and are attributed to the difference in the respective pulse durations used for the two channels, as well as a slight additional contribution arising from the different chromatic dispersion value at the two input carrier wavelengths.

No differences in the static power TF functions were observed in the presence or absence of the interfering channel, which confirms that the spectral broadening was not perturbed by inter-channel nonlinear effects. However at low input power, a constant output levels was achieved for the TF in the presence of the interfering channel, and resulted in a decrease in the maximum output extinction ratio as compared to the single-channel case. For the 40 Gb/s experiment, the reduction is however limited for the second Channel, as the output extinction ratio is slightly reduced to 31.2 dB – as compared to an initial value of 34.8 dB for an initial input extinction ratio of 10 dB as reported in Figure IV-3.

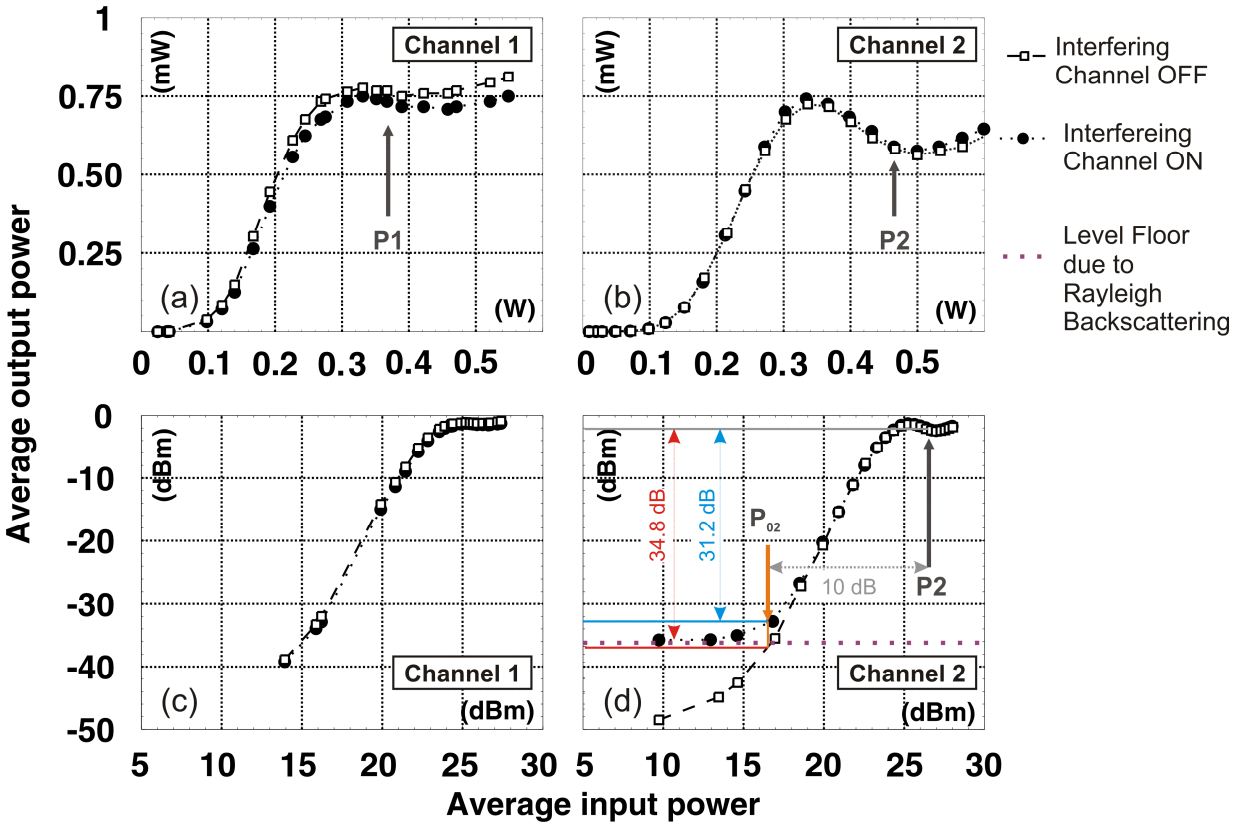

Figure IV-3: Power transfer functions (in linear (a-b) and log (c-d) scales) of Channel 1 & 2 in the presence (channel ON) and in the absence (channel OFF) of the counter-propagating signal.

Finally, the performance was confirmed with Bit-Error Rate (BER) measurements. No significant deterioration associated with this output extinction ratio decrease was observed. As compared to the single-channel case, a power penalty of less than 0.1 dB at a BER=10^{-9} was reported at the output of the optical regenerator for the two channels (as reported in the BER plot in Figure 4(a) of Publication D). These results confirm i) the absence of excessive inter-channel nonlinearities within the HNLF, and ii) the absence of significant degradation resulting from the presence of the power floor level due to Rayleigh scattering from Channel 2.The reshaping capacity of the optical

regenerator in a dynamic environment was not studied due to the lack of realistically degraded optical signals. It was however anticipated that the performance would have been highly similar to the single-channel case.

The origin of the power floor at low input power levels can be attributed to an additional spectral contribution arising from the backscattering of the counter-propagating signal along the HNLF fibre because of Rayleigh backscattering [134]. In Figure IV-4(a), we report the difference in the various spectra that was observed at one end of the HNLF fibre. Depending on the spectral allocation and offset filter position, we highlight that a fraction of this backscattering signal can fall within the filter bandwidth and results in the presence of a constant power floor on the power TF.

The detailed analysis of this cross-talk constitutes the second contribution of this study and theoretical details as well as modelling consideration are reported in Section 3 of Publication C. As depicted in Figure IV-4(b), the corresponding spectral extent of the backscattered signal exhibits a dependence on the average input power of the signal. As expected, the strength of the contribution of the backscattered signal has a strong dependence on the fibre scattering properties, the operating parameter settings (fibre properties, length, and input power) and the wavelength separation of the incoming channels. Much attention is therefore paid to the experimental characterization of the Rayleigh backscattering cross-talk level and its potential impact on the output-extinction ratio with respect to the operating parameters. I proposed a numerical model, which allows computation of the backscattered spectrum. Excellent agreement between the numerical model and experimental data was achieved. For the considered fibre, the

backscattering level was found to be approximately 30 dB below the transmitted signal when considering the operating parameters of the 40 Gb/s experiment.

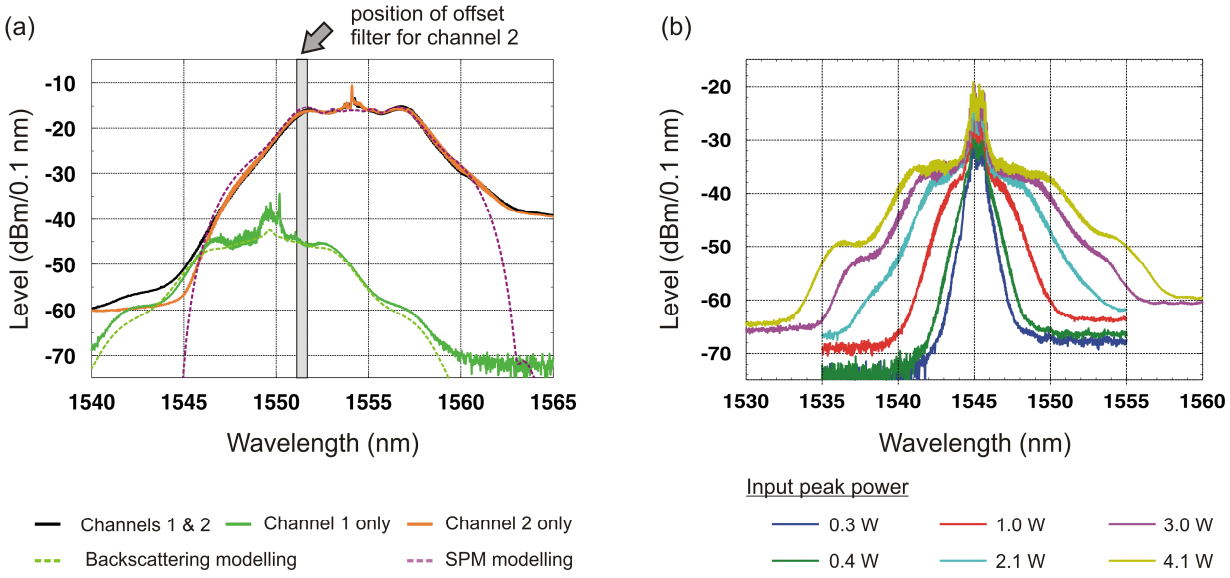

Figure IV-4: (a) Spectra measurement at the Channel 2 output port of the backscattering contribution of Channel 1 alone, of the Channel 2 only spectrum and when both channel are present. The grey-shaded area, represent the optical filter position and bandwidth (δλ=2.8 nm). Modelled Rayleigh backscattering and SPM spectra are reported. (b) Influence of the input peak power of a PRBS sequence of marks pulses on the Rayleigh backscattering spectra. Experimental data correspond to the 10 Gb/s experiment.

2.3. Conclusion

In the previous section, we have examined the possibility to use a counter-propagating scheme to simultaneously regenerate two optical channels within the same optical fibre. The scheme is highly efficient to mitigate the inter-channel nonlinearities by maximising the walk-off between the two channels. The scheme also preserves the benefits of the single-channel design rules, such

that the expected performance of the multi-channel case shall be very similar to that of the single-channel case.

The scheme introduces another source of cross-talk arising from the Rayleigh backscattering contribution that is of a much higher level in HNLF fibre as compared to standard fibre. The impact of the contribution was nevertheless found not to introduce any significant performance deterioration as compared to the single-channel case for the reported operating parameters settings.

The major drawback lies in the fact that only 2 channels can be regenerated using this scheme in isolation.

3. Polarization-multiplexing scheme

In this section, we report the second scheme we have proposed to simultaneously process 4 channels within the same piece of optical fibre. The principle of the scheme is to co-propagate two linear cross-polarized polarized channels within a Polarization-maintaining highly nonlinear fibre (PM-HNLF). The scheme takes benefit from the differential group delay (DGD) existing between the two polarization fibre axes to provide a rapid walk-though of the channels and a sufficient mitigating effect. By adding to this scheme the counter-propagating approach previously proposed, the channel capacity can be doubled up to 4 channels.

Based on modelling work, the existence of a minimum DGD value was identified that allowed sufficient mitigation of the inter-channel nonlinearities for the co-propagating channels.

Finally, we experimentally demonstrated the possibility to simultaneous process 4 channels at 10 Gb/s using a PM-HNLF prototype gratefully provided by the Furukawa Electric Company.

3.1. Principle of operation

The rationale of the scheme takes benefit from the dependence of the cross-modulation strength versus that of SPM on the polarization states of co-propagating pulses [45, 135]. The most deleterious case corresponds to linear and co-polarised beams for which XPM is maximised and is two-fold higher than the SPM term [45, 124] – in absence of any walk-off contribution. Conversely the XPM contribution is minimum for linear and orthogonal polarization states leading to a three-fold reduction of the XPM non-linear phase as compared to the linear co-polarised case [45]. In addition, the phase matching conditions for FWM are also cancelled.

Figure IV-5 depicts the schematic of the proposed implementation, and relies on the use of a polarization maintaining (PM) fibre. Aligning the polarization states of the incoming channels onto the neutral axis of the PM fibre ensures that the polarization states of the incoming channels are preserved during propagation along the fibre. Polarization beam combiners are used to feed (and extract) the orthogonal linear polarization components and align the input state of polarization onto the polarization axis of the fibre.

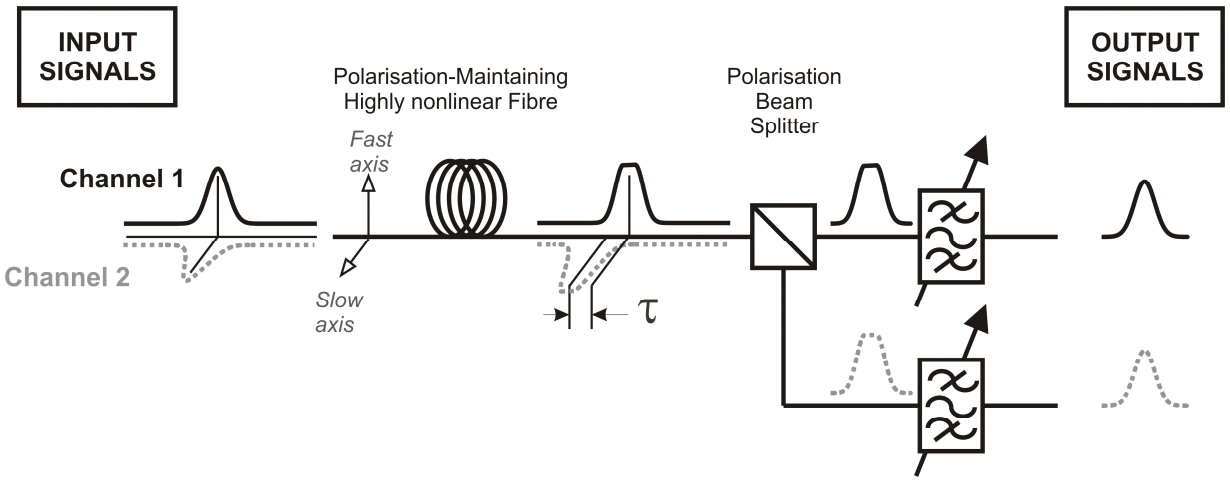

Figure IV-5: Schematic of the polarization- multiplexing optical regenerator based on SPM spectral broadening and offset filtering.

As a maximum three-fold reduction of the XPM-induced cross-talk might not be sufficient to satisfactorily mitigate the inter-channel nonlinearities, the additional mitigating effect stemming from the DGD between the axes of the PM fibre can also be exploited. This DGD arise from the anisotropy of the spatial refractive index profile of the fibre resulting in different group velocities between the two fibre axes that one distinguishes as a fast and a slow axis. The DGD per length unit is expressed from the birefringence parameter B and the light velocity c:

$$DGD(\omega) = \frac{B(\omega)}{c} = \frac{n_{slow}(\omega) - n_{fast}(\omega)}{c} \qquad \text{(IV-4)}$$

Where: n_{slow} and n_{fast} are the effective indices of the optical eigen-modes along the fast and slow axes of the fibre at frequency ω.

With typical birefringence B values ranging from 10^{-4} up to 10^{-3}, the corresponding DGD ranges from a few tenths ps/m up to 3.5 ps/m. These values are more than two orders of magnitude higher than the typical value 25 ps/km arising from the contribution of the group velocity difference for our 40 Gb/s bit-rate case study.

3.2. Numerical investigation

I numerically assessed the existence of the minimum DGD value required to limit XPM-induced output fluctuations on the power transfer function, especially at low input power. As the nonlinear pulse propagation requires a vectorial solution of the NLSE, these studies were completed using a commercial software: VPItranmission from VPI photonics [136].

Figure IV-6 (a) depicts the system investigated. The parameters of the PM-HNLF are reported in Table IV-2. The operating parameters of the regenerator were set so that the power TF of Figure IV-6 (b) is obtained for Channel 1 in the absence of the interfering Channel 2. The input pulse width was 8.25 ps and output filter offset was -0.8 nm. The output power fluctuations at position A along the TF was then computed in the presence of Channel 2 which was cross-polarised relative to Channel 1. The optical signal consisted of alternating marks and spaces for which the average power was set to correspond to the input power of point B (1.5 W peak power). Figure IV-6 (b) represents the relative output power fluctuations as a function of the initial temporal delay τ_0 between the two channels and the fibre birefringence B.

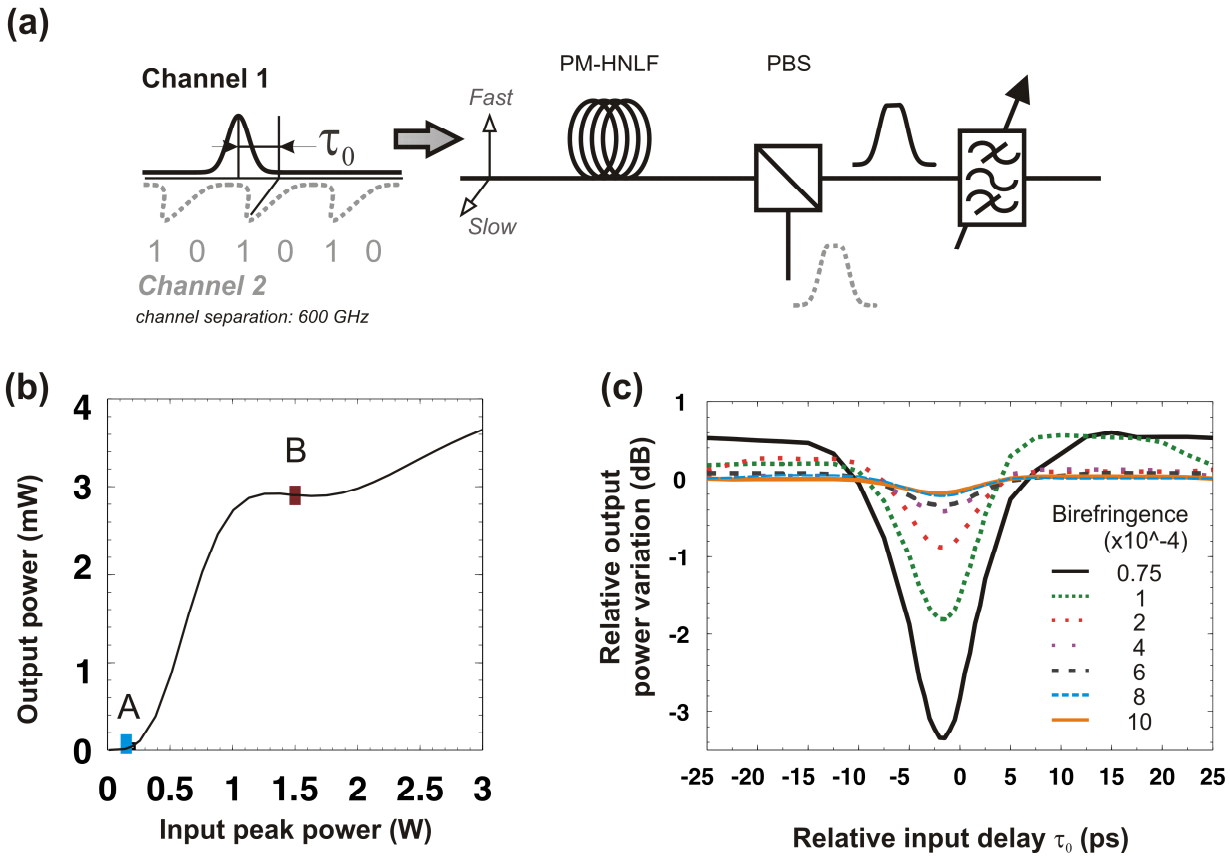

Figure IV-6: (a) Schematic used for the numerical modelling (with initial delay τ_0>0). (b) Static power TF for Channel 1 as a function of input power. Input peak power for position A is set at 10 % of the nominal input peak power corresponding to point B. (c) Influence of birefringence on the TFs variation obtained at point A of the TF (b) as a function of the initial delay τ_0 (pulse peak power of interfering channel set at 1.5 W). Variations are computed from the single-channel scenario (i.e. in the absence of the interfering channel).

Fibre Type	Chromatic Dispersion	Chromatic Dispersion slope	γ	α	L	Effective length	Birefringence	Extinction Ratio
	ps/nm/km	ps/nm²/km	/W/km	dB/km	m	m	-	dB
PM-HNLF	-4.2	0.0046	20	3.2	1,000	707.4	$6.9\ 10^{-4}$	30 (/100m)

Table IV-2: Properties of the Polarization maintaining highly nonlinear fibre used in the experiment (Values are reported at 1550 nm).

It is clear that increasing the birefringence (and equivalently the DGD) decreases the sensitivity to XPM-induced cross-talk and also diminishes the dependence on the initial temporal delay between channels. For the worst- case scenario that corresponds to when the output power fluctuation are maximum (τ_0~2 ps), a minimum birefringence B value of $3.9\ 10^{-4}$ (DGD value of ~1.3 ps/m) is required to limit the XPM –induced output power fluctuations to within +/- 10% at input power A as compared to the single channel case.

3.3. Experimental demonstration at 4x10 Gb/s

The scheme was experimentally assessed by considering 4x10 Gb/s channels case. A suitable fibre with a birefringence value as high as $6.9\ 10^{-4}$ was provided by Furukawa Electric Company. The fibre combined the structure of a PANDA fibre with an elliptical core [137]. The properties of the PM-HNLF are reported in Table IV-2.

Because of the record DGD value of 2.3ps/nm at 1550 nm, a huge mitigating effect was expected. The fibre parameters were appropriate to set-up a device with equipment available in the laboratory considering an output filter detuning of -0.8 nm. The optical power budget was nevertheless very tight when considering all of the contributing optical losses brought by the different optical components. This explains why we were only able to consider a 0.6 nm offset detuning for one of the four channels.

The corresponding set-up is depicted in Figure IV-7. Four 10 Gb/s channels were employed, allocated using a 600 GHz channel grid. The channel allocation to feed the two fibre ports was not symmetrical: the two inner carrier wavelengths channels were fed into the same port, whereas the two remaining channels were fed to the second fibre port. This was done to allow the study of closely spaced co-propagating channels. As the clock signal used to generate the pulse pattern was the same for the four channels, optical delay lines were employed to control the relative temporal delay between the co-propagating channels. By setting the optical delay lines, it was possible to operate in the worst-case scenario regime to ensure and maximize adjacent pulse interaction. The optical delay lines were adjusted to exacerbate the spectral distortions at the output of the fibre when the two co-propagating channels were co-polarized on the same polarization axis of the PM-HNLF.

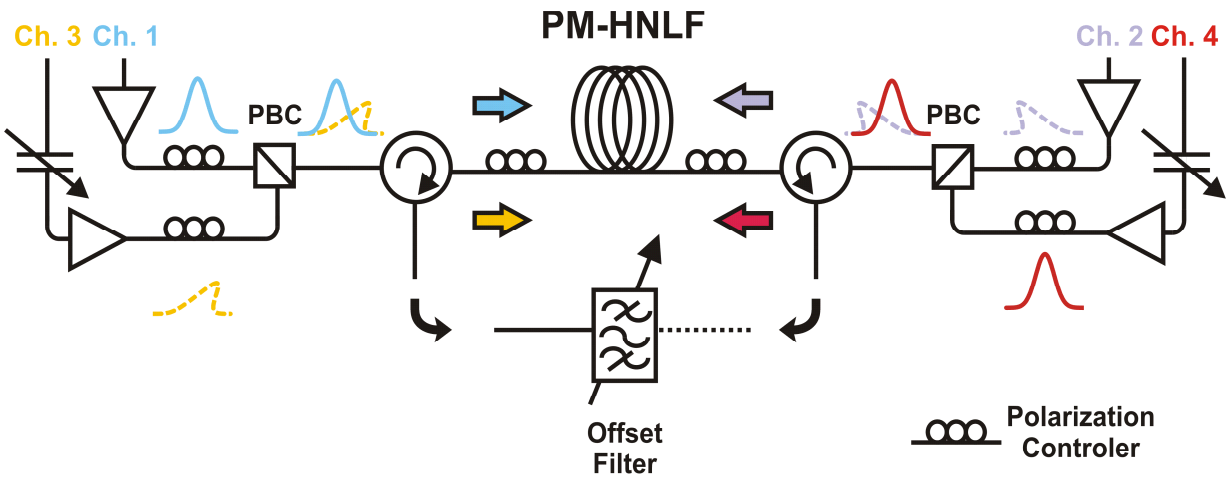

Channel	1	2	3	4
PRBS	$\overline{\text{PRBS 2}}$	PRBS 2	PRBS 1	$\overline{\text{PRBS 1}}$
Input wavelength (nm)	1545.5	1549.9	1554.6	1561.8
Filter Offset (nm)	-0.8	-0.8	-0.8	-0.6

Figure IV-7: Schematic of the experimental set-up used to simultaneously process 4x10 Gb/s channels within the PM-HNLF.

Similar to the counter-propagating approach, the proposed scheme was assessed by successive characterization of the static power TF in the presence and in the absence of an interfering channel, and finally through BER measurements. A power penalty (as low as 0.1 dB) as compared to the back-to-back is reported for the 4 channels. By selecting a sub-optimum modulation bias current at the transmitter, an artificial degradation of Channel 3 was achieved. The regenerator showed good performance and demonstrated that up to 1.8 dB power penalty could be compensated for in the presence of the three interfering channels (as reported in Fig.5 of publication E).

3.4. Conclusion

In this section, we have examined the possibility to use a polarization multiplexing scheme to simultaneously regenerate two co-propagating optical channels within the same optical fibre. By exploiting the huge DGD values existing between the two polarization axes of a PM-HNLF, we were able to demonstrate the applicability of the scheme and demonstrate that excellent mitigation could be obtained by exploiting the polarization walk though and DGD to minimize inter-channel cross-talk.

By combining this scheme with the counter propagating solution, a maximum number of 4 channels can be simultaneously processed within the same piece of optical fibre. I experimentally demonstrated the applicability of the scheme in a 4x10 Gb/s transmission experiment.

4. Experimental demonstration for 2X130 Gb/s channels

In the framework of the European project, the counter-propagating scheme was implemented in the final demonstrator of the optical grooming switch. The optical regenerator demonstrated the processing of two 130 Gb/s optical channels.

The experimental results are reported in the last Publication F given at the end of this manuscript (see page 145), and are published under the following reference:

F.Parmigiani, P.Vorreau, L.Provost, K.Mukasa, M.Takahashi, M.Tadakuma, P.Petropoulos, D.J.Richardson, W.Freude, J.Leuthold, **"2R regeneration of two 130 Gb/s channels within a single fibre",** OFC 2009 San Diego 22-26 Mar 2009 JThA56.

Thanks to the low chromatic dispersion exhibited by the HNLF fibre, a power budget of ~25dBm was necessary for each channel. Because the two channel separation was large as compared to the output filter detuning (2 nm), no degradation due to the Rayleigh backscattering was reported on the BER measurement. Since the separation between the two channels was 14 nm, an HNLF having a reduced chromatic dispersion slope was required to limit the spectral asymmetry in the broadened spectra of the two channels. The HNLF used in the experiment was gratefully provided by The Furukawa Electric Company. The fibre properties are reported in Table IV-3.

Fibre Type	**Chromatic Dispersion**	**Chromatic Dispersion slope**	**γ**	**α**	**L**	**Effective length**
	ps/nm/km	ps/nm²/km	/W/km	dB/km	m	m
HNLF	-0.31	0.0031	22	1.21	310	297

Table IV-3: Properties of the highly nonlinear fibre used in the experiment (values are reported at 1550 nm).

5. Summary and discussion

In this chapter, we have examined the possibility to extend the SPM spectral broadening and offset filtering-based optical 2R regenerator so that several channels can be processed within the same piece of fibre. First I have reviewed the various sources of cross-talk and how they impact the reshaping performance of the regenerator. Using the design rules derived for the single-channel case, it was then demonstrated that a substantial decrease in the nonlinear interactions between co-propagating adjacent pulses could be obtained by changing the walk-off rate in a single piece of fibre in the normal dispersive regime.

I therefore proposed to implement a counter-propagating scheme allowing the processing of two optical channels. Doing so, an additional source of cross-talk due to Rayleigh backscattering was observed. The cross-talk level was sufficiently low to ensure that the scheme was still applicable. However, based on modelling work, we calculated how this Rayleigh scattering was expected to scale with respect to the operating parameter of the optical regenerator and the signal bit rate.

I proposed to use polarization multiplexing to double the processing capacity thanks to a PM-HNLF, in which co-propagating channels are cross-polarized and aligned on the orthogonal polarization axis of the fibre. Numerical modelling work demonstrated the applicability of the scheme at 40Gb/s. Because of the relative high chromatic dispersion of the available fibre, the power budget was limited so that only a 4x10 Gb/s experiment was demonstrated.

Finally, we reported the experimental demonstration of simultaneous processing of 2x130Gb/s optical signals within the same optical fibre using the counter-propagating scheme.

Chapter V: Conclusions and future directions

1. Conclusions

All-optical regeneration allows for flexible optical-signal processing by manipulating and restoring the signal quality directly in the optical domain as compared to the conventional approach of O/E/O circuits, which involves processing the signal in the electrical domain and requires pre- and post-optoelectronic conversion. Numerous optical regeneration schemes have been proposed and experimentally demonstrated over the last decade, but only a few addressed the scalability issue when numerous optical WDM channels are to be processed and which restricts the practical benefits of the all-optical regeneration techniques.

In this thesis, we have investigated several solutions to extend one particular all-optical 2R regenerator to operate in the multi-channel regime. The work proposed in this thesis was thus divided into several parts. First, the single channel 2R all-optical regenerator proposed by P. Mamyshev has been studied allowing one to derive some scaling rules linking the physical parameters of the optical regenerator parts to the optical performance and regeneration output

characteristics. The study permits an assessment of the roles of each physical parameter defining the nonlinear gate (i.e. chromatic dispersion, nonlinear coefficient and optical loss). Doing this, the design of the optical regenerator was drastically simplified.

The extension to a multi-channel processor was then proposed using two simple but efficient mitigation schemes to alleviate for the inter-channel effects occurring within the nonlinear fibre. The first scheme consists of counter propagating two optical signals within the same fibre and is highly similar to the bi-directional architecture of the single channel regenerator reported in [138]. The second scheme exploits the reduction of the inter-channel cross-talk arising from the differential group delay-induced walk-off between two co-propagating signals in a polarization-maintaining highly nonlinear fibre. The combination of the former and latter schemes allows up to 4 optical channels to be processed within the same optical fibre.

For each of the mitigating schemes reported in this work, I report that the inter-channel cross-talk was indeed sufficiently mitigated allowing the signal to be processed as in the single-channel case. An additional cross-talk source arising from the Rayleigh backscattering was identified and found not to be highly problematic for the reported experimental configurations and signal bit-rates.

The main advantages of the bi-directional and polarization multiplexing schemes is that they exhibit a high similarity and therefore should demonstrate similar performance as for the corresponding single-channel case, even if no experimental checking has been done using realistically degraded optical signals. The proposed approach has thus been implemented in the framework of the European Project TRIUMPH to process 2x130 Gb/s channels. We believe this

approach is easier in term of optical design as compared with other unidirectional schemes [96, 98, 99, 139]. The unidirectional scheme on the other hand, benefits from not imposing any hard limits on the maximum number of channels, but is extremely difficult to scale up as the bit-rate is increased due to the limitations caused by the inter-channel XPM.

2. Future directions

The proposed solutions offer varying degrees of resilience to nonlinear cross-talk and differing operational advantages/drawbacks. From a practical and cost perspective, co-propagating schemes are likely to be preferable, although the operation of such systems at very high bitrates (>100 Gb/s) has still to be demonstrated. It is also to be appreciated that the best choice for a given transmission system will depend on the detailed nature of the impairments – for example the final answer may be different depending on whether the system is OSNR or nonlinearity-limited. Such questions have been considered in the case of single channel devices, but similar considerations in the multi-channel case are still limited. Among the critical issues we have identified in our work is the sensitivity of SPM-based schemes to input pulse duration/shape and which may dictate the need for dynamic devices capable of conditioning the individual channels at the regenerator input (e.g. chirp compensation, variable optical attenuation and pre-filtering). However, whatever the ultimate solution, the scope for scaling to higher channel counts is intrinsically limited by the requirement for large inter-channel spacing in order to accommodate the necessary spectral broadening.

Even if the all-optical regeneration could benefit from their extremely low response-time to process very high-bit rate channel as compared to conventional electronics circuits, the large

scale adoption of such all-optical technologies still remains limited, mostly because of their inability to cope with high-channels count systems and also field-related issues (device footprint, system stability, reliability). The development of more compact optical nonlinear gates driven either by optical chip concepts with nonlinear glass substrates [140], or with the development of new highly nonlinear media suitable to operate at high bit-rate [141], could eventually bring benefit to all-optical applications technologies.

Addressing the simultaneous processing of all-optical regeneration of phase-encoded signals could also be beneficial as such modulation format are envisaged with great interest for next-generation high capacity transmission systems.

Appendices

1. Publication A

Publication A was published under the following reference:

L.Provost, C.Finot, P.Petropoulos, K.Mukasa, D.J.Richardson, ”**Design scaling rules for 2R-optical SPM-based regenerators**”, Optics Express 2007 Vol.15 pp.5100–5113.

Design scaling rules for 2R-optical self-phase modulation-based regenerators

Lionel Provost, Christophe Finot, Periklis Petropoulos, Kazunori Mukasa, and David J. Richardson

Optoelectronics Research Centre, University of Southampton, Southampton, SO17 1BJ, United-Kingdom
lap@orc.soton.ac.uk

Abstract: We present simple scaling rules to optimize the design of 2R optical regenerators relying on Self-Phase Modulation in the normal dispersion regime and associated offset spectral filtering. A global design map is derived which relates both the physical parameters of the regenerator and the properties of the incoming signal to the regeneration performance. The operational conditions for optimum noise rejection are identified using this map and a detailed analysis of the system behavior under these conditions presented. Finally, we demonstrate application of the general design map to the design of a regenerator for a specific 160 Gb/s system.

OCIS codes: (060.4370) Fibre optics and optical communications: Nonlinear optics, fibers; (060.4510) Fibre optics and optical communications: Optical communications; (060.7140) Fibre optics and optical communications: Ultrafast processes in fibers.

References and Links

1. R. J. Essiambre, B. Mikkelsen, and G. Raybon, "Intra-channel cross-phase modulation and four-wave mixing in high-speed TDM systems," Electron. Lett. **35**, 1576-1578 (1999).
2. P. V. Mamyshev, "All-optical data regeneration based on self-phase modulation effect," in *Proc. European Conference on Optical Communications (ECOC'98)* (1998), p. 475.
3. G. Raybon, Y. Su, J. Leuthold, R. Essiambre, T.-H. Her, C. Joergensen, P. Steinvurzel, K. Dreyer, and K. Feder, "40 Gb/s pseudo linear transmission over one million kilometers," in *Proc. Optical Fiber Communications (OFC'02)* (Anaheim CA, 2002), p. 42.
4. M. Daikoku, N. Yoshikane, T. Otani, and H. Tanaka, "Optical 40-Gb/s 3R Regenerator With a Combination of the SPM and XAM Effects for All-Optical Networks," J. Lightwave Technol. **24**, 1142-1148 (2006).
5. N. Yoshikane, I. Morita, T. Tsuritani, A. Agata, N. Edagawa, and S. Akiba, "Benefit of SPM-based all-optical reshaper in receiver for long-haul DWDM transmission systems," IEEE J. Sel. Top. Quantum Electron. **10**, 412-420 (2004).
6. Y. Su, G. Raybon, R. J. Essiambre, and T.-H. Her, "All-optical 2R regeneration of 40-Gb/s signal impaired by intrachannel four-wave mixing," Photon.Technol. Lett. **15**, 350 (2003).
7. T.-H. Her, G. Raybon, and C. Headley, "Optimization of pulse regeneration at 40 Gb/s based on spectral filtering of self-phase modulation in fiber," Photon.Technol. Lett. **16**, 200-202 (2004).
8. M. Rochette, L. B. Fu, V. Ta'Eed, D. J. Moss, and B. J. Eggleton, "2R Optical Regeneration: An All-Optical Solution for BER Improvement," IEEE J. Sel. Top. Quantum Electron. **12**, 736-744 (2006).
9. P. Petropoulos, T. M. Monro, W. Belardi, K. Furusawa, J. H. Lee, and D. J. Richardson, "2R-regenerative all-optical switch based on a highly nonlinear fiber," Opt. Lett. **26**, 1233-1235 (2001).
10. J. H. Lee, T. Nagashima, T. Hasegawa, S. Ohara, N. Sugimoto, Y. G. Han, S. B. Lee, and K. Kikuchi, "Output Performance Investigation of Self-Phase-Modulation-Based 2R Regenerator Using Bismuth Oxide Nonlinear Fiber," IEEE Photon.Technol. Lett. **18**, 1296-1298 (2006).
11. F. Parmigiani, S. Asimakis, N. Sugimoto, F. Koizumi, P. Petropoulos, and D. J. Richardson, "2R regenerator based on a 2-m-long highly nonlinear bismuth oxide fiber," Opt. Express **14**, 5038-5044 (2006).
12. X. Liu, C. Xu, and W. H. Knox, "Characteristics of all-optical 2R regenerator based on self-phase modulation in high-nonlinear fibers," in *Proc. Conference on Lasers and Electro-Optics (CLEO'02)*(2002), pp. 612-613.
13. A. G. Striegler and B. Schmauss, "Analysis and Optimization of SPM-Based 2R Signal Regeneration at 40 Gb/s," J. Lightwave Technol. **24**, 2835-2843 (2006).
14. M. Matsumoto, "Performance analysis and comparison of optical 3R regenerators utilizing self-phase modulation in fibers," J. Lightwave Technol. **22**, 1472 (2004).

#78247 - $15.00 USD Received 19 Dec 2006; revised 14 Mar 2007; accepted 20 Mar 2007; published 12 Apr 2007

15. P. Johannisson and M. Karlsson, "Characterization of a self-phase-Modulation-based all-optical regeneration system," Photon.Technol. Lett. **17**, 2667 (2005).
16. L. Provost, C. Finot, P. Petropoulos, and D. J. Richardson, "Design Scaling Laws for Self-Phase Modulation-based 2R-Regenerators," in *Proc. European Conference on Optical Communications (ECOC'06)* (Cannes, 2006), p. We 4.3.2.
17. M. Nakazawa, H. Kubota, and K. Tamura, "Random evolution and coherence degradation of a high-order optical soliton train in the presence of noise," Opt. Lett. **24**, 318-320 (1999).
18. R. Hainberger, T. Hoshida, S. Watanabe, and H. Onaka, "BER estimation in optical fiber transmission systems employing all-optical 2R regenerators," J. Lightwave Technol. **22**, 746 (2004).
19. F. Ohman and J. Mork, "Modeling of Bit Error Rate in Cascaded 2R Regenerators," J. Lightwave Technol. **24**, 1057 (2006).
20. G. P. Agrawal, *Nonlinear Fiber Optics, 3rd Edition* (Academic Press, 2001).
21. D. Anderson, M. Desaix, M. Lisak, and M. L. Quiroga-Teixeiro, "Wave breaking in nonlinear-optical fibers," J. Opt. Soc. Am. B **9**, 1358- (1992).
22. S. Taccheo and L. Boivin, "Investigation and design rules of supercontinuum sources for WDM applications," in *Optical Fiber Communication Conference (OFC) 2000*(2000), Vol. 3, pp. 2-4.
23. W. J. Tomlinson, R. H. Stolen, and A. M. Johnson, "Optical wave breaking of pulses in nonlinear optical fibers," Opt. Lett. **15**, 457 (1985).
24. I. C. M. Littler, M. Rochette, and B. J. Eggleton, "Impact of chromatic dispersion and group delay ripple on self-phase modulation based optical regenerators," Opt. Commun. **265**, 95-99 (2006).
25. N. Yoshikane, I. Morita, and N. Edagawa, "Improvement of dispersion tolerance by SPM-based all-optical reshaping in receiver," Photon.Technol. Lett. **15**, 111-113 (2003).
26. T. Nguyen, M. Gay, L. Bramerie, T. Chartier, J.-C. Simon, and M. Joindot, "Noise reduction in 2R-regeneration technique utilizing self-phase modulation and filtering," Opt. Express **14**, 1737-1747 (2006).
27. J. E. Rothenberg, "Colliding visible picosecond pulses in optical fibers," Opt. Lett. **15**, 443-445 (1990).
28. M. Rochette, I. C. M. Littler, R. W. McKerracher, and B. J. Eggleton, "A dispersionless and bandwidth-adjustable FBG filter for reconfigurable 2R-regeneration," Photon. Technol. Lett. **17**, 1680-1682 (2005).
29. S. Pitois, J. Fatome, and G. Millot, "Generation of a 160-GHz transform-limited pedestal-free pulse train through multiwave mixing compression of a dual-frequency beat signal," Opt. Lett. **27**, 1729-1731 (2002).
30. L. Provost, C. Finot, K. Mukasa, P. Petropoulos, and D. J. Richardson, "Generalisation and experimental validation of design rules for Self-Phase Modulation-based 2R-Regenerators," in *Proc. Optical Fiber Communications (OFC'07)*(Anaheim CA, 2007), p. OThB6.

1. Introduction

All-optical regeneration is likely to be an important function within future optical communication systems providing a route to optical networks of increased scalability, capacity and flexibility, as well as reduced network management complexity and costs. Optical regeneration is progressively more attractive as transmission speeds increase since this places ever more stringent demands on existing impairment mitigation techniques such as dispersion and PMD compensation.

In this paper, our interest is on 2R regeneration i.e Reamplification and Reshaping of optical data pulses. An optical data stream can be corrupted by a variety of physical effects including: uncompensated dispersion, inter- and intra-channel nonlinear effects, the accumulation of Amplified Spontaneous Emission (ASE) noise, and Polarization Mode Dispersion-induced temporal pulse broadening. Intra-channel nonlinear effects, such as intra-channel Four-Wave Mixing (i-FWM) and intra-channel Cross phase modulation (iXPM) for example are responsible for the generation of ghost pulses inside zero-bit slots, amplitude fluctuation in the one-bit pulses and the introduction of timing jitter [1]. These effects are particularly severe and limit the maximum usable span length.

Over the past decade, there have been numerous experimental demonstrations of optical 2R regeneration schemes, designed to work with either On-Off keying amplitude modulated (OOK) and/or phase-shift keyed (PSK) signals. A particularly interesting fiber based regeneration technique for Return-to-Zero (RZ) OOK signals based on Self-Phase Modulation (SPM) followed by offset filtering has been proposed and experimentally demonstrated by Mamyshev [2]. This method has drawn much attention due mainly to its ease of implementation and robustness. Its main advantages include a reduced sensitivity both to environmental instabilities, as compared to systems relying on interferometric effects (e.g. nonlinear optical loop mirrors), and its low polarization sensitivity relative to other regenerating schemes based on effects such as Four-Wave Mixing. Finally, unlike other technologies that exhibit a longer response time (such as semiconductor optical amplifiers),

#78247 - $15.00 USD Received 19 Dec 2006; revised 14 Mar 2007; accepted 20 Mar 2007; published 12 Apr 2007

the quasi-instantaneous response time of Kerr nonlinearities in optical fibers makes the scheme directly applicable to high bit-rate operation. Using the Mamyshev approach a number of 2R and more recently 3R optical regenerators (i.e. 2R regenerators with an additional retiming operation) have been experimentally reported at 10 Gb/s and 40 Gb/s with either OOK-RZ [2, 3] or Carrier-Suppressed RZ (CS-RZ) formats [4, 5]. The ability to handle data impaired either by iFWM [6] or ASE [7, 8] has also been confirmed. Significant advances in fiber technology, such as the emergence of holey fibres [9], fibers made of compound materials (for instance chalcogenide [8]) or bismuth oxide [10, 11], have further enhanced interest in this technique. Due to their high nonlinearity coefficient, these latter waveguides are proposed as attractive media for reducing the power budget and/or increasing the compactness of the devices.

Despite the numerous experimental demonstrations, the design optimization of such regenerators is not straightforward, because of both the wide variety of input signal parameters (pulse width, duty cycle, input power), and the numerous physical properties of the fibers (chromatic dispersion D, nonlinearity coefficient γ, and length L). To date, only a few works have introduced any form of design guideline [2, 7, 12-14] and even these have addressed the problem either within the context of a pure nonlinear regime [13, 15], or have considered only a fixed fiber length [3]. However, neither of these approaches facilitates cross-comparison between different fiber systems. In this work, we report the development of global scaling rules for the 2R regenerator based on Mamyshev's technique. We first introduce the physical parameters of the regenerator and define associated parameters that can be used to assess the regeneration performance. From this process, we identify an optimum operation regime in terms of rejection of amplitude noise [16]. We study the quality of the regenerated pulses at the output of the regenerator for operation under these optimal conditions, and extend our conclusions with a simulation example showing the applicability of the design rules for a regenerator operating at 160 Gb/s.

2. Regenerator and regeneration parameters

2.1 Regenerator principles and associated parameters

In this first section, we recall the principle of the SPM-based Mamyshev regenerator as shown schematically in Fig. 1. The degraded optical pulse streams are first fed into an optical amplifier which is used to boost the power to a suitably high level at the input to the highly nonlinear fiber (HNLF). (Note that an additional filter is often inserted after the amplifier to reject the out-of-band ASE noise). The amplified pulses are then propagated in the HNLF during which they experience spectral broadening due to Kerr-induced SPM. A narrow-band filter is used to carve into the broadened spectrum at the output of the HNLF acting both to provide intensity discrimination as discussed below, and as a pulse shaping element.

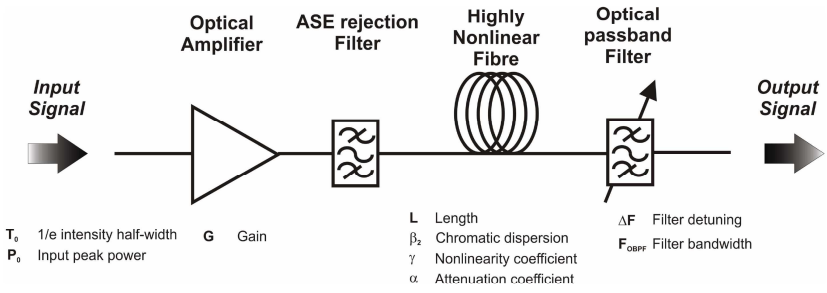

Fig. 1. Schematic of a typical optical regenerator based on Self-Phase Modulation.

The amount of spectral broadening experienced by the signal in the HNLF is to first order proportional to the time-derivative of the pulse intensity profile. This allows one to

#78247 - $15.00 USD Received 19 Dec 2006; revised 14 Mar 2007; accepted 20 Mar 2007; published 12 Apr 2007

discriminate between high and low peak power pulses simply by detuning the narrow-band filter away from the input signal carrier frequency. A detuned optical filter will collect only a small fraction of the energy of low-peak-power pulses (nominal 'zeros'), which experience less spectral broadening than high-peak-power pulses (nominal 'ones'). Thus, undesired ghost pulses can be suppressed at the output of the regenerator and the overall mark-to-space extinction ratio can consequently be improved.

In addition, the regenerator should perform amplitude equalization on the 'ones', and also the nominal shape and width of the transmitted pulses should be retained. In general this requires a condition under which the spectrum broadens in proportion to an increase in the signal power. Although this condition can be satisfied both in the normal and the anomalous dispersion regimes, nonlinear propagation within the normal dispersion regime is preferable in that it does not allow the development of modulational instability, or the nonlinear interaction of the signal with ASE, both of which can introduce additional noise [17]. Furthermore, the SPM spectra generated under conditions of normal dispersion are generally flatter, thus leading to smoother pulse shapes at the output of the regenerator.

In the work presented here, we have assumed transform-limited Gaussian pulses at the input, with a variable peak power P^{in} and a half-width at the 1/e-intensity point T_0. Figure 1 lists the remaining parameters of the regenerator. The customizable parameters of the HNLF are the chromatic dispersion (D or β_2), the nonlinearity coefficient γ and the fiber length L. The output optical band-pass filter (OBPF) is detuned from the carrier frequency by an offset value ΔF. To adhere with our previous statements, the filter is Gaussian with a 1/e half-bandwidth of Γ_{OBPF}, which matches the corresponding input pulse 1/e half-bandwidth F_0 (i.e. $F_{OBPF} = F_0 = 1/(2\pi T_0)$), and has a flat phase response. In order to distinguish the impact of the ASE noise from the intrinsic ability of the regenerator to eliminate ghost pulses, we have not considered any ASE noise in our simulations. (Nevertheless, the effects of ASE are qualitatively discussed in a separate section in the paper).

It should also be noted here that in order to be able to devise some general scaling rules, we have chosen not to consider the impact of fiber loss in this study. Although the effects of attenuation can be quite significant, the general trends described in the following sections are still valid when this is considered. Quantification of the precise effects of fiber losses will be the subject of a separate study.

2.2 Assessment of the regeneration function

The ability of the regenerator to offer both extinction ratio improvement and amplitude equalization is defined by the transfer function (TF). The TF simply describes the variation of the output pulse energy as a function of the input pulse energy. In the particular type of regenerator considered here, input pulses of the same peak power and shape but with different duration, (and hence energy), do not exhibit the same output response. As detailed in Ref. [8], the principle of the regeneration is based on the temporal derivative of the intensity profile of the pulse and not on an instantaneous power response as in an interferometric switch. As a result, the regenerator can ultimately exhibit as many TFs as there are input pulse shapes. In this work, we overcome this limitation by considering only the case of Gaussian pulses at the input. The same remarks apply also to the output pulses. We have therefore considered that the pulse width T_0 and pulse shape remain largely unchanged at the regenerator output, so that we can define the TF as a function of the output pulse peak power P_{out} versus the input peak power P_{in} (the validity of this statement will be shown in Section 4 below).

Depending on the interplay between the broadened pulse spectrum and the detuned filter position, three possible regimes for the TF can be identified, as graphically illustrated in Fig. 2. The variation of the output power relative to the input can either be non-monotonous (regime 'A'), exhibit a locally flat region on the one-level (regime 'B'), or be purely monotonous (regime 'C'). It is clear that regime 'B' offers the largest power equalization ability, and represents the preferred operational regime.

#78247 - $15.00 USD Received 19 Dec 2006; revised 14 Mar 2007; accepted 20 Mar 2007; published 12 Apr 2007

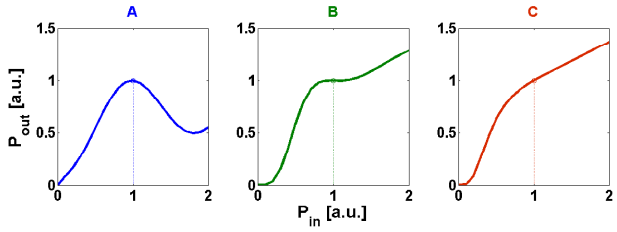

Fig. 2. Illustration of the three possible TF types for the SPM-based regenerator: non-monotonic evolution (A), locally flat evolution (B), or monotonous variation (C).

Parameterization of the TF shape has been previously proposed in order to analytically predict the regeneration performance and concatenation effects [18, 19]. In these earlier studies, the TFs were approximated by *tanh*-like, sigmoid or more drastically by linear piecewise functions. Unlike these authors in our global approach we chose to define parameters directly extracted from the TFs, and to evaluate the regenerator performance on this basis. The three parameters that we use are graphically illustrated in Fig. 3, and are described below:

- The nominal input peak power for the marks P_1^{in}. This value is defined as the input peak power for a 'one' bit that locally exhibits maximum peak power compression at the output. Mathematically, this value corresponds to the input peak power at which there is either a local maximum (type A), a sign change in the curvature of the TF (type B,) or a local minimum in the TF derivative (type C),
- Taking into consideration this P_1^{in} value, an output extinction ratio ER^{out} is computed for an arbitrarily fixed input extinction ratio of $ER^{in} = -10$ dB. We define the extinction ratio as the ratio between the peak powers of a 'zero' and a 'one' pulse.
- Finally, the assessment of the output power equalization on the marks is quantified by introducing the difference ε, which is defined as the total variation in output peak power for an input peak power ranging between -7.5 % and +7.5 % around P_1^{in}. The output peak power compression ρ is defined as the normalized ratio $|\varepsilon|/P_1^{out}$.

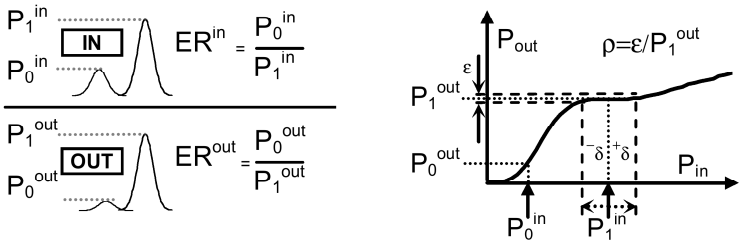

Fig. 3. Definition of the parameters used to parameterize the power TF of the regenerator. Left: Definition of the input (ER^{in}) and output (ER^{out}) extinction ratios. Right: An example showing these parameters on a model TF.

It will become obvious in the following section that although the precise choice of various of these values (e.g. $ER^{in} = -10$ dB and variation in the incoming pulse peak power of ± 7.5 %) might seem somewhat arbitrary, they do not affect the generality of the developed model. These values are only used to provide an indication of the quality of the TF for a physically reasonable choice of input signal parameters, rather than a specification of particular operating conditions.

#78247 - $15.00 USD Received 19 Dec 2006; revised 14 Mar 2007; accepted 20 Mar 2007; published 12 Apr 2007

Finally, it is also worth noting that the TF alone does not provide any information on the pulse quality at the regenerator output, or the corresponding power efficiency. These effects will be studied separately in Section 4 of this paper.

3. Modeling results

We now consider the nonlinear Schrödinger equation (NLSE) that governs the propagation of the pulse within an optical fiber. We limit the contributions of the dispersive effects to the group velocity dispersion β_2 term and the nonlinear contributions to the effects of SPM. The medium is assumed to be lossless (α=0). We follow the well-known analysis (which can be found in [20]) which allows us to express the slowly varying pulse envelope in a standard form using the following set of normalized parameters:

$$u(z,t)=\sqrt{N^2}\,U(z,t);\qquad \xi=\frac{z}{L_D};\qquad \tau=\frac{T}{T_0}=\frac{t-\beta_1 z}{T_0} \tag{1}$$

$$L_D=\frac{{T_0}^2}{|\beta_2|};\qquad L_{NL}=\frac{1}{\gamma P_p};\qquad N^2=\frac{L_D}{L_{NL}} \tag{2}$$

with t and z the time and the longitudinal position along the fiber respectively. Here, β_1 is the group velocity, P_p the pulse peak power, U(z, t) the normalized slowly varying field envelope of the pulses, and L_D and L_{NL} are defined as the dispersion and nonlinear lengths respectively. The NLSE can then be written as:

$$i\frac{\partial u(\xi,\tau)}{\partial \xi}-\frac{\mathrm{sgn}(\beta_2)}{2}\frac{\partial^2 u(\xi,\tau)}{\partial \tau^2}+|u(\xi,\tau)|^2\,u(\xi,\tau)=0 \tag{3}$$

Our approach benefits from the use of scaling factors and allows us to derive a global set of solutions by only considering any one solution of the standard form. For example, if $u(z/L_D,T/T_0)$ satisfies Eq. 3, then for any real number δ, the pulse envelope $\delta.u(\delta^2.z/L_D,\delta.T/T_0)$ is still a solution of Eq. 3 [20]. From a practical point of view, if we consider two pulses with different initial peak powers (P_1, P_2), and different initial pulse widths (T_1, T_2) but of the same initial shape, then these pulses will evolve to the same scaled profiles in both time and frequency when two conditions are fulfilled: (a) that the fiber length in the two cases is the same proportion of the dispersion length ($L_1/L_{D1}=L_2/L_{D2}$); and (b) that they exhibit the same N^2 value ($L_{NL1}/L_{D1}=L_{NL2}/L_{D2}$). This scaling rule drastically reduces the complexity of the problem, as global bit-rate-independent conclusions can be derived from the analysis of a single case in which the four aforementioned parameters T_0, P_p, β_2 and γ are arbitrarily fixed.

By using these scaling factors, and by virtue of the normalized quantities N, L_{NL} and L/L_D, where L_{NL} is defined with respect to the nominal input peak power P_1^{in}, our calculations demonstrate that it is possible to relate the three TF parameters (P_1^{in}, ER^{out} and ρ) to the physical parameters of the regenerator (fiber parameters L, γ, β_2 and filter detuning ΔF). The interdependencies between the three parameters can be represented in the two-dimensional space formed by the normalized fiber length L/L_D and the normalized output filter detuning $\Delta F/F_0$, as shown in the multi-contour plot of Fig. 4.

Figure 4 shows that the two-dimensional space is split into two distinct areas that correspond to the 'A' and 'C' TF regimes, with the 'B' regime lying along the common boundary. For a fixed $\Delta F/F_0$ ratio, a small L/L_D ratio yields a non-monotonous TF variation (regime 'A'), whereas a monotonic variation (regime 'C') is experienced at high L/L_D ratios. This illustrates the spectral evolution of the pulse along the fiber length: For short fiber lengths the SPM-spectrum is characterized by ripples which lead to the features of regime 'A', whereas for longer lengths the SPM-broadening has saturated and the extra energy of higher power pulses only contributes to an increase in the power that passes through the offset filter (regime 'C'). More interestingly, we identify the region of maximum power equalization

#78247 - $15.00 USD Received 19 Dec 2006; revised 14 Mar 2007; accepted 20 Mar 2007; published 12 Apr 2007

(regime 'B') over a large range of N values when operating under specific conditions for the fiber length and filter detuning.

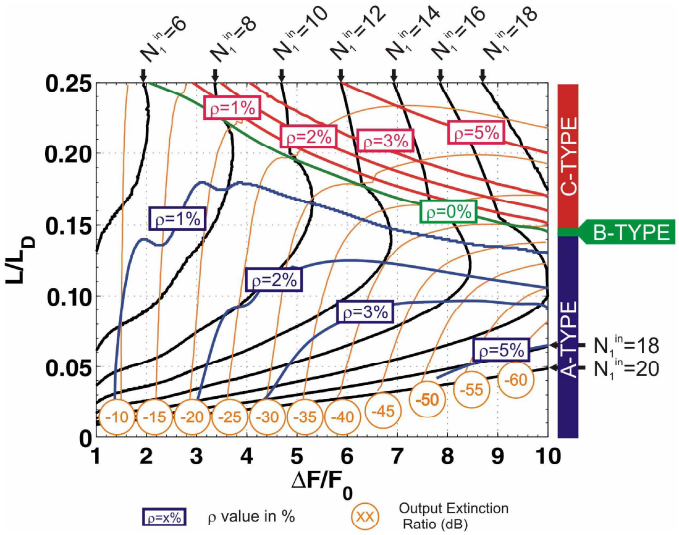

Fig. 4. Normalized map for input unchirped Gaussian pulses linking the regenerator parameters to the regeneration performance: Bold plain lines correspond to ρ contours. Orange plain lines correspond to ER^{out} contours (in dB), and black lines correspond to N_1^{in} contours.

The map directly provides simultaneous access to the parameters to be employed and to the expected performance. Additionally, some interesting observations can be made at this stage. As it might be expected, the output extinction ratio improvement is mainly determined by the position of the output filter and a minimum offset detuning value of $1.5xF_0$ is necessary to significantly improve the input extinction ratio. The extinction ratio improvement has a remarkable dependence on the length of propagation as, the variation of the output extinction ratio for high input peak powers is progressively altered and tends to saturate when increasing $\Delta F/F_0$ for a fixed L/L_D ratio. This behavior is accounted for by the development of pedestal structures in the wings of ghost pulse spectra (i.e. the onset of wave-breaking), which are more likely to be sampled by the detuned filter.

As far as the optimal regime 'B' is concerned, we have found a relationship between the optimal fiber length $L_{opt,B}$ and the corresponding N_1^{in} value (defined as $(\gamma P_1^{in} T_0^2/\beta_2)^{1/2}$):

$$\frac{L_{opt,B}}{L_D} = \sqrt{\frac{K_0}{N_1^{in}}} \tag{4}$$

where K_0 is a fitting constant equal to 0.382 (with a ±4% error) over a range of N values between 5.5 and 23. Although this relation has been found numerically rather than analytically, we note that it is of a similar form as the relations describing both the optical wave-breaking distance for Gaussian pulses [21] and supercontinuum design rules [22]. There is a linear relationship between the optimal normalized filter detuning $\Delta F/F_0$ and the corresponding N_1^{in} value:

$$\frac{\Delta F}{F_0} \approx 0.71\, N_1^{in} - 2.13 \tag{5}$$

Equation 4 shows that a balance needs to be maintained between the dispersive and nonlinear contributions and demonstrates that a design consideration based solely on the value

#78247 - $15.00 USD Received 19 Dec 2006; revised 14 Mar 2007; accepted 20 Mar 2007; published 12 Apr 2007

of the fiber nonlinearity is therefore insufficient. Again, we emphasize that the proposed rules, as well as the map of Fig. 4, are directly applicable to any bit-rate systems by an appropriate setting of the input pulse duration T_0 and only depend on the pulse shape characteristics.

According to Fig. 4, the fiber length and filter position need to be carefully chosen to ensure operation in the optimal regime 'B'. However, it is interesting to note that there is a quite broad region close to the boundary between regimes 'A' and 'B', where the ratio ρ does not change significantly. This provides a convenient route towards relaxing the design considerations without greatly affecting the TF shape.

Finally, it follows from Eq.2 and 4 that the optimum length $L_{opt,B}$ scales inversely to the square root of the $\beta_2^3\gamma$ product. This favors the use of highly nonlinear, compound glass fibers (see e.g. [8, 10, 11]), whose extremely high nonlinearities are usually accompanied by large values of chromatic dispersion. However, these fibers also exhibit significantly higher propagation losses, which are likely to compromise the validity of this observation.

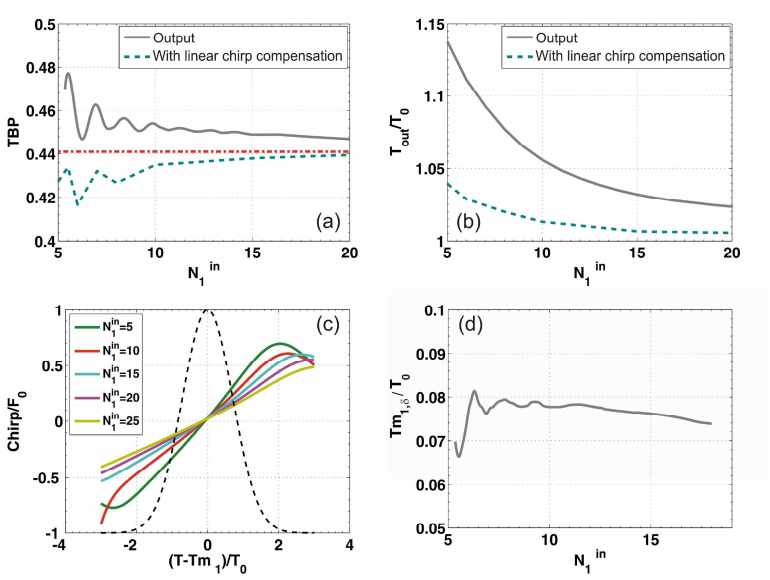

Fig. 5. (a): TBP of the regenerated pulse as a function of N_1^{in}. Red dashed line represents the value for transform-limited Gaussian pulses. (b): Variation of the normalized temporal pulse FWHM as a function of N_1^{in}. (c): Normalized output pulse chirp for various N_1^{in} values. As a reference, the initial Gaussian pulses are also shown. (d): Variation of the timing jitter induced by the regenerator over a ± 7.5% input peak power range as a function of N_1^{in}. Dashed lines in (a) and (b) show the performance that can be achieved when chirp compensation is considered.

4. Properties of the regenerated pulses

As mentioned earlier, for the design optimization of a 2R regenerator, an analysis of the TF characteristics should also be accompanied by in-depth assessment of the quality of the regenerated pulses. We therefore examine the characteristics of the optical pulses at the output of the regenerating system, in terms of time-bandwidth product (TBP), pulse width, chirp and induced timing jitter. We specifically focus on the preferred operation regime 'B'. Then, according to Eq. (4), Eq. (5) and Fig. 4 each value of N_1^{in} corresponds to a unique set of regenerator parameters.

In Fig. 5(a) we plot the variation observed in the TBP, as we move along the 'B' contour. It is to be noted that the pulses deviate only slightly from the transform-limited case (0.441),

#78247 - $15.00 USD Received 19 Dec 2006; revised 14 Mar 2007; accepted 20 Mar 2007; published 12 Apr 2007

especially for larger values of N_1^{in}. We attribute the degradation of the TBP at small values of N_1^{in} to the more pronounced peaked structure of the SPM broadened spectrum which is reflected in the filtered spectrum at the output of the regenerator. Unlike the TBP, the temporal FWHM of the pulse is decreases smoothly with increasing N_1^{in} [see Fig. 5(b)]. As far as the shape of the output pulse is concerned, a slight asymmetry can be observed – however this is found to be negligible and it is even less noticeable at high values of N_1^{in} as depicted in Fig. 6.

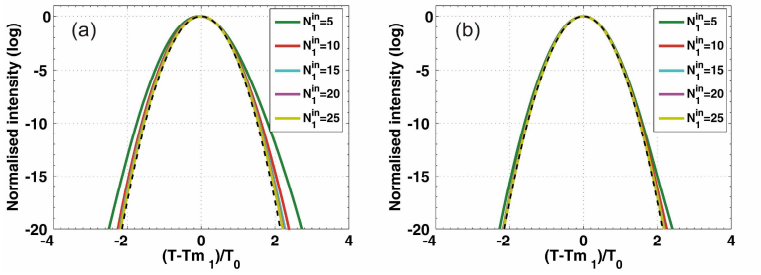

Fig. 6. Normalized intensity profiles: (a) before linear chirp compensation, and (b) and after linear chirp compensation. As a reference, an initial Gaussian pulse is also shown (dashed lines).

A closer examination of the chirp reveals that it varies in a rather linear fashion across the largest portion of the output pulses for all values of N_1^{in}, and that the chirp rate is positive [Fig. 5(c)]. This behavior is characteristic of the pulse evolution close or above the optical wave breaking condition [23]. A consequence of the chirp on the pulses is that they acquire an additional timing delay relative to linearly propagating pulses, which is a function of N_1^{in}. In order to quantify this power-dependent timing delay we introduce the quantity $Tm_{1,\delta}$ as follows:

$$Tm_{1,\delta} = \left| Tm_1\left[(1+\delta)P_1^{in} \right] - Tm_1\left[(1-\delta)P_1^{in} \right] \right| \tag{6}$$

where

$$Tm_1\left[P_1^{in} \right] = \frac{\int_{-\infty}^{\infty} t\, I(L,t)\, dt}{\int_{-\infty}^{\infty} I(L,t)\, dt} \tag{7}$$

$Tm_{1,\delta}$ traces the relative variation of the temporal position (i.e. the timing jitter) of the output pulses over an input peak power variation of ±7.5% (i.e. δ=0.075) around P_1^{in}. The temporal position of the pulse is defined as the first-order moment integral (center of gravity) Tm_1 of the output pulse intensity profile I, obtained for an input pulse with peak power P_1^{in} (Eq. 7). We demonstrate in Fig. 5(d) that this variation is almost independent of the operating value N_1^{in}, so that the same amount of timing jitter is introduced whatever the operating condition along the 'B' contour. The amount of timing jitter is found to be around 8% of the initial pulse width T_0. The abrupt variation at small values of N_1^{in} is explained by the presence of a small asymmetry of the output pulses which affects the computed Tm_1 value.

Since the output pulses have a smooth and linear chirp, it is possible to consider offset filter with a phase response designed to compensate this chirp (alternatively a suitable length of anomalously dispersive fiber can be used for the same purpose). In Figs. 5(a), 5(b), and 6 we have included the corresponding plots that represent the TBP, the normalized pulse width and the pulse shapes respectively after optimum linear chirp compensation is applied, demonstrating that it is possible to achieve almost identical characteristics to the input pulses.

#78247 - $15.00 USD Received 19 Dec 2006; revised 14 Mar 2007; accepted 20 Mar 2007; published 12 Apr 2007

5. Discussion

In the following subsections we examine the impact of various system parameters on the regenerator performance. In particular, we consider: how some variation in the input pulse parameters (i.e. the pulse width and temporal chirp) can affect the regenerator TF; how the power efficiency and extinction ratio of the regenerating system are affected by the operating conditions; and how coherent interference between adjacent pulses nonlinearly propagating in the HNLF can degrade the regeneration. In addition, we provide qualitative comments on the contribution of ASE noise, and discuss the consequences of using an output filter with a bandwidth other than the nominal F_0 value considered above on the TF parameters. Finally, we summarize our observations and draw some conclusions on how to go about choosing the best operating conditions for a given system.

5.1 Pulse width variation and residual dispersion

In order to ensure robust operation, a regenerator should be able to demonstrate tolerance to input pulse width variations and residual chirp, since these are both likely to be affected during transmission by environmentally-driven chromatic dispersion variations, ASE-signal interaction and polarization-mode dispersion. Since the TF is dependent on the intensity derivative of the input pulse [8], a variation in the input pulse width would be translated into a variation in the output pulse energy. For the case of unchirped pulses, the consequence of this variation can be appreciated from a study of Fig. 4, where an increase (decrease) in the pulse width may shift the operating condition e.g. from regime 'B' to regime 'A' ('C'), due to the dependence of L_D on T_0. In Fig. 7(a), we show TFs obtained when the pulse width is varied from -20% up to 20% of its nominal value T_0, when the system is operating in regime 'B' with a fixed value N_1^{in}=10 (defined for the nominal value T_0).

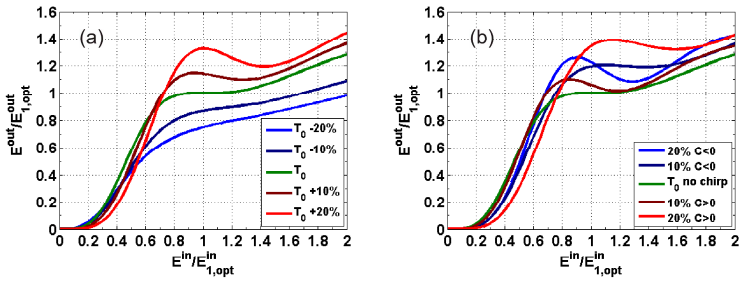

Fig. 7. (a). TFs for an input pulse width variation between -20% and +20% relative to T_0. (b): TFs for linearly chirped input pulses with either positive (C>0) or negative (C<0) linear chirp. The axes correspond to normalized pulse energies with respect to energies $E_{1,opt}^{in}$ and $E_{1,opt}^{out}$ of the unchirped nominal case for N_1^{in}=10.

The appreciation of the effects of residual chirp is less straightforward to establish. Following [24, 25], we have adopted a simple approach that consists of positively (negatively) prechirping the input pulse by linear propagation in a segment of anomalous (normal) dispersion fiber. This has allowed us to vary the pulse width at the input of the regenerator by either +10% or +20 % of the nominal T_0 value. The corresponding TFs are plotted in Fig. 7(b), again for nominal operation in regime 'B' with a value N_1^{in}=10. All modified TFs are of type 'A' and exhibit a higher output pulse energy than the unchirped case. This behavior originates from the fact that the SPM spectra are not as flat when the input pulses are chirped [21].

From these results, we can conclude that the regeneration is not significantly compromised by the presence of large variations in both the input pulse width and the residual chirp. It could be argued that cascading a second regeneration stage, as is frequently done with

#78247 - $15.00 USD Received 19 Dec 2006; revised 14 Mar 2007; accepted 20 Mar 2007; published 12 Apr 2007

Mamyshev regenerators to eliminate any overall-frequency shift, might be beneficial in terms of offering an additional power equalization step. In this way all power fluctuations at the end of the first stage could be fully compensated.

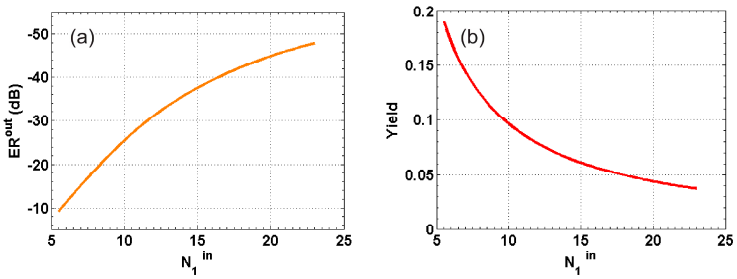

Fig. 8. Output extinction ratio ER_{out} improvement (a) and energy yield (b) as a function of N_1^{in} when operating along the optimal regime 'B'.

5.2 Output Extinction ratio, energy yield

On the basis of the discussion presented so far, it follows that operation at high values of N_1^{in} is favorable in terms of both extinction ratio improvement and pulse quality. However, when operating at high powers, the power spectral density of the signal reduces, since the SPM-induced spectral broadening is more pronounced. Therefore, the proportion of energy that passes through the offset filter decreases with increasing N_1^{in}. Additionally, this reduction in spectral density at high values of N_1^{in} is accompanied by optical signal-to-noise ratio (OSNR) degradation in the presence of out-of-band ASE noise [26]. These considerations lead to a trade-off between the improvement in the regenerator performance and the energy yield of the system (i.e. the ratio of the power at the output of the filter to the power at the input of the fiber), as shown in Fig. 8. Inter-pulse interactions during their propagation in the HNLF are also likely to further restrict the maximum value of N_1^{in} that can be used in the systems as discussed below.

5.3 Interaction between adjacent pulses

Up to this point, we have concerned ourselves with the study of the propagation of single Gaussian pulses in the regenerator. It is important however, to study the limits at which the consideration of a stream of pulses will affect the system operation. Under the combined effects of normal dispersion and nonlinearity, Gaussian pulses typically broaden and evolve into trapezoidal-shaped pulses, as illustrated in Fig. 9(a). The extent of the pulse broadening has therefore to be investigated to address the possibility for adjacent pulses to spread and as a result partially collide within the HNLF. In that case, both coherent interference and nonlinear interactions would result in strong oscillations in the temporal profile of overlapping pulses [27]. The possibility of a collision is determined by the pulse duration with respect to its time slot, that is to say the pulse duty cycle.

Figure 9(a) shows that the pulse width within the HNLF increases with the value of N_1^{in}. Interactions between adjacent pulses are therefore likely to be more severe when operating at high peak powers. We have simulated the propagation of three adjacent pulses of the same nominal peak power P_1^{in}, when operating under regime 'B'. We have observed the fluctuations in peak power between adjacent filtered output pulses, caused by pulse-to-pulse interactions, and compared them to the pulse peak power obtained for the single pulse case. Fig. 9(b) summarizes the results we obtained for three different duty cycles, namely 33%, 25% and 20%. It is clear that there is a maximum N_1^{in} value below which adjacent pulse interaction does not compromise the regeneration. These N_1^{in} values were quantified as 10, 20 and more than 25 respectively for the three values of duty cycles that we considered. One can

#78247 - $15.00 USD Received 19 Dec 2006; revised 14 Mar 2007; accepted 20 Mar 2007; published 12 Apr 2007

therefore operate at high peak powers when the pulse duty cycle is sufficiently low. However, the possibility that the incoming pulses suffer from timing jitter should also be considered, since this will further restrict the maximum N_1^{in} value.

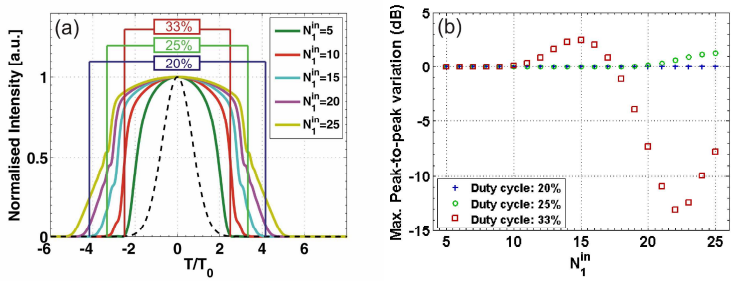

Fig. 9. (a). Temporal evolution of the input pulse for various N_1^{in} values; the bit slot occupation for 20, 25, and 33% duty cycle is also shown. (b). Variation of the peak power of three propagating pulses relative to the single pulse case as a function of N_1^{in}, for duty-cycle values of 20%, 25% and 33%.

5.4 ASE noise contribution

Having explored the design of the 2R regenerator in the absence of any incoherent noise, we take the opportunity to present some qualitative statements on the main consequences of the contribution of ASE. Firstly, the presence of in-band ASE noise will critically affect the 'one' pulses by introducing some distortions in the pulse shape, thereby affecting both the pulse width T_0 and the peak power. By assuming an OSNR value higher than ~20dB [8], any variations in the pulse width will affect the operation of the regenerator in the same fashion as was described in Subsection 5.1 above. Additionally, it is obvious that the filtering action of the regeneration system favors the elimination of ASE noise. Any in-band ASE can be rejected by operating with a large filter offset value, whereas out-of-band ASE can be rejected by placing an ASE rejection filter at the input of the HNLF [26].

5.5 Impact of the filter bandwidth

So far, we have required that the pulse width at the output is maintained the same as that at the input. However, it is possible to consider a different filter bandwidth at the output for duty cycle conversion applications [28]. A variation in the output filter bandwidth does not affect the global trends presented in Fig. 4. For a fixed fiber length, it is possible to retrieve a 'B'-type regime by simply adjusting the filter position. For example, use of a broader (narrower) filter requires smaller (larger) filter offset ΔF, which will affect the regenerator performance by reducing (increasing) the output extinction ratio, while at the same time, the energy efficiency of the system will also be increased (decreased). However, it also needs to be appreciated that a broader (narrower) filter bandwidth will increase (reduce) the output pulse asymmetry, since a larger (smaller) amount of rippled spectrum will be allowed to pass through the filter.

6. Applying the design rules to specific optical systems

The study presented in this paper links the system parameters, such as bit rate and pulse duty cycle, to the various parameters of the regenerating system, such as the fiber properties, the required power levels and the filter offset. Using the specifications of the map presented in Fig. 4 as a starting point, it is evident that the optimum operating conditions for such a regenerator will depend on several factors, such as the available spectral bandwidth, the power budget and even the nature of the predominant impairments targeted during the regeneration process. In the discussions above we have highlighted the various performance trade-offs that

#78247 - $15.00 USD Received 19 Dec 2006; revised 14 Mar 2007; accepted 20 Mar 2007; published 12 Apr 2007

have to be taken into account when designing a regenerator for a specific system. For example, taking all of the above into account we concluded that for a 33% duty-cycle a maximum N_1^{in} value somewhere in the range 7-10 is likely to provide the best overall compromise between the different effects (see Fig. 9).

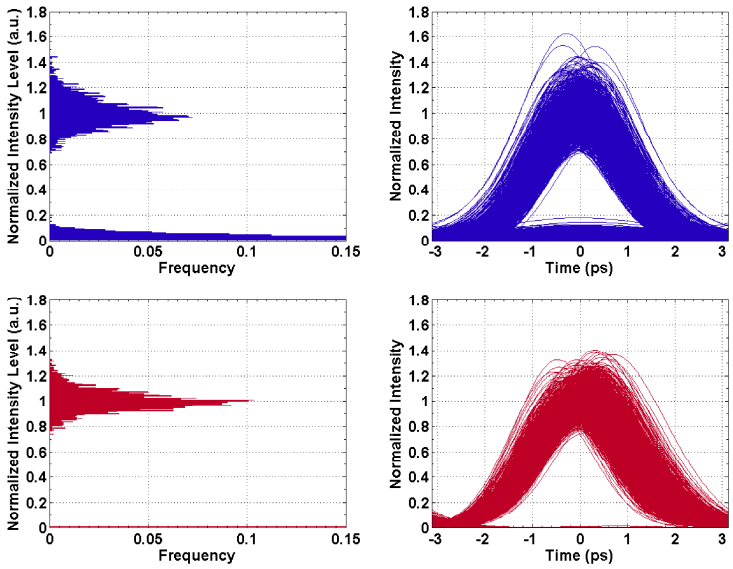

Fig. 10. Peak power distributions and temporal pulse shape at the input of the regenerator (top) and at the output (bottom) for a data signal at 160 Gb/s.

We tested the applicability of our design rules in a simulation example that considered 33% RZ Gaussian data pulses at 160 Gb/s. Note that such pulses can be generated using a source like that reported in Ref. [29], or by using simple OTDM techniques. We transmitted a 212-bit-long Pseudo-Random Bit Sequence with an average power of 15.5 dBm into two segments of 80 km of standard fibre with complete dispersion compensation (second and third-order). The simulation was performed by using commercial software (VPI TransmissionMaker from VPISystems). Intrachannel cross-phase modulation and four-wave mixing introduced noise into the signal, as shown in the optical eye diagram of Fig. 10 (top). The data sequence was then fed into a 2R regenerator, which was designed according to our design rules. The HNLF included in the regenerator had a chromatic dispersion D=-0.78 ps/nm-km, a nonlinearity coefficient γ=20 $W^{-1}km^{-1}$ and a total length L=347 m. According to Fig. 4, this regenerator operates in regime 'B' when the normalized output filter offset is 3.3 and N_1^{in} is 7.75. This value corresponds to a pulse peak power P_1^{in}=1.92 W, or an average power of 340 mW at the input of the regenerator. We considered ideal amplification, i.e. no ASE noise within the link. Figure 10 compares the optical eye diagrams at the input and the output of the regenerator. Corresponding intensity distributions for the one- and zero-bit pulses are also plotted [as calculated at the center of the eye corresponding to the center position of the bit slot (t=0)].

The statistical data show that both suppression of the ghost pulses and reduction in the amplitude noise distribution on the ones is achieved. According to Fig. 10, the variance of the distribution of the amplitude noise is reduced by a factor of ~2. The introduction of timing jitter manifests itself by adding some asymmetry on the output optical eye diagram.

#78247 - $15.00 USD Received 19 Dec 2006; revised 14 Mar 2007; accepted 20 Mar 2007; published 12 Apr 2007

7. Conclusion

We have presented simple and generalized scaling rules for the design of 2R optical regenerators based on SPM in normally dispersive fibers. Our present study, which was restricted to the case of Gaussian input pulses and lossless fibers, has shown that the regenerator performance can be mapped onto a parameter space defined by the fiber properties (as expressed by L/L_D), and the filter offset position. Our scaling rules show how the bit-rate (pulse width) affects the system performance, and we have identified the optimal operating conditions which ensure power equalization for a broad range of incoming powers. We have also identified the trade-off that exists between performance and energy efficiency, and have examined the characteristics of the regenerated pulses under different operating conditions. A detailed extension of the study to include the effects of fiber loss is naturally of great practical interest, as is extension of the mapping concept to other pulse forms. Our initial studies in both of these directions confirm that the trends that we have identified in the present study can be extended directly to both of these cases, albeit with quantitative changes to the design maps [30]. A study of the impact of other high-order effects (e.g. Stimulated Brillouin Scattering, Stimulated Raman Scattering or Two Photon Absorption) is also likely to be of interest depending on the precise nature of the fiber host material (e.g. silica- or non silica-based).

Acknowledgments

Christophe Finot gratefully acknowledges the financial support of European Union through a Marie Curie grant. This work was partially supported by the STREP/EU project TRIUMPH IST-027638 and the EU Network of excellence e-Photon/ONE (Project IST-027497).

#78247 - $15.00 USD Received 19 Dec 2006; revised 14 Mar 2007; accepted 20 Mar 2007; published 12 Apr 2007

2. Publication B

Publication B was published under the following reference:

L.Provost, C.Finot, K.Mukasa, P.Petropoulos, D.J.Richardson, "**Generalisation and experimental validation of design rules for SPM-based 2R-regenerators**", Optical Fiber Communication conference (OFC 2007), 25-29 Mar 2007, OThB6.

The paper can be found at the following URL on the IEEE*Xplore*® website: http://ieeexplore.ieee.org/xpl/freeabs_all.jsp?arnumber=4348652

3. Publication C

Publication C was published under the following reference:

*L.Provost, F.Parmigiani, C.Finot, K.Mukasa, P.Petropoulos, D.J.Richardson, "***Analysis of a two-channel 2R all-optical regenerator based on a counter-propagating configuration***", Optics Express 2008 Vol.16(3) pp.2264-2275.*

Analysis of a two-channel 2R all-optical regenerator based on a counter-propagating configuration

L. Provost, F. Parmigiani, C. Finot*, K. Mukasa+, P. Petropoulos, D.J. Richardson

Optoelectronics Research Centre, University of Southampton, Southampton SO17 1 BJ, United Kingdom
lap@orc.soton.ac.uk

Abstract: We report a 2R optical regenerator based on the Self-Phase Modulation and offset filtering technique in a bi-directional architecture for the simultaneous processing of two optical channels at 10 Gb/s within a single highly nonlinear fiber. Whereas excellent mitigation of the inter-channel nonlinear crosstalk is experimentally demonstrated, we identify Rayleigh backscattering as the major source of crosstalk and show how it is related to the regenerator parameters and operational settings. Finally, we demonstrate that this crosstalk does not introduce any significant additional penalties as compared to single channel operation.

OCIS codes: (060.4370) Fiber optics and optical communications: Nonlinear optics fibers; (060.4510) Fiber optics and optical communications: Optical communications; (060.7140) Fiber optics and optical communications: Ultrafast processes in fibers

References and links:

1. O. Leclerc, B. Lavigne, E. Balmefrezol, P. Brindel, L. Pierre, D. Rouvillain, and F. Seguineau, "Optical regeneration at 40 Gb/s and beyond," J. Lightwave Technol. **21**, 2779-2790 (2003).
2. G. Raybon, Y. Su, J. Leuthold, R. Essiambre, T.-H. Her, C. Joergensen, P. Steinvurzel, K. Dreyer, and K. Feder, "40 Gb/s pseudo linear transmission over one million kilometers," in *Proc. Optical Fiber Communications (OFC'02)*(Anaheim CA, 2002), p. 42.
3. S. Wanatabe, F. Futami, R. Okabe, Y. Takita, S. Ferber, R. Ludwig, C. Schubert, C. Schmidt, and H. G. Weber, "160 Gbit/s optical 3R-regenerator in a fiber transmission experiment," in *Optical Fiber Communications Conference (OFC 2003)* (Atlanta, GA, 2003), p. PD 16.
4. M. Daikoku, N. Yoshikane, T. Otani, and H. Tanaka, "Optical 40-Gb/s 3R Regenerator With a Combination of the SPM and XAM Effects for All-Optical Networks," J. Lightwave Technol. **24**, 1142-1148 (2006).
5. P. V. Mamyshev, "All-optical data regeneration based on self-phase modulation effect," in *European Conference on Optical Communications (ECOC'98)* (Madrid, Spain, 1998), p. 475.
6. M. Matsumoto, "Efficient all-optical 2R regeneration using self-phase modulation in bidirectional fiber configuration," Opt. Express **14**, 11018-11023 (2006).
7. L. Provost, F. Parmigiani, C. Finot, P. Petropoulos, and D. J. Richardson, "Self-phase modulation-based 2R optical regenerator for the simultaneous processing of two WDM channels," in *CLEO/Europe-IQEC* (Munich, Germany, 2007), pp. CI2-1-TUE.
8. R. J. Essiambre, B. Mikkelsen, and G. Raybon, "Intra-channel cross-phase modulation and four-wave mixing in high-speed TDM systems," Electron. Lett. **35**, 1576-1578 (1999).
9. L. Provost, C. Finot, K. Mukasa, P. Petropoulos, and D. J. Richardson, "Design scaling rules for 2R-optical self-phase modulation-based regenerators," Opt. Express **15**, 5100-5112 (2007).
10. G. P. Agrawal, *Nonlinear Fiber Optics, 3rd Edition* (Academic Press, 2001).
11. T. Ohara, H. Takara, A. Hirano, K. Mori, and S. Kawanishi, "40-Gb/s x 4-channel all-optical multichannel limiter utilizing spectrally filtered optical solitons," Photon.Technol. Lett. **15**, 763-765 (2003).
12. D. V. Kuksenkov, S. Li, M. Sauer, and D. A. Nolan, "Nonlinear Fibre Devices Operating on Multiple WDM Channels," in *European Conference on Optical Communications (ECOC'05)* (Glasgow, UK, 2005), p. Mo.3.5.1.
13. T. I. Lakoba, and M. Vasilyev, "A new robust regime for a dispersion-managed multichannel 2R regenerator," Opt. Express **15**, 10061-10074 (2007).
14. E. Brinkmeyer, "Analysis of the backscattering method for single-mode optical fibers," J. Opt. Soc. Am. **70**, 1010-1012 (1980).

#89944 - $15.00 USD Received 19 Nov 2007; revised 20 Jan 2008; accepted 20 Jan 2008; published 1 Feb 2008

15. T. H. Wood, R. A. Linke, B. L. Kasper, and E. C. Carr, "Observation of coherent Rayleigh noise in single-source bidirectional optical fiber systems," J. Lightwave Technol. **6**, 346-352 (1988).
16. S. Radic, and S. Chandrasekar, "Limitations in dense bidirectional transmission in absence of optical amplification," Photon. Technol. Lett. **14**, 95-97 (2002).
17. M. O. Van Deventer, "Polarization properties of Rayleigh backscattering in single-mode fibers," J. Lightwave Technol. **11**, 1895-1899 (1993).
18. P. Gysel, and R. K. Staubli, "Spectral properties of Rayleigh backscattered light from single-mode fibers caused by a modulated probe signal," J. Lightwave Technol. **8**, 1792-1798 (1990).
19. P. Di Vita, and U. Rossi, "Backscattering measurements in optical fibres: separation of power decay from imperfection contribution," Electron. Lett. **15**, 467-469 (1979).
20. L. Provost, F. Parmigiani, K. Mukasa, M. Takahashi, J. Hiroishi, M. Tadakuma, P. Petropoulos, and D. J. Richardson, "Simultaneous all-optical 2R regeneration of 4x10 Gbit/s wavelength division multiplexed channels," in *European Conference on Optical Communications (ECOC'07)* (Berlin, Germany, 2007), p. Di 4.5.1.

1. Introduction

Over the recent years, all-optical signal processing has attracted much attention in the field of optical telecommunications. The main argument for optical processing techniques is that they can easily support high bitrate operations (far beyond 40 Gb/s) thereby bridging the gap between the ultra-high capacity of optical transmission systems and the limited bandwidth of electronic equipment. Within this context, all-optical regeneration schemes (either just signal Re-amplification and Reshaping (2R) or complete with Retiming (3R) operation) have been proposed as an alternative to the conventional approach based on optical-electronic-optical conversion [1]. Numerous reported implementations exploiting nonlinear effects either in optical fibers [2-4], or in semiconductor optical amplifiers (SOAs) [1] have proven without doubt the power of the approach. However, the true potential of all-optical techniques will only be realized in a cost effective manner if it proves possible to process multiple channels simultaneously in a single device. The challenge in achieving multi-channel operation is to mitigate coexisting cross-channel nonlinear effects, which give rise to crosstalk.

In this paper, we experimentally investigate an optical scheme based on the Mamyshev regenerator [5] which allows the simultaneous processing of two optical channels. The technique uses a bi-directional architecture [6, 7], which allows the use of a single highly nonlinear optical fiber (HNLF) without giving rise to nonlinear crosstalk between the channels. After a first brief description of the working principle, we identify the presence of a different source of crosstalk originating from the backscattering contribution. An analysis of this contribution is presented allowing the determination of the crosstalk levels. We then experimentally validate the proposed model, and move on to demonstrate that the presence of a second channel does not impose any additional power penalty to the operation of the regenerator.

2. Principle of operation

The optical 2R regenerator under consideration is based on the scheme proposed by Mamyshev in Ref. [5]. Its operation relies on the dependence of the Self-Phase Modulation (SPM) induced spectral broadening on the gradient of the pulse intensity profile. The incident pulse train to be regenerated passes through a length of HNLF and an offset filter and is then used to carve into the broadened spectrum, providing pulse reshaping on the marks and noise removal from the spaces, which originates both from noise accumulation and generation of ghost pulses due to intra-channel nonlinearities [8]. This regeneration process results in better discrimination between the marks and spaces. This scheme is suitable for the on-off keying modulation format, and has drawn much attention to date, mainly due to its simplicity and ease of implementation using HNLF. In a previous work, we have provided some generalized rules that link the physical design of the optical regenerator to its performance [9].

The extension of the regenerator to a multi-channel environment requires an effective mitigation of the inter-channel crosstalk arising from Kerr nonlinearities, such as Cross-Phase

#89944 - $15.00 USD Received 19 Nov 2007; revised 20 Jan 2008; accepted 20 Jan 2008; published 1 Feb 2008

Modulation (XPM) and Four-Wave Mixing (FWM), which compete with SPM [10]. Nonlinear crosstalk typically manifests itself as the introduction of strong asymmetries in the broadened spectrum, which result from an incomplete pulse interaction between the co-propagating adjacent channels. In order to alleviate these nonlinearities, one has to minimize the interaction time between pulses by ensuring a complete and fast walk-through. Such mitigation is usually achieved by providing a suitable chromatic dispersion map. In the past, this has been achieved through either a specific arrangement of fiber assemblies of alternating dispersion [11], highly specialized fibers [12], or dispersion compensating devices with spectrally periodic responses[13]. In Ref. [6], Matsumoto proposed a wavelength-conversion-free all-optical 2R regeneration scheme, where a single channel is transmitted twice along the same fiber taking advantage of a bidirectional architecture to enhance the regenerative performances. Herein, we propose a mitigation scheme that relies on a similar bi-directional configuration in which two different optical channels are propagating in opposite directions within the same optical fiber [7].

Figure 1(a) schematically illustrates the corresponding implementation. The major benefit of this solution lies in the extremely high relative walk-off value T_W between the two counter-propagating channels, which is typically $\sim 2/V_g(\lambda)$, where $V_g(\lambda)$ is the group velocity at wavelength λ (e.g. for silica-based fibers: T_w=10 ns/m). Interestingly, this value is almost independent of the chromatic dispersion and the spectral separation of the channels. The immediate result of a high T_W value is that the nonlinear (NL) phase ϕ_{NL} induced by XPM manifests itself as a constant phase shift across the whole pulse (proportional to the ratio between the pulse peak power and T_w), as illustrated in Fig. 1(b). It follows that no additional frequencies are generated from this XPM contribution, reducing the distortion induced on the SPM-broadened spectrum. Note that any frequency chirp due to incomplete pulse collisions occurring at the two ends of the HNLF is expected to be negligible due to the large T_w. (see Fig. 1(b)). Similarly, because of the relatively high walk-off, there is no FWM phase-matching condition between the two counter-propagating pulses. More generally, each signal evolution is insensitive to other propagation-related issues (e.g. the variation in the pulse intensity profile along the fiber, or change in the polarization states) as well as to the cumulative effects of a large number of pulse collisions. Last but not least, the general operating principles relating to the single channel regenerator [9] are preserved and can be applied directly to the bi-directional configuration.

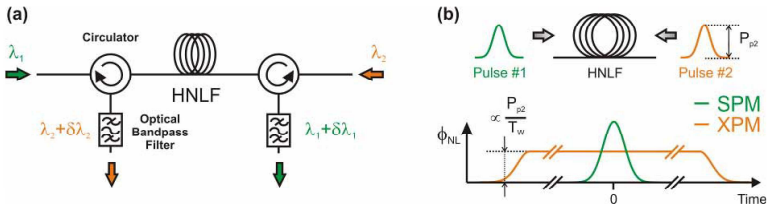

Fig. 1. (a) Schematic of the bi-directional regenerator. (b) Variation of the nonlinear phase self-induced on the first pulse by SPM (green curve) and XPM (orange curve) arising from the interaction with a second counter-propagating pulse. The NL phases are plotted across the temporal window of the first pulse.

3. Crosstalk due to backscattering

Despite the reduction in the XPM crosstalk, the proposed bi-directional architecture introduces a new source of crosstalk resulting from the reflections of the counter-propagating signal as it propagates along the HNLF. Since these reflections co-propagate with the second signal, they may give rise to some performance degradation, and therefore their contribution needs to be thoroughly investigated.

#89944 - $15.00 USD Received 19 Nov 2007; revised 20 Jan 2008; accepted 20 Jan 2008; published 1 Feb 2008

These reflection contributions come from either local defects generating a strong signal reflection (e.g. reflections at connections and splices, or extraordinary defects in the fibers), or more predominantly from the backscattering experienced along the HNLF. The fiber backscattering mechanism is essentially governed through a Rayleigh scattering process, and originates from sub-wavelength non-uniformities along the fiber. For an optical fiber, these defects are found at regions of refractive index variation across the transverse fiber profile. Given the localized nature of the process, the overall backscattering results from the summation of the elementary scattering contributions created both across and along the optical fiber. The strength of the process is quantified through two parameters [14]: the local scattering coefficient - $\alpha_R(\lambda,z)$, representing the strength of the backscattering-process, and the backscatter re-capture fraction $S_R(\lambda,z)$, that represents the fraction of the backscattered light that is recollected within the fiber core. The backscattering properties of an optical fiber are generally highly dependent on their refractive index profile as well as the manufacturing and drawing conditions and might vary from fiber to fiber. Due to their higher core-cladding refractive index difference and the resulting higher numerical aperture, HNLFs exhibit higher backscattering coefficients than conventional transmission fibers.

Intuitively, the impact of Rayleigh backscattering will depend on the spectral position and evolution of the incoming signal as well as the relative position of the output offset filters: the strength of this crosstalk will be expected to increase as the spectral separation between the two channels decreases. This kind of crosstalk was previously highlighted in a wavelength-conversion-free all-optical single channel regenerator [6]. Here we present a simple approach that allows one to derive the backscattered spectrum induced by a nonlinearly propagating signal. The validity of the theoretical expressions presented in Section 3.1 below is then experimentally verified in Section 3.2. This will allow us to draw some general and useful conclusions on the impact of Rayleigh backscattering on SPM-based devices that follow a bi-directional configuration. It will be shown in the second part of this paper, where extensive system measurement are reported that this effect only slightly affects the device performance.

3.1 Theoretical prediction

So far, the limitations imposed by Rayleigh backscattering have theoretically and experimentally been studied for the cases of bidirectional transmission links or distributed amplification in optical communication systems. These studies have represented Rayleigh crosstalk as either coherent (intra-channel) or incoherent (inter-channel) sources of interference [15, 16], and have also accounted for the partial depolarization effect experienced by the backscattered signal [17]. However, these studies have been limited to regimes where nonlinear effects could be neglected. In this Section, we derive an expression for the power spectral density of the Rayleigh backscattering contribution of a propagating signal. We propose a simple model to extend the estimation of the Rayleigh backscattering contribution when a distributed spectral broadening of the propagating signal is experienced along the optical fiber. Following the analysis in Ref. [18], the power spectral density of the backscattered field is directly proportional to the power spectral density of the incoming signal. This statement is still valid for modulated signals provided that: (a) the signal is cyclostationary (e.g. such as a Pseudo Random Bit Sequence (PRBS)), and (b) the bit slot duration T_b is very short compared to the fiber round trip time T_L, defined as $2L/V_g(\lambda)$, where L is the fiber length. The average backscattered intensity can be interpreted then as an incoherent summation of a large number of elementary uncorrelated backscattered contributions. High bitrate systems (e.g. >10 Gb/s) and typical fiber lengths (of the order of several hundreds of meters) fully satisfy these conditions.

Let $S(t, \lambda, z_0)$ be the power spectrum of the incoming signal obtained at a distance z_0 from the fiber input at an instant t. Defining S_{BS} as the corresponding backscattered power spectral density of the backscattered field integrated over the fiber length, L, we have:

#89944 - $15.00 USD Received 19 Nov 2007; revised 20 Jan 2008; accepted 20 Jan 2008; published 1 Feb 2008

$$S_{BS}(t,\lambda)=\int_{z_0=0}^{L}\alpha_R(\lambda,z_0)\,S_R(\lambda,z_0)\,S\left(t-\frac{2z_0}{V_g(\lambda)},\lambda,z_0\right)\int_{z=0}^{z_0}e^{-\alpha(\lambda)z}\,dz\,dz_0 \qquad (1)$$

with $2z_0/V_g(\lambda)$ being the retardation term corresponding to the round trip time over the distance z_0, and $\alpha(\lambda)$ the attenuation coefficient of the fiber.

The corresponding power spectrum of the total average contribution $S_{BS,TOTAL}(\lambda)$ is obtained averaging Eq. (1) over time:

$$S_{BS,TOTAL}(\lambda)=\langle S_{BS}(t,\lambda)\rangle_t=\alpha_R(\lambda)\,S_R(\lambda)\int_{z_{0=0}}^{L}\left\langle S\left(t-\frac{2z_0}{V_g(\lambda)},\lambda,z_0\right)\right\rangle_t\frac{1-e^{-\alpha(\lambda)z_0}}{\alpha(\lambda)}\,dz_0 \qquad (2)$$

with $\langle\cdot\rangle_t$ denoting the time average. One should note that the relations shown above are valid under the assumptions that (a) the level of backscattering is small enough, so that the reflected signal does not experience any nonlinear effects; the backscattered contribution only experiences power decay due to the fiber attenuation; and (b) the state of polarization of the backscattered signal is preserved. Equation 2 also assumes that the parameters α_R and S_R do not vary along the length of the fiber.

3.2 Experimental characterization of the backscattered spectrum

In order to validate the expressions and assumptions made in the previous Section, we experimentally measured the backscattered spectra as a function of the input power of a pulsed signal. The measurements were performed using the experimental set-up depicted in Fig. 2.

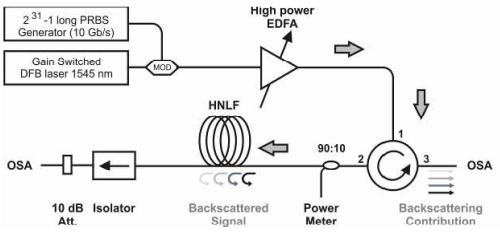

HNLF parameters at 1550 nm		
Length	1	km
Attenuation	-2.13	dB/km
Effective length	0.79	km
2nd order dispersion	2.30	ps²/km
3rd order dispersion	0.03	ps³/km
Nonlinear coefficient	18	/W/km

Fig. 2. Experimental set-up used for the characterization of the backscattered signal, and the corresponding HNLF parameters.

A gain-switched laser diode operating at 1545 nm generated 6.8 ps-long Gaussian pulses at a 10 GHz repetition rate. The pulse stream was intensity-modulated by a $LiNbO_3$ modulator using a 2^{31}-1-long PRBS and fed into an optical amplifier delivering up to ~25 dBm average output power at the fiber input. The signal was then launched into the HNLF (see Fig. 2 for the fiber parameters) after being first coupled into a circulator, which was used to separate the incoming signal from the outgoing backscattered signal. At the fiber output, an optical isolator was employed to block any undesirable Fresnel reflections created at the fiber end facet. Both transmitted and reflected spectra were measured. The power at the input of the HNLF was monitored using a 90:10 optical power splitter.

Figure 3 compares (a) the backscattered spectra to (b) the SPM broadened spectra obtained in the forward direction for various input power levels. Consecutive spectral traces are vertically offset in the two plots by 5 dB for easier reading. As the input peak power increases, the variation in the backscattered and forward-propagating spectra becomes ever more noticeable – both in terms of shape and spectral extent. We observe that the

#89944 - $15.00 USD Received 19 Nov 2007; revised 20 Jan 2008; accepted 20 Jan 2008; published 1 Feb 2008

backscattered spectra exhibit a common flat-top shape, which becomes more pronounced as the input power increases. This behavior is explained by the weighted summation of all the spectral ripples exhibited in the SPM-induced broadened spectrum (see Eq. 2). Additionally, a saturation effect arising from the fiber losses restricts the backscattered spectral extent by limiting the contribution of frequencies generated at longer distances. Note that in our experiment, the presence of a strong contribution of constant bandwidth (equivalent to the input signal bandwidth) which can be observed at the wavelength of the incoming signal was due to the presence of a parasitic reflection (around -23 dB) experienced at the connection between the circulator port 2 and the tap coupler input port.

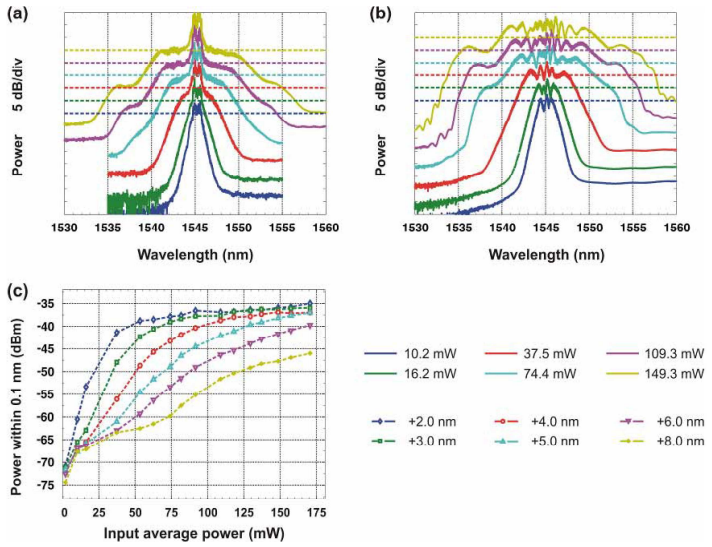

Fig. 3. (a) Measured backscattered spectra as a function of the input average power of the signal. (b) Measured transmitted spectra as a function of the retrieved input average power of the pulses. Consecutive spectra in (a) and (b) are offset by 5 dB for clarity and acquired with a 0.1 nm resolution bandwidth. Color dashed lines correspond to same power level for each spectrum. (c) Backscattered levels within a 0.1 nm bandwidth as a function of the input average power for various offset positions from the input central wavelength. Input average powers are given at the input port of the fiber.

As can be noted, increasing the input power, the strength of the frequency components around the flat-top region remains constant, while the overall spectral bandwidth broadens. To underline this, the backscattered level within a 0.1 nm bandwidth is reported in Fig. 3(c) as a function of the input average power of the signal (or alternatively as a function of the input average power) when various offset positions are considered. The combined results of the spectral broadening and backscattering are clearly summarized in this figure and allow prospecting the level of the backscattering signal for the bi-directional configuration. We clearly observe a saturation effect with an asymptotic convergence to about -35 dBm. The presence of this saturated regime undoubtedly allows a certain degree of freedom in the choice of the regenerator parameters. For instance, an increase in the input power and a consequent increase in the offset filter position can be chosen without significantly changing the backscattering contribution, which remains at a nearly constant level. Finally, when a two-channel configuration is considered, Fig. 3(c) facilitates the determination of the backscattering levels as a function of the channels separation and the relative position of the offset filters.

#89944 - $15.00 USD Received 19 Nov 2007; revised 20 Jan 2008; accepted 20 Jan 2008; published 1 Feb 2008

3.3 Comparison between theoretical and experimental results

In this Section we compare the experimentally measured backscattered spectra to those obtained by the expression reported in Section 3.1. Equation. (2) is evaluated by considering the experimental parameters, the insertion losses of the system, the properties of the optical fiber and the nonlinear propagation of an incoming Gaussian pulse that is governed by the Nonlinear Schrödinger Equation [10]. Parameter α_R was retrieved from a spectral attenuation measurement and found to be ~5.5 dB/km/μm^4, while S_R was acquired from a bi-directional high resolution optical time-domain reflectometry measurement [19]. Moreover, this last measurement confirmed the excellent longitudinal homogeneity of the scattering properties of the HNLF used and the absence of any detrimental localized defects. The $S_R\alpha_R$ product was eventually estimated to be -32.8 dB/km at 1550 nm.

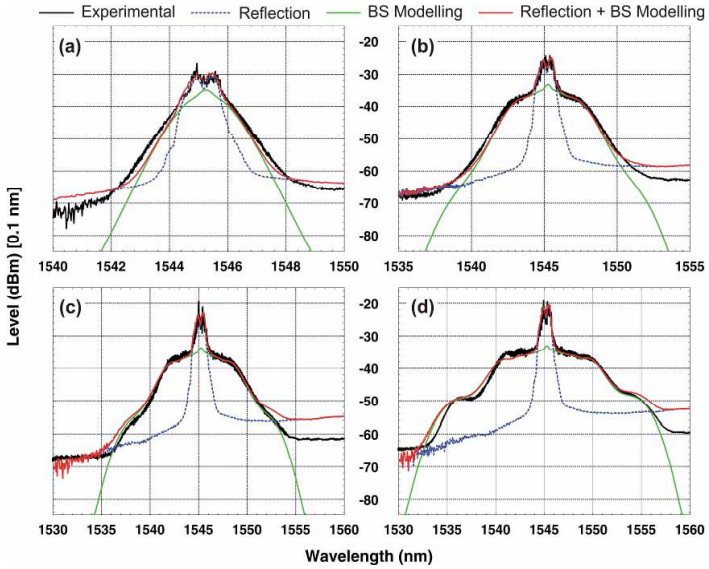

Fig. 4. (a-d) Comparison between experimental (black curves) and computed backscattered spectra (red curves) obtained from the contributions of the sole backscattering modeling (green curves) and the experimentally measured point-reflection (blue dashed curves) for four different input average powers. (a): 16.2 mW; (b): 53.3 mW; (c) 74.4 mW; and (d) 149.1 mW. Resolution bandwidth: 0.1 nm.

Some computed spectra are reported in Fig. 4 together with their corresponding experimental ones for four different input average powers (16.2, 53.3, 74.4, and 149.1 mW respectively). In order to achieve a better accuracy in our simulations, we used a measured spectral trace at port 2 of the circulator as our starting data corresponding to case (a) in Fig. 4, and derived the remaining cases by properly scaling the input power. The green curves in Fig. 4 show the numerical backscattering spectra, while the blue dashed curves show the spectra of parasitic reflection previously mentioned. The red curves are the final calculated spectra, formed by summing these two contributions (green and blue curves). The agreement with the experimental traces (black curves) is extremely good as the mismatch over the flat region range is within 0.8 dB, which is attributed to insertion loss measurement uncertainties.

From the previous discussion, we can conclude that the optical noise induced by Rayleigh backscattering crosstalk can be accurately quantified when the conditions set in Section 3.1

#89944 - $15.00 USD Received 19 Nov 2007; revised 20 Jan 2008; accepted 20 Jan 2008; published 1 Feb 2008

are satisfied. However these conditions depend strongly on the fiber properties (i.e. chromatic dispersion, nonlinear coefficient, attenuation loss, and scattering properties), its length and the properties of the incoming signal (pulse width duration, bit-rate). Nevertheless it is interesting to point out that the fiber length directly determines the number of pulses that contribute to the backscattered signal and can be estimated as $\eta=\frac{1}{2}L/(V_g \cdot T_B)$ where ½ holds for the mark probability ratio. Referring to our setup, one finds $\eta \sim 2.5 \cdot 10^5$ pulses. This large number of pulses gives rise to strong averaging effects and subsequently the individual properties of the pulses (e.g. amplitude jitter, mark density probabilities) become insignificant, so that the backscattered contribution is likely to remain constant for a degraded incoming signal when strong amplitude variation is experienced.

Although the results presented in this section have allowed us to derive some conclusions regarding the level of the induced Rayleigh backscattered signal in a simple manner, a more precise study would require the exact statistics of the data signals to be considered in order to accurately assess the effects of the interaction of this type of noise with the transmitted signal at the detection stage. However, since the degradation introduced by Rayleigh backscattering appears to be low enough, so that it does not affect the optical signal-to-noise ratio to any significant extent, it is unlikely to alter the performance of the system.

4. Experimental implementation of the two-channel optical regenerator

In this Section, we describe the implementation of an optical regenerating device using the proposed bi-directional architecture at 10 Gb/s in order to evaluate i) the mitigation of XPM, and ii) the impact of the presence of the Rayleigh backscattering noise. To assess the performance of the XPM mitigation, we characterized the regenerator in a single- and dual-channel operation, and for various filter offsets. Finally, we present bit-error rate (BER) measurements on the two channels taken under conditions for which backscattering crosstalk is present.

4.1 Experimental set-up

Figure 5 depicts the experimental set-up of the optical regenerator. Two optical channels sitting at λ_1=1549.7 nm (Channel 1) and λ_2=1554.2 nm (Channel 2) respectively, were generated by two chirp-compensated Gain-switched laser diodes. The pulses were Gaussian with a similar temporal duration of ~6.3 ps. Both signals were intensity-modulated using two complementary 2^{31}-1 long PRBS running at a repetition rate of 10 GHz. The HNLF used was the same as in the previous experiment (see Fig. 2 for fiber parameters). Two adjustable optical filters (0.57 nm bandwidth each) were employed as the offset filtering elements at the HNLF output ports. In the following $\delta\lambda_i$ denotes the corresponding wavelength-detuning value with respect to the initial carrier wavelength λ_i, where i = (1, 2) is the channel number.

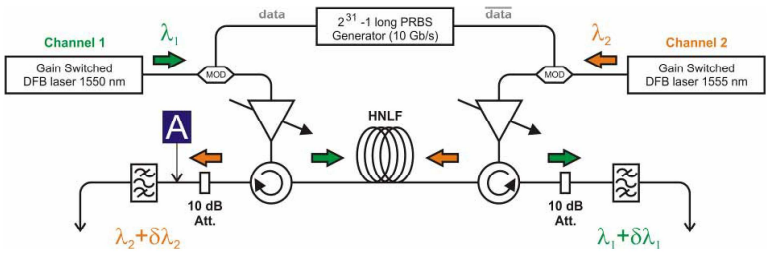

Fig. 5. Experimental setup of the optical 2R optical regenerator.

#89944 - $15.00 USD Received 19 Nov 2007; revised 20 Jan 2008; accepted 20 Jan 2008; published 1 Feb 2008

4.2 Characterization of the regenerator properties

We characterized the optical regenerator both in the presence (ON case) and in the absence (OFF case) of the second interfering optical channel. We firstly considered the evolution of the power transfer functions (TFs) of the two channels, by representing the output power variation as a function of the nominal input power. It is worth noting that we have mainly focused our study in the spectral range where the broadened channel spectrum and the backscattered spectrum were overlapping, which corresponds to the worst-case scenario. Note that we have taken more detailed measurements for Channel 1, but similar results are also expected for Channel 2.

For each considered filter offset position, the power P_1 (and P_2), corresponding to the optimal (nominal) operation power of channel 1 (channel 2) for the OFF case, was directly measured from the TFs. Examples of measured TFs obtained for the two channels are shown in Fig. 6(a) on a linear and a logarithmic scale in order to clearly appreciate the characteristics of the regeneration at high- (linear scale) and low- input power levels (logarithmic scale) respectively. To better appreciate the effect of crosstalk, the TFs for channel 1 are reported for various filter detuning values. As $\delta\lambda_1$ increases, the corresponding nominal operating point P_1 obviously increases, due to the requirement for a broader SPM spectrum [9]. The corresponding values of P_1 and P_2 as a function of the offset filter positions are summarized in Fig. 6(b). Note that the slight dependence of the operating power on the sign of $\delta\lambda_i$ shown for Channel 1 can be explained by the slightly asymmetric SPM spectral broadening. Similar measurements were repeated in the presence of the second channel (ON case), the average power of which was set to the previously determined nominal value (P_1 or P_2) for $\delta\lambda_i$ = -2.8 nm. The corresponding TFs are also shown in Fig. 6(a).

A comparison between the TFs of the ON and OFF cases for a given $\delta\lambda$ clearly shows that whereas at high input power levels (marks) the overlapping of the TFs for both cases is satisfactory, at low input powers (spaces) a constant power floor is clearly experienced. From these results, we can conclude that the mitigation of the XPM and FWM-induced interchannel crosstalk is particularly efficient, since there is no variation in the TF evolution. However, the presence of the power floor limits the maximum achievable output extinction ratio (defined as the ratio between the power in a 'one' and a 'zero' slot [3]. The presence of this power floor is obviously explained by the presence of the Rayleigh backscattered signal that falls within the bandpass of the optical filter. This noise floor becomes more significant as the wavelength of the output signal approaches the central wavelength of the second channel, as anticipated from a direct observation of the results shown in Fig. 3(c).

In Fig. 6(c), we compare the evolution of the output extinction ratios as a function of the operating filter offset position for an initial extinction ratio of 13 dB. For Channel 1, we clearly see that there is no change when the filter position is placed far apart from the second channel ($\delta\lambda_1<0$). In contrast, when the filter is centered between λ_1 and λ_2 (i.e. $\delta\lambda_1>0$), the higher the offset position, the higher the output extinction ratio degradation. A similar trend is observed for Channel 2. A more clear view of the crosstalk level is given in Fig. 7(a), where the spectra measured for all possible ON/OFF cases are shown (taken at point A in Fig. 5). Considering $\delta\lambda_2$=-2.8 nm, the backscattered contribution of Channel 1 within the filter bandwidth (grey-shaded band) can clearly be observed. The power calculated from the backscattered spectrum within the filter bandwidth is ~-37 dBm, which corresponds to the observed noise floor level obtained for the corresponding TF (Channel 2) in Fig. 6(a). Similar conclusions are drawn when operating at different offset values. To facilitate a direct extraction of the backscattered levels, a factor of ~2.4 should be applied on the input average powers of Fig. 3(c) to match the convention of Fig. 6 (i.e. input powers are expressed at the output of the high power amplifiers and not at the fiber input). This coefficient represents the insertion losses of the components employed between the high power amplifier and the input fiber port. Recalling that the backscattered levels are reported with a 0.1 nm bandwidth resolution and that an additional 10 dB attenuator is used in this Section, a good agreement is

#89944 - $15.00 USD Received 19 Nov 2007; revised 20 Jan 2008; accepted 20 Jan 2008; published 1 Feb 2008

found between the observed TF power level floors and corresponding counter-propagating backscattered levels.

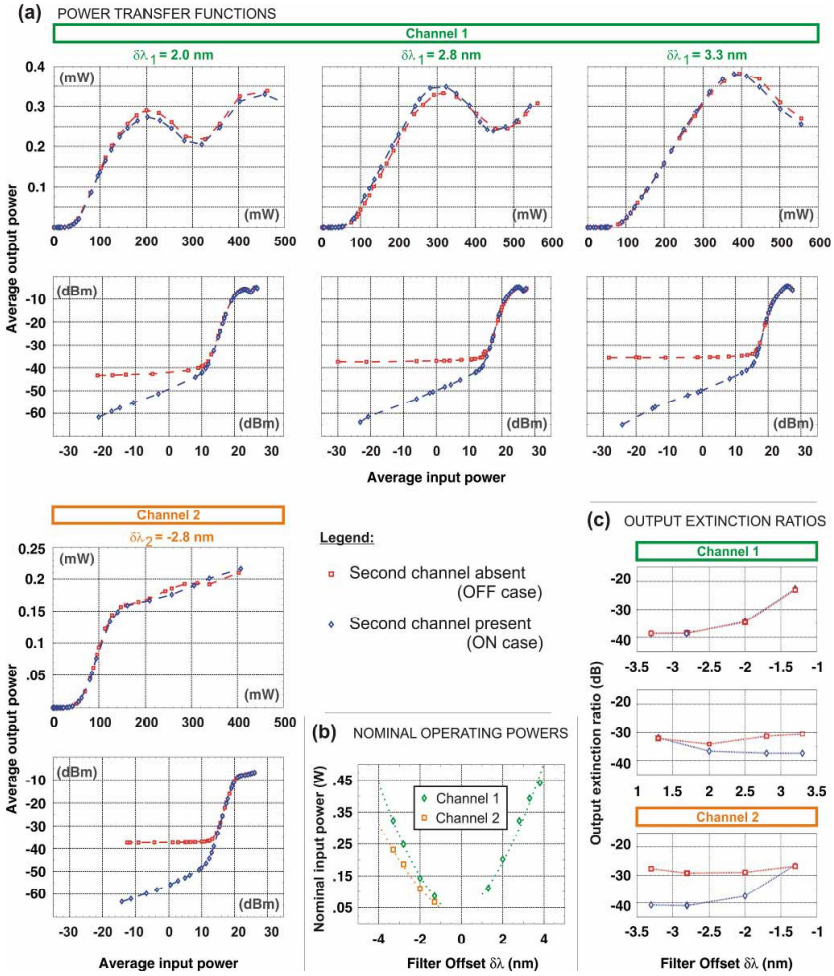

Fig. 6. (a) Power TFs for Channels 1 and 2 for different filter detunings in the presence and in the absence of the second channel. (b) Nominal input power as a function of the filter offset position for both channels. (c) Output extinction ratio as a function of the filter offset value for both channels in the presence and in the absence of the second channel for an input extinction ratio of 13 dB. The reported input powers are measured at the output of each high power amplifier.

Finally, BER measurements were carried out to assess the overall system performance. As a working point we chose again an offset detuning of 2.8 nm for both channels. Fig. 7(b) shows the corresponding BER traces for the two channels in the presence/absence of the other channel. As compared to the back-to-back measurement, under single channel operation, the

#89944 - $15.00 USD Received 19 Nov 2007; revised 20 Jan 2008; accepted 20 Jan 2008; published 1 Feb 2008

regenerator introduces a negligible power penalty for Channel 1 and a negative power penalty of -0.6 dB for Channel 2 at error free operating conditions (BER=10^{-9}). In the presence of the second channel, the results demonstrate that a small extra power penalty is introduced due to the backscattering process. The corresponding additional penalty remains however limited to just 0.1 dB for Channel 1 and 0.4 dB for Channel 2 at error-free operation, which can be attributed to the different backscattering level (~-32.9 dB, and ~-29.4 dB for channel 1 and channel 2 respectively) by referring to Fig. 3(c). No evidence of stimulated Brillouin scattering was experienced in any of the reported characterization measurements on the regenerator.

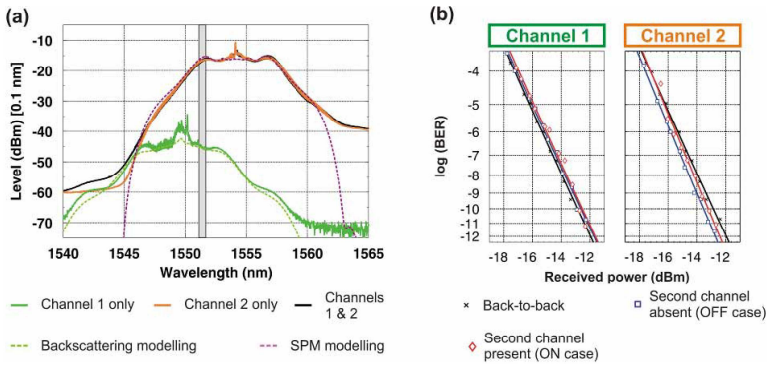

Fig. 7. (a) Experimental spectra measured at point A of Fig. 5 when either of Channels 1 or 2 are present or not and for operating powers P_1 and P_2 set for $\delta\lambda_1$=-$\delta\lambda$2=2.8 nm. (0.1 nm resolution bandwidth). Gray-shaded area represents the offset filter 3 dB bandwidth used for Channel 2. (b) BER measurements of the regenerator for the two Channels (operating powers set for $\delta\lambda_1$=-$\delta\lambda$2=2.8 nm). 3 dB-bandwidth of the electrical filter ~6.5 GHz.

5. Discussion and conclusion

We have presented a bi-directional optical regeneration scheme to simultaneously process two optical channels in a single HNLF, by minimizing the otherwise strong impact of the crosstalk induced by inter-channel nonlinearities (XPM, FWM). The interchannel crosstalk is largely mitigated, due to the extremely high walk-off value between the two counter-propagating signals. Nevertheless, a new source of crosstalk is identified arising from the Rayleigh backscattering contribution along the HNLF. We have demonstrated that this contribution can be predicted within an excellent degree of confidence, by considering the evolution of the distributed spectral broadening of the propagating signal and the operating parameters of the regenerator. The presence of this backscattering contribution limits the maximum achievable output extinction ratio of the regenerator by contributing a constant background level on the regenerator TF at low input powers. This level is directly dependent not only on the fiber properties (namely backscattering properties and presence of local defects along the fiber), but also on the operating conditions of the regenerator (input power, channel separation, detuning filter position). Through BER measurements we have confirmed however, that this backscattering contribution is generally not likely to introduce any significant penalties to the operation of the regenerator.

Ghost pulses should only slightly contribute to the spectral extent of the backscattering spectrum as they experience less spectral broadening than the marks. Consequently, it is expected that this scheme should exhibit similar performance to the single channel Mamyshev regenerator, when degraded signals are considered.

#89944 - $15.00 USD Received 19 Nov 2007; revised 20 Jan 2008; accepted 20 Jan 2008; published 1 Feb 2008

It is not straightforward to generalize this analysis for systems operating at higher bit-rates, or regenerators with different HNLF parameters. This difficulty originates from the existence of a close relationship between the fiber parameters (e.g. length, chromatic dispersion, loss) and the performance of the regenerator (e.g. input power, TF behavior, filter detuning) [9]. The spectral extent of the backscattered contribution is determined by the selected filter offset position (which dictates the spectral broadening of the signal in the forward direction), whereas the corresponding backscattering noise level mainly arises from the fiber parameters and the input average power, which both depend directly on the bitrate. However, an interesting observation is that as the bit-rate increases (i.e. the pulse width decreases), the fiber length required to achieve a certain level of regenerative performance decreases [3]. Hence, it is likely that the impact of the increase in the input power levels due to the higher bit-rates in Eq. (2) will be counterbalanced by this reduction in the fiber length. A precise quantification of these counter-balancing effects is beyond the scope of this study.

Finally, the proposed architecture can be used to offer a wavelength-transparent two-channel optical regenerator by cascading a second regenerator to the one described above. It is important to appreciate that any crosstalk due to backscattering in such a two-stage configuration would not accumulate within the second regenerator stage, since these contributions have too low a power to give rise to any substantial spectral broadening. This could overcome the limitations induced by coherent backscattering crosstalk as anticipated from [6, 16] when considering a single channel regenerator operating in a bidirectional configuration, as the overall contribution of the backscattered crosstalk would exclusively arise from the second channel in the second stage. Recently the proposed scheme has been extended to the simultaneous processing of up to four WDM channels within the same HNLF, combining this proposed bidirectional architecture with a polarization multiplexing scheme [20].

Acknowledgements

This work has been supported by the European Commission under TRIUMPH project IST-027638. The authors gratefully acknowledge the Furukawa Electric Company (Japan) for the loan of the highly nonlinear fiber used in the experiments.

* C. Finot is now with the Institut Carnot de Bourgogne (ICB), UMR-CNRS 5209, Université de Bourgogne, 9 avenue Alain Savary, 21078 Dijon, France.

+ K. Mukasa is now with The Furukawa Electric Company, Fitel Photonics Laboratory, 6 Yawata-Kaigandori, Ichihara, Chiba Prefecture, Japan.

#89944 - $15.00 USD Received 19 Nov 2007; revised 20 Jan 2008; accepted 20 Jan 2008; published 1 Feb 2008

4. Publication D

Publication D was published under the following reference:

L.Provost, F.Parmigiani, P.Petropoulos, D.J.Richardson, "**Investigation of simultaneous 2R regeneration of two 40 Gb/s channels in a single optical fibre**", *Photonics Technology Letters 2008 Vol.20(4) pp.270-272*.

The paper can be found at the following URL on the IEEE*Xplore*® website: http://ieeexplore.ieee.org/xpl/freeabs_all.jsp?arnumber=4439745.

---

5. Publication E

Publication E was published under the following reference:

L.Provost, F.Parmigiani, P.Petropoulos, D.J.Richardson, K.Mukasa, J.Takahashi, J.Hiroishi, M.Tadakuma, "**Investigation of four-wavelength regenerator using polarization-and-Direction-Multiplexing**", *Photonics Technology Letters 2008 Vol.20(20) pp.1676-1678.*

The paper can be found at the following URL on the IEEE*Xplore*® website: http://ieeexplore.ieee.org/xpl/freeabs_all.jsp?arnumber=4604682.

---

6. *Publication F*

Publication F was published under the following reference:

*F.Parmigiani, P.Vorreau, L.Provost, K.Mukasa, M.Takahashi, M.Tadakuma, P.Petropoulos, D.J.Richardson, W.Freude, J.Leuthold, "***2R regeneration of two 130 Gb/s channels within a single fibre***", OFC 2009 San Diego 22-26 Mar 2009 JThA56.*

The paper can be found at the following URL on the IEEE*Xplore*® website: http://ieeexplore.ieee.org/xpl/freeabs_all.jsp?arnumber=5032322.

References

[1] Verizon_Newscenter. *Verizon's Second Field Trial of 10 Gigabit-per-Second XG-PON Fiber-to-the-Premises System Affirms FiOS Network Design Is Future-Ready*. [cited 2010 July]; Available from: http://newscenter.verizon.com/press-releases/verizon/2010/Verizon-s-Second-Field-Trial-of-10-Gigabit-per-Second-XG-PON-Fiber-to-the-Premises-System-Affirms-FiOS-Network-Design-Is-Future-Ready.html.

[2] Desurvire, E.B., *Capacity Demand and Technology Challenges for Lightwave Systems in the Next Two Decades*. J. Lightwave Technol., 2006. **24**(12): p. 4697-4710.

[3] Nakazawa, M., *1 Tb/s OTDM technology*, in *27th European Conference on Optical Communications (ECOC)*. 2001: Amsterdam (The Netherlands). p. 184-187.

[4] Winzer, P.J. and R.J. Essiambre, *Advanced Modulation Formats for High-Capacity Optical Transport Networks*. J. Lightwave Technology, 2006. **24**(12): p. 4711-4728.

[5] Salsi, M., et al., *155x100Gbit/s coherent PDM-QPSK transmission over 7,200km*, in *35th European Conference on Optical Communication (ECOC)*. 2009: Vienna (Austria). p. PostDeadline Session.

[6] Tzanakaki, A., et al., *Broadband building Blocks*, in *IEEE Circuits & Devices*. 2004. p. 32.

[7] Morioka, T., *Ultrafast optical technologies for large-capacity TDM/WDM photonic networks.* Journal of Optical and Fiber Communications Reports, 2007. **4**(1): p. 14-40.

[8] Yoo, S.J.B., *Wavelength conversion technologies for WDM network applications.* J. Lightwave Technol., 1996. **14**(6): p. 955-966.

[9] Yamamoto, T. and M. Nakazawa, *Ultrafast OTDM transmission using novel fiber devices for pulse compression, shaping, and demultiplexing.* Journal of Optical and Fiber Communications Reports, 2005. **2**(3): p. 209-225.

[10] Bigo, S., et al., *All-optical RZ-to-NRZ format conversion at 10 Gbit/s with nonlinear optical loop mirror*. Electron. Lett., 1994. **30**(22): p. 1868.

[11] Bigo, S., et al., *All-optical fiber signal processing and regeneration for soliton communications.* IEEE J. Sel. Top. Quantum Electron., 1997. **3**(5): p. 1208.

[12] Leclerc, O., et al., *Optical regeneration at 40 Gb/s and beyond.* J. Lightwave Technol., 2003. **21**(11): p. 2779.

[13] Essiambre, R.J., et al., *Intra-channel cross-phase modulation and four-wave mixing in high-speed TDM systems.* Electron. Lett., 1999. **35**(18): p. 1576.

[14] Mamyshev, P.V., *All-optical data regeneration based on self-phase modulation effect*, in *24th European Conference on Optical Communications (ECOC'98)* 1998: Madrid, Spain. p. 475.

[15] The_University_of_Karlsruhe. *TRIUMPH Website : Transparent Ring Interconnection Using Multi-wavelength PHotonic switches*. [cited 2010 July]; Available from: www.ihq.uni-karlsruhe.de/research/projects/TRIUMPH/

[16] Boscolo, S., et al., *All-optical passive 2R regeneration for N x 40 Gbit/s WDM transmission using NOLM and novel filtering technique.* Optics Communications, 2003. **217**(1-6): p. 227.

[17] Leclerc, O., et al., *Simultaneously regenerated 4x40 Gbit/s dense WDM transmission over 10000 km using single 40 GHz InP Mach-Zehnder modulator.* Electron. Lett., 2000. **36**(18): p. 1574-1575.

[18] Chi, N., et al., *2R regeneration based on dispersion-imbalanced loop mirror and its applications in WDM systems.* J. Lightwave Technol., 2002. **20**(10): p. 1809.

[19] Chi, N., et al., *All-optical wavelength conversion and multichannel 2R regeneration based on highly nonlinear dispersion-imbalanced loop mirror.* IEEE Photon.Technol. Lett., 2002. **14**(11): p. 1581.

[20] Kuksenkov, D.V., et al., *Simultaneous 2R regeneration and dynamic dispersion compensation at 40 Gb/s in a nonlinear fiber-based device*. 2003. p. PD5.

[21] Kuksenkov, D.V., et al., *Nonlinear Fibre Devices Operating on Multiple WDM Channels*, in *31th European Conference on Optical Communications (ECOC'05)* 2005: Glasgow, UK. p. Mo.3.5.1.
[22] Vasilyev, M. and T.I. Lakoba, *All-optical multichannel 2R regeneration in a fiber-based device.* Opt. Lett., 2005. **30**: p. 1458-1460.
[23] Ohman, F., et al., *Noise and regeneration in semiconductor waveguides with saturable gain and absorption.* IEEE Journal of Quantum Electronics, 2004. **40**(3): p. 245-255.
[24] Chayet, H., et al., *Regenerative all-optical wavelength converter based on semiconductor optical amplifier and sharp frequency response filter*, in *Optical Fiber Communication Conference (OFC'04)*. 2004. p. ThS2.
[25] Leuthold, J., et al., *All-optical wavelength conversion and regeneration*, in *Optical Fiber Communication Conference (OFC) 2004*. 2004. p. WN1.
[26] Usami, M. and K. Nishimura, *Optical nonlinearities in semiconductor optical amplifier and electro-absorption modulator: their applications to all-optical regeneration.* Journal of Optical and Fiber Communications Reports, 2005. **2**(6): p. 497-529.
[27] Sakurai, T. and N. Kobayashi, *Optical nonlinearities in semiconductor optical amplifier and electro-absorption modulator: their applications to all-optical regeneration.* Journal of Optical and Fiber Communications Reports, 2005. **2**(6): p. 530-557.
[28] Liu, Y., et al., *160 Gb/s SOA-based wavelength converter assisted by an optical bandpass filter*, in *Optical Fiber Communication Conference, 2005. Technical Digest. OFC/NFOEC.* 2005. p. 49.
[29] Akiyama, T., et al., *Nonlinear gain dynamics in quantum-dot optical amplifiers and its application to optical communication devices.* IEEE Journal of Quantum Electronics, 2001. **37**(8): p. 1059.
[30] Sugawaraa, M., et al., *Quantum-dot semiconductor optical amplifiers.* SPIE Proceedings of Materials and Devices for Optical and Wireless Communications, 2002. **4905**: p. 259-275.
[31] Uchiyama, K., et al., *100-Gb/s multiple-channel output all-optical OTDM demultiplexing using multichannel four-wave mixing in a semiconductor optical amplifier.* IEEE Photon. Technol. Lett., 1998. **10**(6): p. 890.
[32] Cho, P.S., et al., *All-optical regeneration at the receiver of 10-Gb/s RZ data transmitted over 30 000 km using an electroabsorption modulator.* IEEE Photon.Technol. Lett., 2000. **12**(2): p. 205-207.
[33] Otani, T., et al., *40 Gbit/s signal transmission using optical 3R regenerator based on electroabsorption modulators*, in *Optical Fiber Communication Conference (OFC)*. 2000. p. 226-228.
[34] Otani, T., et al., *40 Gbit/s optical 3R regenerator for all-optical networks*, in *27th European Conference on Optical Communication (ECOC)*. 2001. p. 278-281.
[35] Nakagawa, J., et al., *All-optical 3R regeneration technique using injection-locking in gain-switched DFB-LD.* Electron. Lett., 2001. **37**(4): p. 231-232.
[36] Webster, M., et al., *All-optical 2R regeneration and wavelength conversion at 10 Gb/s in an integrated semiconductor optical amplifier/distributed feedback laser*, in *27th European Conference on Optical Communication (ECOC)*. 2001. p. 578-579.
[37] Dumeige, Y., et al., *Integrated all-optical pulse restoration with coupled nonlinear microring resonators.* Opt. Lett., 2006. **31**(14): p. 2187-2189.
[38] Foster, M.A., et al., *Nonlinear optics in photonic nanowires*. Opt. Express, 2008. **16**(2): p. 1300-1320.
[39] Salem, R., et al., *All-optical regeneration on a silicon chip.* Opt. Express, 2007. **15**(12): p. 7802-7809.
[40] Biberman, A., et al., *Wavelength multicasting in silicon photonic nanowires.* Opt. Express, 2010. **18**(17): p. 18047-18055.
[41] Armstrong, J.A., et al., *Interactions between light waves in a nonlinear dielectric.* Phys. Rev., 1962. **127**: p. 1918-1939.
[42] Gallo, K. and G. Assanto, *Analysis of lithium niobate all-optical wavelength shifters for the third spectral window.* J. Opt. Soc. Amer. A,, 1999. **16**(5): p. 741-7523.
[43] Ohara, T., et al., *160 Gbit/s optical-time-division multiplexing with PPLN hybrid integrated planar lightwave circuit.* IEEE Photon. Technol. Lett., 2003(15): p. 302–304.
[44] Ta'eed, V.G., et al., *Integrated all-optical pulse regenerator in chalcogenide waveguides.* Opt. Lett., 2005. **30**(21): p. 2900-2902.
[45] Agrawal, G.P., *Nonlinear Fiber Optics, 3rd Edition.* Optics and Photonics. 2001: Academic Press.
[46] Stolen, R.H. and C. Lin, *Self-phase-modulation in silica optical fibers.* Phys. Rev. A, 1978. **1448-1454**(4): p. 1448-1454.
[47] Doran, N.J. and D. Wood, *Nonlinear-optical loop mirror.* Opt. Lett., 1988. **13**(1): p. 56-58.

[48] Bogoni, A., et al., *Nonlinear optical loop mirrors: investigation solution and experimental validation for undesirable counterpropagating effects in all-optical signal processing.* IEEE Journal of Selected Topics in Quantum Electronics, 2004. **10**(5): p. 1115-1123.
[49] Seguineau, F., et al., *Experimental Loop demonstration of cascaded 42.7 Gbit/s NOLM-based 2R regeneration performance versus timing jitter and optical noise*, in *30th European Conference on Optical Communications (ECOC) 2004*. 2004.
[50] Inoue, K., *Four-wave mixing in an optical fiber in the zero-dispersion wavelength region.* J. Lightwave Technol., 1992. **10**(11): p. 1553.
[51] Ciaramella, E. and S. Trillo, *All-optical signal reshaping via four-wave mixing in optical fibers.* IEEE Photon. Technol. Lett., 2000. **12**(7): p. 849.
[52] Inoue, K., *Suppression of level fluctuation without extinction ratio degradation based on output saturation in higher order optical parametric interaction in fiber.* IEEE Photon.Technol. Lett., 2001. **13**(4): p. 338-340.
[53] Ciaramella, E., et al., *All-optical signal reshaping by means of four-wave mixing in optical fibers.* IEEE Photon.Technol. Lett., 2001. **13**(2): p. 142.
[54] Torii, K. and S. Yamashita, *Efficiency improvement of optical fiber wavelength converter without spectral spread using synchronous phase/frequency modulations.* J. Lightwave Technol., 2003. **21**(4): p. 1039.
[55] Yamashita, S. and M. Shahed, *Optical 2R regeneration using cascaded fiber four-wave mixing with suppressed spectral spread.* IEEE Photon.Technol. Lett., 2006. **18**(9): p. 1064-1066.
[56] Radic, S., et al., *All-optical regeneration in one- and two-pump parametric amplifiers using highly nonlinear optical fiber.* IEEE Photon.Technol. Lett., 2003. **15**(7): p. 957-959.
[57] Nakazawa, M., et al., *Random evolution and coherence degradation of a high-order optical soliton train in the presence of noise.* Opt. Lett., 1999. **24**(5): p. 318-320.
[58] Grosz, D.F., et al., *Modulation instability induced resonant four-wave mixing in WDM systems.* IEEE Photon.Technol. Lett., 1999. **11**(3): p. 379.
[59] Hirano, A., et al., *All-optical limiter circuit based on four-wave mixing in optical fibres.* Electron. Lett., 1998. **34**(14): p. 1410-1411.
[60] Ciaramella, E., *A new scheme for all-optical signal reshaping based on wavelength conversion in optical fibers*, in *Optical Fiber Communication Conference (OFC)*. 2000. p. WM37.
[61] Argyris, A., et al., *Extinction ratio improvement by four-wave mixing in dispersion-shifted fibre.* Electron. Lett., 2003. **39**(2): p. 230-232.
[62] Bogris, A. and D. Syvridis, *Regenerative properties of a pump-modulated four-wave mixing scheme in dispersion-shifted fibers.* J. Lightwave Technol., 2003. **21**(9): p. 1892.
[63] Lee, J.H., et al., *Four-wave mixing based 10-Gb/s tunable wavelength conversion using a holey fiber with a high SBS threshold.* IEEE Photon.Technol. Lett., 2003. **15**(3): p. 440.
[64] Tosi-Beleffi, G.M., et al., *10 Gbit/s all-optical 2R fiber based regeneration.* Opt. Commun., 2004. **236**: p. 323–327.
[65] Chow, K.K., et al., *Extinction ratio improvement by pum pmodulated four-wave mixing in a dispersion flattened nonlinear photonic crystal fiber.* Opt. Express, 2005. **13**(22): p. 8900-8905.
[66] Mazumder, S. and S. Yamashita, *Optical 2R Regeneration of 10Gbps Signal Using Cascaded Fiber Four Wave Mixing*, in *31th European Conference on Optical Communications (ECOC)* 2005. p. Mo3.5.3.
[67] Mok, J., et al., *Investigation of group delay ripple distorted signals transmitted through all-optical 2R regenerators.* Opt. Express, 2004. **12**(19): p. 4411-4422.
[68] Suzuki, J., et al., *All-Optical Regenerator Using Wavelength Shift Induced by Cross-Phase Modulation in Highly-Nonlinear Fibers*, in *Optical Fiber Communication Conference (OFC) 2005*. 2005. p. OME-64.
[69] Ito, C. and J.C. Cartledge, *Polarization Independent All-Optical 3R Regeneration Based on the Kerr Effect in Highly Nonlinear Fiber and Offset Spectral Slicing.* IEEE J. Sel. Top. Quantum Electron., 2008. **14**(3): p. 616-624.
[70] Wanatabe, S., et al., *160 gbit/s optical 3R-regenerator in a fiber transmission experiment*, in *Proc. Optical Fiber Communications (OFC'03)*. 2003: Atlanta, GA.
[71] Pender, W.A., et al., *Error free operation of a 40 Gbit/s all-optical regenerator.* Electron. Lett., 1996. **32**(6): p. 567.
[72] Hansryd, J., et al., *Fiber-based optical parametric amplifiers and their applications.* IEEE J. Sel. Top. Quantum Electron., 2002. **8**(3): p. 506.

[73] Wang, W., et al., *Raman-enhanced regenerative ultrafast all-optical fiber XPM wavelength converter*. J. Lightwave Technol., 2005. **23**(3): p. 1105-1115.
[74] Akhmediev, N. and M. Karlsson, *Cherenkov radiation emitted by solitons in optical fibers.* Phys. Rev. A, 1995. **51**: p. 2602-2607.
[75] Asobe, M., et al., *Noise reduction of 20 Gbit/s pulse train using spectrally filtered optical solitons.* Electron. Lett., 1998. **34**(11): p. 1135.
[76] Ohara, T., et al., *160-Gb/s all-optical limiter based on spectrally filtered optical solitons.* IEEE Photon.Technol. Lett., 2004. **16**(10): p. 2311-2313.
[77] Her, T.-H., et al., *Optimization of pulse regeneration at 40 Gb/s based on spectral filtering of self-phase modulation in fiber.* Photon.Technol. Lett., 2004. **16**(1): p. 200-202.
[78] Leuthold, J., et al., *All-optical transmission and wavelength conversion of 40 Gb/s signals over ultra-long haul distances*, in *IEEE LEOS Summer topical Meeting 2002*. 2002. p. WB1.
[79] Olsson, B.E. and D.J. Blumenthal, *Pulse width restoration and PMD suppression using fiber self-phase modulation*, in *Proc. European Conference on Optical Communication (ECOC'02)*. 2002. p. P1.2.
[80] Matsumoto, M., *Polarization-mode dispersion mitigation by a fiber-based 2R regenerator combined with synchronous modulation.* IEEE Photon.Technol. Lett., 2004. **16**(1): p. 290-292.
[81] Yoshikane, N., et al., *Improvement of dispersion tolerance by SPM-based all-optical reshaping in receiver.* IEEE Photon.Technol. Lett., 2003. **15**(1): p. 111-113.
[82] Rochette, M., et al., *An All-Optical Regenerator that Discriminates Noise from Signal*, in *31th European Conference on Optical Communications (ECOC) 2005*. 2005. p. We2.4.1.
[83] Irina O. Nasieva, S.B., and Sergei K. Turitsyn, *Bit error rate improvement by nonlinear optical decision element.* Opt. Lett., 2006. **31**(9): p. 1205-1207.
[84] Rochette, M., et al., *2R Optical Regeneration: An All-Optical Solution for BER Improvement.* IEEE J. Sel. Top. Quantum Electron., 2006. **12**(4): p. 736-744.
[85] Su, Y., et al., *All-optical 2R regeneration of 40-Gb/s signal impaired by intrachannel four-wave mixing.* Photon.Technol. Lett., 2003. **15**(2): p. 350.
[86] Johannisson, P. and M. Karlsson, *Characterization of a self-phase-Modulation-based all-optical regeneration system.* Photon.Technol. Lett., 2005. **17**(12): p. 2667.
[87] Raybon, G., et al., *40 Gb/s pseudo linear transmission over one million kilometers*, in *Proc. Optical Fiber Communications (OFC'02)*. 2002: Anaheim CA. p. PD10.
[88] Nguyen, T.N., et al. *Caractérisation théorique du régénérateur 2R exploitant l'automodulation de phase dans une fibre optique*. in *26èmes Journées Nationales d'Optique Guidée (JNOG)* 2007. Grenoble, France.
[89] Finot, C., et al., *Numerical study of an optical regenerator exploiting self-phase modulation and spectral offset filtering at 40 Gbit/s.* Optics Communications, 2008. **281**(8): p. 2252-2264.
[90] Spyropoulou, M., et al., *Investigation of Multi-Wavelength Regeneration Employing Quantum-Dot Semiconductor Optical Amplifiers beyond 40Gb/s*, in *International Conference on Transparent Optical Networks (ICTON '07)*. 2007. p. 102-105.
[91] Ohara, T., et al., *40-Gb/s x 4-channel all-optical multichannel limiter utilizing spectrally filtered optical solitons.* IEEE Photon.Technol. Lett., 2003. **15**(5): p. 763.
[92] Evangelides, S.G., Jr., et al., *Polarization multiplexing with solitons.* IEEE J. Lightwave Technol., 1992. **10**(1): p. 28-35.
[93] Suzuki, K.I., et al., *Unrepeatered 40 Gbit/s RZ signal transmission over 240 km conventional singlemode fibre.* Electron. Lett., 1998. **34**(8): p. 799-800.
[94] Cuenot, B. and A.D. Ellis, *WDM signal regeneration using a single all-optical device.* Opt. Express, 2007. **15**(18): p. 11492-11499.
[95] Mollenauer, L.F., et al., *Experimental test of dense wavelength-division multiplexing using novel, periodic-group-delay-complemented dispersion compensation and dispersion-managed solitons.* Opt. Lett., 2003. **28**(21).
[96] Lakoba, T.I. and M. Vasilyev, *A new robust regime for a dispersion-managed multichannel 2R regenerator.* Opt. Express, 2007. **15**(16): p. 10061-10074.
[97] Tomkos, I., et al., *Performance studies of multi-wavelength all-optical 2R regeneration subsystems based on highly nonlinear fibers*, in *International Conference on Transparent Optical Networks (ICTON'07)* 2007: Rome, Italy. p. Tu.C1.1.

[98] Kouloumentas, C., et al., *Four-Channel All-Fiber Dispersion-Managed 2R Regenerator*. Photonics Technology Letters, IEEE, 2008. **20**(13): p. 1169-1171.
[99] Vorreau, P., et al., *Simultaneous Processing of 43 Gb/s WDM Channels by a Fiber-Based Dispersion-Managed 2R Regenerator*, in *34th European Conference on Optical Communications (ECOC'08)* 2008: Brussels, Belgium. p. Th.1.B.3.
[100] Liu, X., et al., *Characteristics of all-optical 2R regenerator based on self-phase modulation in high-nonlinear fibers*, in *Proc. Conference on Lasers and Electro-Optics (CLEO'02)*. 2002. p. 612-613.
[101] Gruner-Nielsen, L., et al., *Dispersion-compensating fibers.* J. Lightwave Technol., 2005. **23**(11): p. 3566-3579.
[102] Asobe, M., et al., *Applications of highly nonlinear chalcogenide glass fibers in ultrafast all-optical switches.* IEEE J. Quantum Electron., 1993. **29**(8): p. 2325-2333.
[103] Feng, X., et al., *Extruded singlemode, high-nonlinearity, tellurite glass holey fibre.* Electronics Letters, 2005. **41**(15): p. 835-837.
[104] Kikuchi, K. and K. Taira, *Highly nonlinear bismuth oxide-based glass fibres for all-optical signal processing.* Electronics Letters, 2002. **38**(4): p. 166-167.
[105] Her, T., et al. *Experimental demonstration of a fiber-based optical 2R regenerator in front of an 80Gbit/s receiver*. 2003.
[106] Nakanishi, T., et al., *Silica-based highly nonlinear fiber with γ =30 /W/km and its FWM-based conversion efficiency*, in *Conference on Optical Fiber Communications (OFC)*. 2006. p. OTuH7.
[107] OFS, *Highly nonlinear fiber product datasheet.* 2002.
[108] Yusoff, Z., et al., *A 36-channel /spl times/ 10-GHz spectrally sliced pulse source based on supercontinuum generation in normally dispersive highly nonlinear holey fiber.* IEEE Photon.Technol. Lett., 2003. **15**(12): p. 1689.
[109] Hansen, K.P., et al., *Fully Dispersion Controlled Triangular-Core Nonlinear Photonic Crystal Fiber*, in *Optical Fiber Communications Conference (OFC) 2003*. 2003. p. PD02.
[110] Parmigiani, F., et al., *2R regenerator based on a 2-m-long highly nonlinear bismuth oxide fiber.* Opt. Express, 2006. **14**(12): p. 5038-5044.
[111] Sugimoto, N., et al., *Bismuth-based optical fiber with nonlinear coefficient of 1360 W/sup -1/ km/sup -1*, in *Optical Fiber Communication Conference, 2004. OFC 2004* 2004. p. 3.
[112] Nagashima, T., et al., *Dispersion Shifted Bi_2O_3-based Photonic Crystal Fiber*, in *32th European Conference on Optical Communications (ECOC)* 2006. p. We 1.3.2.
[113] Nagashima, T., et al., *Fusion-Spliceable Bi_2O_3-Based Photonic Crystal Fiber*, in *Optical Fiber Communication Conference (OFC) 2007*. 2007: Anaheim, CA. p. OTuC5.
[114] Lamont, M.R.E., *2R optical regenerator in As2Se3 chalcogenide fiber characterized by a frequency-resolved optical gating analysis.* Applied Optics, 2006. **45**(30): p. 7904-7907.
[115] Petropoulos, P., et al., *2R-regenerative all-optical switch based on a highly nonlinear fiber.* Opt. Lett., 2001. **26**(16): p. 1233-1235.
[116] Chow, K.K., et al. *All-optical pulse compression and reshaping by spectral fitering from Self-Phase modulation in a nonlinear photonics crystal fiber*. in *Optical Fiber Communication Conference (OFC)*
[117] Monro, T.M., et al., *Chalcogenide holey fibres.* Electron. Lett., 2000. **36**(24): p. 1998-2000.
[118] Fu, L.B., et al., *Investigation of self-phase modulation based optical regeneration in single mode As Se chalcogenide glass fiber.* Opt. Express, 2005. **13**(9): p. 7637-7644.
[119] Brilland, L., et al., *Fabrication of complex structures of holey fibers in chalcogenide glass.* Opt. Express, 2006. **14**(3): p. 1280-1285.
[120] Asimakis, S., et al., *A 2-m-long Reshaping Regenerator Based on a Highly Nonlinear Bismuth Oxide Fiber*, in *Optical Fiber Communication Conference (OFC) 2006* 2006. p. OThB5.
[121] Lee, J.H., et al., *Output Performance Investigation of Self-Phase-Modulation-Based 2R Regenerator Using Bismuth Oxide Nonlinear Fiber.* IEEE Photon.Technol. Lett., 2006. **18**(12): p. 1296-1298.
[122] Finot, C., et al., *Regenerative 40 Gbit/s wavelength converter based on similariton generation.* Opt. Lett., 2005. **30**(14): p. 1776-1778.
[123] Goto, H., et al., *All optical intensity equalizer based on effective control of spectral modulation induced by self-phase-modulation using super-Gaussian signals*, in *10th Anniversary International Conference on Transparent Optical Networks, 2008. ICTON 2008.* . 2008. p. 124-127.

[124] Chernikov, S.V. and J.R. Taylor, *Measurement of normalization factor of n_2 for random polarization in optical fibers.* Opt. Lett., 1996. **21**: p. 1559.
[125] Tomlinson, W.J., et al., *Optical wave breaking of pulses in nonlinear optical fibers.* Opt. Lett., 1985. **15**(10): p. 457.
[126] Anderson, D., et al., *Wave breaking in nonlinear-optical fibers.* J. Opt. Soc. Am. B, 1992. **9**(8): p. 1358-1361.
[127] Finot, C., et al., *Beneficial impact of wave-breaking for coherent continuum formation in normally dispersive nonlinear fibers.* J. Opt. Soc. Am. B, 2008. **25**(11): p. 1938-1948.
[128] Rothenberg, J.E., *Colliding visible picosecond pulses in optical fibers.* Opt. Lett., 1990. **15**(8): p. 443-445.
[129] Mamyshev, P.V. and N.A. Mamysheva, *Pulse-overlapped dispersion-managed data transmission and intrachannel four-wave mixing.* Opt. Lett., 1999. **24**(21): p. 1454.
[130] Nguyen, T., et al., *Noise reduction in 2R-regeneration technique utilizing self-phase modulation and filtering.* Opt. Express, 2006. **14**(5): p. 1737-1747.
[131] Baveja, P.P., et al., *Optimization of All-Optical 2R Regenerators Operating at 40~Gb/s: Role of dispersion.* IEEE J. Lightwave Technol., 2009. **17**(17-20): p. 3831-3836
[132] Provost, L., et al., *2R Regeneration Architectures Based on Multi-Segmented Fibres*, in *34th European Conference on Optical Communications (ECOC'08)* 2008: Brussels, Belgium. p. Th.1.B.1.
[133] Matsumoto, M., *Efficient all-optical 2R regeneration using self-phase modulation in bidirectional fiber configuration.* Opt. Expr., 2006. **14**(23): p. 11018-11023.
[134] Hartog, A. and M. Gold, *On the theory of backscattering in single-mode optical fibers.* J. Lightwave Technol., 1984. **2**(2): p. 76-82.
[135] Potasek, M.J., et al., *Analytic and numerical study of pulse broadening in nonlinear dispersive optical fibers.* J. Opt. Soc. Amer. B, 1986. **2**(2): p. 205-211.
[136] *VPI Photonics Website: VPItransmissionMaker™ Optical Systems*. [cited 2010 July]; Available from: http://www.vpiphotonics.com/TMOpticalSystems.php.
[137] Hiroishi, J., et al., *Development of Highly Nonlinear Fibers for Optical Signal Processing.* Furukawa Review, 2005. **23**: p. 21-25.
[138] Matsumoto, M., *Efficient all-optical 2R regeneration using self-phase modulation in bidirectional fiber configuration.* Opt. Express, 2006. **14**(23): p. 11018-11023.
[139] Patki, P.G., et al., *Recirculating-loop study of dispersion-managed 2R regeneration*, in *Conference on Lasers and Electro-Optics/Quantum Electronics and Laser Science (CLEO US)*. 2007. p. CMZ3.
[140] Madden, S.J., et al., *Chalcogenide Glass Photonic Chips.* Opt. Photon. News, 2008. **19**(2): p. 18-23.
[141] Koos, C., et al., *All-optical high-speed signal processing with silicon-organic hybrid slot waveguides.* Nature Photonics, 2009. **3**(4): p. 216–219.

List of Publications

Journal

1. **L. Provost**, C. Finot, P. Petropoulos, D. Richardson, "A 2R Mamyshev Regeneration Architecture Based on a Three-Fibre Arrangement", to be published in Journal of Lightwave Technology 2010.

2. C. Finot, B. Kibler, **L. Provost**, and S. Wabnitz, "Beneficial impact of wave-breaking for coherent continuum formation in normally dispersive nonlinear fibres," *J. Opt. Soc. Am. B,* vol. 25, pp. 1938-1948, 2008.

3. C. Kouloumentas, P. Vorreau, **L. Provost**, P. Petropoulos, W. Freude, J. Leuthold, I. Tomkos, "All-fibreized dispersion-managed multi-channel regeneration at 43 Gb/s", *IEEE Photonics Technology Letters* 2008 Vol. 20(20) pp. 1854-1856

4. F. Parmigiani, M. Ibsen, T. T. Ng, **L. Provost**, P. Petropoulos, D. J. Richardson, "An efficient wavelength converter exploiting a grating based saw-tooth pulse shaper", *Photonics Technology Letters* 2008 Vol. 20(17) pp. 1461-1463

5. **L. Provost**, F. Parmigiani, P. Petropoulos, D. J. Richardson, K. Mukasa, J. Takahashi, J. Hiroishi, M. Tadakuma "Investigation of four-wavelength regenerator using polarization-and-Direction-Multiplexing", *Photonics Technology Letters* 2008 Vol. 20(20) pp. 1676-1678

6. C. Kouloumentas, **L. Provost**, F. Parmigiani, S. Tsolakidis, P. Petropoulos, I. Tomkos, D. J. Richardson, "Four-channel all-fibre dispersion-managed 2R regenerator, *Photonics Technology Letters* 2008 Vol. 20(13) pp. 1169-1171

7. **L. Provost**, F. Parmigiani, C. Finot, K. Mukasa, P. Petropoulos, D. J. Richardson, "Analysis of a two-channel 2R all-optical regenerator based on a counter-propagating configuration", *Optics Express* 2008 Vol. 16(3) pp. 2264-2275.

8. **L. Provost**, F. Parmigiani, P. Petropoulos, D. J. Richardson, "Investigation of simultaneous 2R regeneration of two 40 Gb/s channels in a single optical fibre", *Photonics Technology Letters* 2008 Vol. 20(4) pp. 270-272

9. **L. Provost**, C. Finot, P. Petropoulos, K. Mukasa, D. J. Richardson, "Design scaling rules for 2R-optical SPM-based regenerators", *Optics Express* 2007 Vol. 15 pp. 5100-5113

10. C. Finot, **L. Provost**, P. Petropoulos, D. J. Richardson, "Parabolic pulse generation through passive nonlinear pulse reshaping in a normally dispersive two segment fibre device", *Optics Express* 2007 Vol. 15 pp. 852-864

11. S. Pitois, C. Finot, **L. Provost**, "Asymptotic properties of incoherent waves propagating in an all-optical regenerators line", *Optics Letters* 2007 Vol. 32(22) pp. 3263-3265

Conferences

12. F. Parmigiani, **L. Provost**, P. Petropoulos, D. J. Richardson, "Multi-wavelength all-optical regeneration techniques", *IEEE/LEOS Summer Topicals 2009,* Newport Beach 20-22 Jul 2009. *Invited Talk*

13. P. Petropoulos, **L. Provost**, F. Parmigiani, C. Kouloumentas, C. Finot, K. Mukasa, P. Vorreau, I. Tomkos, S. Sygletos, W. Freude, J. Leuthold, A. D. Ellis, D. J. Richardson, "Simultaneous 2R regeneration of WDM signals in a single optical fibre", *LEOS Winter Topicals,* Innsbruck 12-14 Jan 2009, We2.2. *Invited Talk*

14. **L. Provost**, P. Petropoulos, D. J. Richardson, "Optical WDM regeneration: status and future prospects", *OFC 2009,* San Diego 21-25 Mar 2009, OWD7. *Invited Talk*

15. F. Parmigiani, P. Vorreau, **L. Provost**, K. Mukasa, M. Takahashi, M. Tadakuma, P. Petropoulos, D. J. Richardson, W. Freude, J. Leuthold, "2R regeneration of two 130 Gb/s channels within a single fibre", *OFC 2009,* San Diego 22-26 Mar 2009, JThA56.

16. **L. Provost**, C. Finot, P. Petropoulos, D. J. Richardson, "2R regeneration architectures based on multi-segmented fibres", *ECOC 2008,* Brussels 21-25 Sep 2008, Th.1.B.1

17. S. Pitois, C. Finot, **L. Provost**, "Generation of Localized Pulses from Incoherent Wave in Optical Fiber Lines Made of Concatenated Mamyshev Regenerators", PHOTONICS PRAGUE 2008, 6th International Conference on Photonics, Devices and Systems, Prague 27-29 Aug. 2008.

18. **L. Provost**, F. Parmigiani, P. Petropoulos, D. J. Richardson, "Investigation of timing-jitter reduction in a bi-directional 2R all-optical Mamyshev regenerator", *OFC 2008* San Diego 24-28 Feb 2008 OThJ4
19. **L. Provost**, C. Kouloumentas, F. Parmigiani, S. Tsolakidis, I. Tomkos, P. Petropoulos, D. J. Richardson, "Experimental investigation of a dispersion-managed multi-channel 2R optical regenerator", *OFC 2008* San Diego 24-28 Feb 2008 OThJ3

20. F. Parmigiani, M. Ibsen, T. T. Ng, **L. Provost**, P. Petropoulos, D. J. Richardson, "Efficient wavelength conversion using triangular pulses generated using a superstructured fibre Bragg grating", *OFC 2008* San Diego 24-28 Feb 2008 OMP3

21. S. Pitois, C. Finot, **L. Provost**, "Generation de sequences d'impulsions picoseconds aperiodiques a partir d'ondes optiques incoherentes", *PhoNoMi2* Montpellier 25-27 Oct 2007

22. S. Pitois, C. Finot, **L. Provost**, "Generation of aperiodic picosecond pulses sequences from incoherent optical waves", *BGPP/NP 2007* Quebec 2-6 Sep 2007 NTuA3

23. **L. Provost**, F. Parmigiani, K. Mukasa, M. Takahashi, J. Hiroishi, M. Tadakuma, P. Petropoulos, D. J. Richardson, "Simultaneous all-optical 2R regeneration of 4x10 Gb/s wavelength division multiplexed channels", *ECOC 2007* Berlin 16-20 Sep 2007.

24. C. Finot, **L. Provost**, "Étude numérique des performances d'un régénérateur 2R à fibre", *26th National Conference on Guided Optics* 2007. Grenoble, France (Poster).

25. **L. Provost**, F. Parmigiani, C. Finot, P. Petropoulos, D. J. Richardson, "SPM-based 2R optical regenerator for the simultaneous processing of two WDM channels", *CLEO/Europe-IQEC 2007* Munich 17-22 Jun 2007 CI2-1-TUE

26. C. Finot, **L. Provost**, P. Petropoulos, D. J. Richardson, "Parabolic pulse generation through passive reshaping of Gaussian pulses in normally dispersive fibre", *OFC 2007* Anaheim 25-29 Mar 2007 OTuJ3

27. **L. Provost**, C. Finot, K. Mukasa, P. Petropoulos, D. J. Richardson, "Generalisation and experimental validation of design rules for SPM-based 2R-regenerators", *OFC 2007* Anaheim 25-29 Mar 2007 OThB6

28. **L. Provost**, C. Finot, P. Petropoulos, D. J. Richardson, "Regles de conception pour les regenerateurs optiques 2-R exploitant l'auto-modulation de phase", *25th National Conference on Guided Optics* Metz 7-9 Nov 2006 (Poster)

29. **L. Provost**, C. Finot, P. Petropoulos, D. J. Richardson, "Design scaling laws for SPM-based 2R-Regenerators", *ECOC 2006* Cannes 24-28 Sep 2006 We4. 3. 2

30. C. Finot, P. Dupriez, **L. Provost**, F. Parmigiani, P. Petropoulos, D. J. Richardson, C. Billet, J. Dudley, S. Pitois, G. Millot, "Impulsions paraboliques et similaritons dans les fibres

optiques (Parabolic pulses and similaritons in optical fibres)", *PAMO 2006 - Atomic & Molecular Physics Optics* Dijon 5-7 Jul 2006.

31. K. Mukasa, M. N. Petrovich, F. Poletti, A. Webb, J. R. Hayes, A. van Brakel, R. Amezcua-Correa, **L. Provost**, J. K. Sahu, P. Petropoulos, D. J. Richardson, "Novel fabrication method of highly nonlinear silica holey fibres", *CLEO/QELS 2006* Long Beach 21-25 May 2006 CMC5.